Toward Dendrite-Free Metallic Lithium Anodes: From Structural Design to Optimal Electrochemical Diffusion Kinetics

Jian Wang,* Linge Li, Huimin Hu, Hongfei Hu, Qinghua Guan, Min Huang, Lujie Jia, Henry Adenusi, Kun V. Tian, Jing Zhang,* Stefano Passerini,* and Hongzhen Lin*

ABSTRACT: **Lithium metal anodes are ideal for realizing high-energy-density batteries owing to their advantages, namely high capacity and low reduction potentials. However, the utilization of lithium anodes is restricted by the detrimental lithium dendrite formation, repeated formation and fracturing of the solid electrolyte interphase (SEI), and large volume expansion, resulting in severe "dead lithium" and subsequent short circuiting. Currently, the researches are principally focused on inhibition of dendrite formation toward extending and maintaining battery lifespans. Herein, we summarize the strategies employed in interfacial engineering and current-collector host designs as well as the emerging electrochemical catalytic methods for evolving-accelerating-ameliorating lithium ion/atom diffusion processes. First, strategies based on the fabrication of robust SEIs are reviewed from the aspects of compositional constituents including inorganic, organic, and hybrid SEI layers derived from electrolyte additives or artificial pretreatments. Second, the summary and discussion are presented for metallic and carbon-based three-dimensional current collectors serving as lithium hosts, including their functionality in decreasing local deposition current density and the effect of introducing lithiophilic sites. Third, we assess the recent advances in exploring alloy compounds and atomic metal catalysts to accelerate the lateral lithium ion/atom diffusion kinetics to average the spatial lithium distribution for smooth plating. Finally, the opportunities and challenges of metallic lithium anodes are presented, providing insights into the modulation of diffusion kinetics toward achieving dendrite-free lithium metal batteries.**

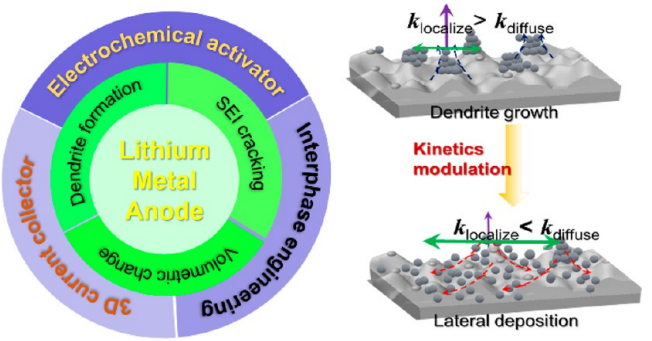

KEYWORDS: *lithium metal battery, lithium dendrite, artificial SEI layer, 3D current collector, electrochemical diffusion modulation, single atomic catalyst, lithium ion/atom diffusion, lithiophilic site, kinetics enhancement, lateral plating/deposition*

1. INTRODUCTION

The ever-increasing dependency and demands on consumable electronics, electric vehicles (EVs), and smart grid storages have stimulated the rising demands for high-energy-density rechargeable batteries.[1−4] Although lithium-ion batteries dominate the current consumer markets, the capacities of cathodes and graphitic anodes have both reached bottlenecks.[5−13] Fortunately, the lithium metal anode has been regarded as the "Holy Grail" for high-energy-density batteries due to its unrivaled theoretical specific capacity (∼3860 mA h g^{-1}), nearly 10 times higher than that of a graphite anode (∼372 mA h g^{-1}), and lower electrochemical potential (∼−3.04 V) relative to the standard hydrogen electrode (SHE).[14−16] More importantly, the utilization of a Li metal anode broadens the range of applicable cathode materials, from lithium-rich intercalated cathodes (e.g., $LiFePO_4$, $LiCoO_2$, and $LiNi_xCo_yMn_{1-x-y}O_2$) to lithium-free conversion cathodes (e.g., sulfur and air), for the realization of differing types of lithium batteries with higher energy densities (Figure 1A).[17−22] Due to these advantageous electrochemical properties, lithium metal batteries (LMBs) have the potential to reach the energy

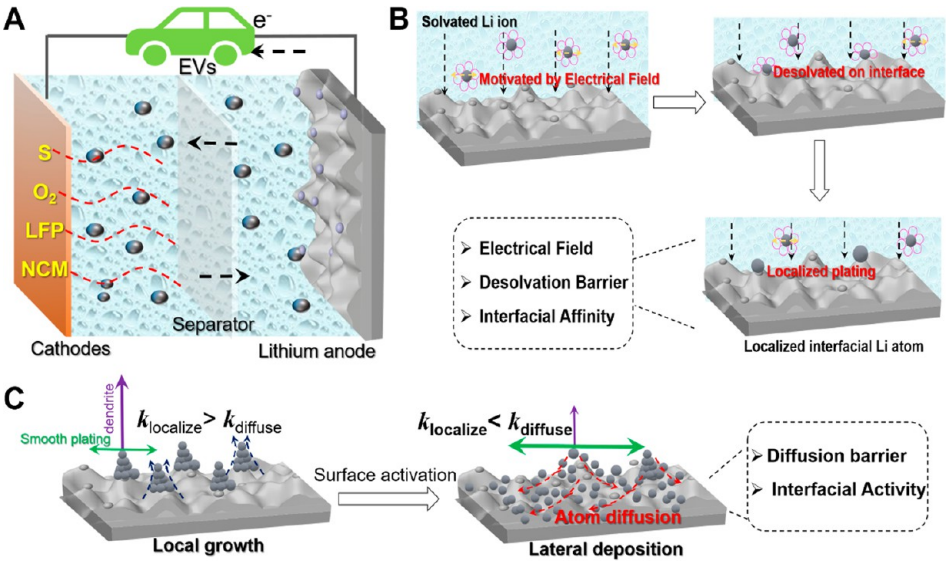

Figure 1. (A) Illustration of the lithium metal battery. (B) The systematic scheme of the formation of lithium atoms from solvated Li ions to desolvation to lithium atoms with localized plating. (C) The competing kinetics between lithium atom localization with dendrite growth and lithium atom diffusion with lateral deposition.

density milestone of 500 Wh kg^{-1} in the next few years to satisfy industrial goals and practical utilizations in EVs and grid energy storage.[23−28]

Despite these potentials, the large-scale commercialization of Li metal anodes is still plagued by numerous technical and industrial challenges, as follows: (1) high reactivity of lithium metal anodes, manifested in repeated interaction with electrolyte constituents to form discontinuous solid−electrolyte interphase (SEI) layers, exhausting the limited amount of electrolyte; (2) formation of Li dendrites and the subsequent partial cracking of these fragile Li from the root, forming isolated "dead Li" and diminishing Li utilization; (3) large volume changes caused by the breakdown of the unstable SEI and "dead Li".[6,17,19,21,29−45] Usually, the electrochemically generated SEI results from the side reactions between Li metal and electrolyte salts/solvents, forming an electron-insulative but ion-conductive nanoscale layer. For example, in commercial carbonate-based electrolyte, organic or inorganic Li salts such as RCOOLi or LiF are generated along with the decomposition of solvents or electrolytes. However, the electrochemically generated SEI layer is usually uneven and discontinuous so that the exposed Li surface will further exhaust more electrolyte, generating progressively thicker passivated layers. Accordingly, from the dynamic view, the Li plating process is also associated with the Li diffusion kinetics in the electrode/electrolyte interface.[34,39,46,47]

To overcome these challenges and to realize the commercialization of LMBs, considerable efforts have been devoted to lithium metal protection. Commonly used strategies can be divided into two categories: (i) SEI interfacial engineering: to form robust SEI layers on metallic lithium surfaces by using electrolyte additives or artificial pretreatments, in order to prevent electrolyte components from decomposition to continuously form fresh SEI layer;[1,38,41,48−60] and (ii) constructing three-dimensional (3D) ion/electron conductive architectures for hosting thermally infused/electrochemically plated lithium, lowering the local deposition current density and alleviating volume changes.[61−68] The SEI interfacial engineering is usually performed through adding suitable active electrolyte additives, e.g., fluoroethylene carbonate (FEC), vinylene carbonate (VC), lithium nitrate ($LiNO_3$), to generate thin SEI in situ during the electrochemical processes.[59,69,70] Another effective way is precoating inorganic/organic artificial layers on metallic lithium surfaces to strengthen the SEI in order to suppress the dendrite-induced short-circuiting. For example, the LiF-derived inorganic layer helps to provide robust mechanical properties to resist dendrite formation while maintaining a good conductivity to lithium ions.[70,71] To further improve the mechanical properties of the SEI, organic polymers are incorporated into the inorganic layer to form a robust yet flexible hybrid artificial layer, which is not only helpful to suppress the dendrite formation but also beneficial for the long-term cycling stability due to its good contact compatibility with the electrolyte.[48,72] Furthermore, conductive carbon-based protective films that spread over the lithium electrode surfaces can uniformize the surface distribution of current density and avoid the current cusp effect that triggers the vertical Li deposition, prohibiting the formation of both dendrites and "dead Li".[73] However, the insufficient lithiophilicity of nanocarbon surfaces may weaken its regulating capability toward uniform plating. On the contrary, the coating layers with heteroatoms doping are more polar and can provide more lithiophilic sites to capture Li ions/atoms toward more uniform plating. In terms of the host architecture designs, the 3D current collectors with reserved voids are capable of effectively accommodating volume expansion. In this manner, the 3D matrix significantly enhances the active interfacial electrochemical surface area between the electrodes and electrolyte, which effectively averages the electric field distribution and lowers the local deposition current density, resulting in uniform Li electrodeposition.[2,66,74,75] Unfortunately, the lithiophilicity of the host matrix is still inadequate for the loading of metallic Li or accommodating lithium effectively, since a relatively large weight content of the 3D matrix is required which inevitably compromises the entire energy density.

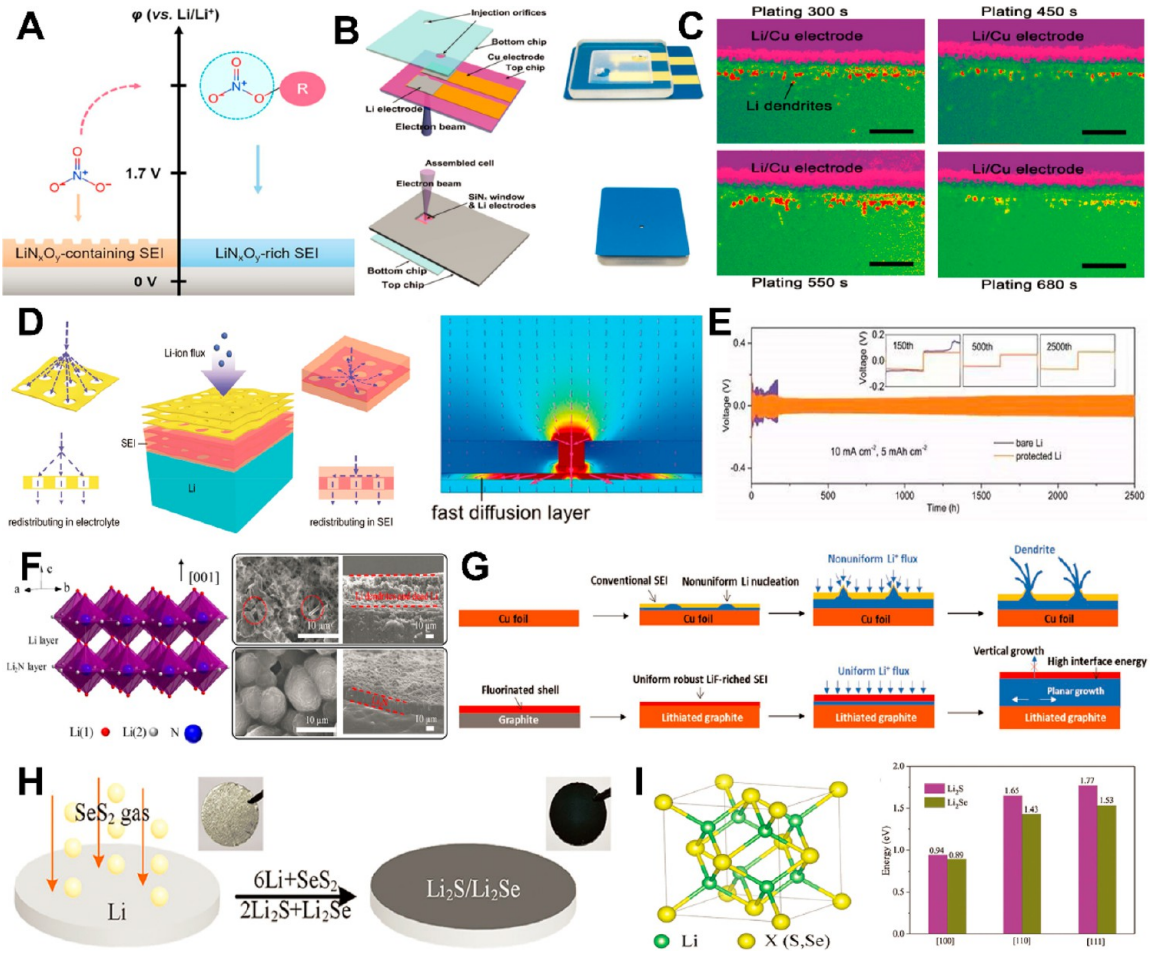

Figure 2. Typical ion-conductive inorganic SEI layer on metallic Li surface: (A) Illustration of $LiNO_3$ in forming SEI layer on Li surface. Reproduced with permission from ref 53. Copyright 2020, Wiley-VCH. (B) Configuration of self-made liquid EC-SEM cell and (C) corresponding Li plating morphologies on Cu electrode with Li_2S_8 and $LiNO_3$ electrolyte additives. Reproduced with permission from ref 69. Copyright 2017, Wiley-VCH. (D) Illustration of Li-ion redistribution behaviors regulated by aligned holey-nanosheets and corresponding simulation as fast diffusion layer. (E) Long-term stability test at 10 mA cm^{-2}. Reproduced with permission from ref 101. Copyright 2020, Wiley-VCH. (F) Li_3N crystal structure and SEM images of bare Li and Li_3N modified Li. Reproduced with permission from ref 109. Copyright 2019, Elsevier. (G) Functions of MCMB-F in averaging lithium ion flux for uniform deposition surface. Reproduced with permission from ref 112. Copyright 2020, Wiley-VCH. (H) The fabrication process of LSSe@Li anode via gas treatment. (I) The structure image and migration barriers in Li_2S and Li_2Se, respectively. Reproduced with permission from ref 115. Copyright 2020, Wiley-VCH.

As detailed in Figure 1B, the localized electric field, the heterogeneous interfacial affinity, and the high desolvation barriers are responsible for the failure of the Li metal anodes.[15,76] Such a failure may cause low Coulombic efficiency (CE), shortened life-span, and even safety risks of fire and explosion in LMBs.[16,76−82] During the multistep lithium plating (Figure 1B), the lithium ion/atom has to overcome the sluggish kinetics due to the high barriers of desolvation, nucleation and diffusion,[34,39,83] which are the main causes of the random plating, dendrite growth and SEI failure.[24] Currently, there is a lack of methods for manipulating the intrinsic nucleation and diffusion kinetics toward lateral growth of Li deposition. From the dynamical viewpoint, enhancing the surface affinity of the conductive matrix to lithium ions/atoms can create a thermodynamically favorable environment for smooth lithium deposition: Increasing the Li-ion/atom diffusion rates, especially those along the electrode surface, can kinetically ensure the rapid and uniform distribution of the lithium flux to the nucleation sites, even at large current densities.[34,84] Therefore, a combination of these two strategies would be the most effective solution for achieving dendrite-free Li plating. To decrease the diffusion energy barriers, one can apply the fundamentals of conventional catalysis for reducing the energy barriers of chemical reactions.[76,85−88] Actually, the concept of lithium bonding, as an analogue to hydrogen bonding, has been well established and widely applied to the understanding of lithium ionic/atomic behaviors in lithium batteries.[89,90] The solvation, desolvation, transfer, and migration of lithium ions/atoms can be regarded as a sequence of "reactions" involving the formation and breaking of different types of lithium bonds.[83,91] Therefore, the catalyst design principles can be readily implemented for modulating the lithium diffusion kinetics. This offers an alternative method for covering the pristine lithium metal surface with catalysis/modulation layer to regulate the lithium plating behaviors. We note that an ideal catalyst for accelerating the lithium diffusion kinetics should possess a moderate affinity to Li ions/atoms, rather than the common belief in "the stronger the better," in order to circumvent poisoning by the strongly adsorbed lithium species.[92] Hence, the dendrite formation and growth

can be ascribed to the localized aggregation of the formed lithium atoms (Figure 1C), when the lateral diffusion rate of the lithium atoms is far slower than the local deposition rate at the vertical direction. The high surface diffusion barriers and low surface activity are the main factors responsible for this issue.[93]

In this review, the interfacial layer structural designs toward robust mechanical properties and solvent-isolation with high ion conductivity are first summarized and classified according to the constituent of the SEI: inorganic, organic and hybrid layers. Second, the recent literature on using multidimensional current collectors made from metal to carbon networks for hosting lithium metal to capture and uniformize initial Li nucleation by decreasing the localized deposition current density are reviewed. Third, the state-of-the-art approaches for modulating Li-ion/atom diffusion kinetics with alloy layers or highly active single atomic catalysts (SACs) are introduced. Although advancements have been made in the three aspects, with the dynamic studies of lithium diffusion still at the early stage, the understanding of the dynamic processes of Li electrodeposition remains insufficient, and there lacks evaluation of practical large pouch cells. Promising research perspectives of LMBs are suggested for the future development of lithium metal anodes.

2. ROBUST INTERFACIAL ENGINEERING DESIGNS OF SEI ON LI METALS

Although Li metal electrode encounters the issue of dendrite formation and volumetric changes in the electrochemical plating process, it is still considered the "Holy Grail" anode candidate for batteries in large-scale energy storage applications because of its high capacity and low relative potential. It is widely accepted that Li dendrite formation occurs when nonuniform Li-ion flux is induced under the morphology and time-dependent local electric field. Inspired by the successful commercialization of graphite anode, on which the spontaneously formed SEI is capable of enhancing the cycling stability of the electrode, constructions of robust SEI layers via electrolyte component tunings, or artificial pretreatments have been employed to average the lithium flux across the SEI, to confine the growth of lithium dendrites and to passivate the metallic lithium from continuous side reactions with the electrolytes. An ideal SEI layer should possess features such as good mechanical strength and flexibility, smooth morphology and lithiophilicity for uniform Li^+ distribution, compactness for resisting the penetration of solvents, and sufficient channels for Li^+ transport.[2,59,72,94] An appropriate SEI layer on the Li electrode surface can effectively inhibit the undesirable Li dendrite formation and related issues such as volumetric fluctuations and cracking of the SEI. The SEI formation derived from the decomposition of anions can be classified into two categories: (1) potential-driving redox ability of the anions to form stable organic or inorganic SEI and (2) activity-driving decomposition to generate inorganic or organic SEI in comparison with the common electrolyte salts or solvents. Based on composition, the obtained SEI layers can be classified into inorganic, organic/polymeric, and organic/inorganic hybrid ones.

2.1. High Ionic Conductive Inorganic SEI Layers. It has been established that the SEI should be ionically conductive but electronically insulating. A facile strategy to develop the inorganic layer on the metallic Li electrode surface is to regulate the constituents of liquid electrolytes, i.e., solvents, Li salts, and (salt) additives.[52,56,69,71] It is possible to optimize the inner structures of solvated Li^+ since additives do not disrupt the compatibility between the electrolyte and electrodes.[95] Meanwhile, these inorganic layers possess wide electrochemical/structural stability as well as high mechanical strength. For instance, $LiNO_3$ is a widely adopted additive in ether-based or carbonate-based electrolytes for developing the SEI layer on metallic Li surface. $LiNO_3$ is usually reduced under the potential of 1.7 V, and the product of the side reactions is LiN_xO_y (Figure 2A).[53] Therefore, the introduction of $LiNO_3$ in the electrolyte is expected to improve the reversibility with the formation of a LiN_xO_y-rich SEI on the surface. Although the functions of $LiNO_3$ in prohibiting dendrite formation and extending cycle life have been extensively studied with electrochemical and theoretical methods, direct observation of Li plating under the influence of $LiNO_3$ remains scarce. In this regard, an in situ liquid electrochemical scanning electron microscopy (EC-SEM) technique to investigate the plating/stripping behaviors of Li atom on the Cu current collector, where a thin SiN_x membrane was selected as the observation window, was developed.[69] With this delicately designed in situ EC-SEM cell (Figure 2B), the synergistic effects of polysulfide and $LiNO_3$ additives in prohibiting dendrite formation were observed: a competing deposition and dissolution phenomenon along with increased plating time (Figure 2C). During the entire process, the height of formed dendrite was limited within 3 μm, much smaller than that formed with the addition of $LiNO_3$ or polysulfide alone. After disassembling, the ex situ SEM also revealed the smooth surface without dendrite formation in the coin cell, demonstrating the indisputable role of $LiNO_3$ in realizing dendrite-free Li electrode. Other in situ characterization methods such as in situ X-ray absorption spectroscopy (XAS) and in situ transmission electronic microscopy (TEM) have also been explored to aid the understanding of the specific functions of various additives.[96−98]

The ideal inorganic SEI layer should also possess mechanical robustness to withstand the focused stress exerted by dendrite growth. In contrast to the uncontrollable naturally formed SEI film derived from functional additives, the artificially engineered interphase layer is more compact and can tolerate dendrite penetration during repeated plating/stripping processes.[54,72] Some lithiophilic metal compounds with certain polarity can strongly interact with lithium ions/atoms and display satisfactory wettability to Li flux, thus they are viable candidates for building artificial interphase layers with the capability to average the distribution of Li ions/atoms over the electrode surface.[99,100] Parallelly aligned holey (porous) MgO nanosheets were introduced on the Li metal surface to redistribute Li-ion flux (Figure 2D).[101] Such holey (porous) nanosheets provide a tunnel for lithium ion transport reinforcing the simultaneous formation of multilayer SEI. Outside the SEI, these nanosheets redistribute the ionic flux through the homogeneous pores. As simulated by the dynamic COMSOL multiphysics software (Figure 2D), holey (porous) nanosheets incorporation enabled a fast diffusion layer with enhanced Li^+ diffusion coefficient to uniformly redistribute the Li-ion flux in the electrolyte, in sharp contrast to the simulation of nonuniform Li^+ flux that emerged in the pristine SEI. Thanks to the guiding and sieving effect of the holey (porous) MgO nanosheets, even cycled at a high current density of 10 mA cm^{-2} (Figure 2E), the symmetric cell possessed a ultralong cycle life span over 2500 h under 5 mA h cm^{-2} and the paired

full cell also displayed a much higher capacity retention rate of 90.9% after 500 cycles at 1 C. Apart from porous metal oxides, the sieve-like SiO_2 nanosheet-modified SEI film seems more suitable to adjust the Li-ion flux than the other types, i.e., nanospheres and nanocubes. Due to the stronger blocking effect of the permselective property of SiO_2 nanosheets, Li dendrite propagation is significantly prohibited by the microchannels where only Li-ions can pass through. Besides the intrinsic ion transfer regulation, interfacial stability and electrolyte compatibility on the metal oxide surface should also be considered. Chen et al. discovered that depositing inorganic aluminum oxide (Al_2O_3) layer on the metallic Li surface via atomic layer deposition method presented a good wettability toward both carbonate and ether-based electrolytes, resulting in reduced electrolyte consumption during battery operation from 20 to 5 μL.[102] More significantly, the advantageous electrolyte compatibility and stabilizing effect of the Al_2O_3 coating on Li surface have expanded the cycle life by 4-fold compared to the pristine counterpart.

Fast plating ability under practical capacities above 3 mA h cm^{-2} is prerequisite for the development of fast charging technique, which means fast Li-ion diffusion kinetics should be guaranteed across the SEI interfaces.[103−107] In situ grown elemental Li-based compounds possess high Li-ion conductivity. Among various elemental Li-based compounds, lithium nitride (Li_3N) has recently been considered as an ideal artificial SEI layer because it offers extremely high ionic conductivity ($\approx 10^{-3}$ S cm^{-1}), high Young's modulus of elasticity, and thermodynamic stability.[19,77,108] Chen et al. fabricated the multifunctional Li_3N protective layer on the lithium metal surface through N_2 plasma activation.[109] The generated Li_3N layer is composed of α-phase Li_3N crystal, offering an excellent lithium ion conductivity to facilitate dendrite inhibition: needle-like lithium dendrites could be observed on the surface of pristine Li, while the cycled Li_3N-activated Li exhibited stable and smooth nanomorphology on the SEM micrographs. In the cross-sectional SEM images, the Li_3N-activated Li exhibited a more compact interface layer while loose dead lithium formed on the bare lithium (Figure 2F). In another work, Xiong's group also constructed an artificial inorganic Li_3N-based SEI layer with abundant grain boundaries on the Li metal via an in situ spontaneous reaction between zirconyl nitrate ($ZrO(NO_3)_2$) and Li metal. The numerous grain boundaries helped to facilitate Li-ion diffusion across the interface, thereby enabling uniform and stable stripping/plating at high current densities.[110] On the other hand, the generated inorganic Li_3N and ZrO_2 provided ultrahigh mechanical strength and chemical stability, inhibiting the penetration of undesirable Li dendrites into the SEI and preventing the continuous electrolyte consumption. Thus, the symmetric cell assembled with the $LiZrO(NO_3)_2$@Li anodes exhibited cycling stability even at an ultrahigh current density of 10 mA cm^{-2} (10 mA h cm^{-2}).[110]

Besides Li_3N, lithium fluoride (LiF) is also electrochemically stable within the working window of 0−6.4 V. More importantly, with a relatively high shear modulus of 55 GPa, even higher than metallic Li, the LiF film can tolerate the dendrite growth.[111] Beneficially, LiF film can be deposited directly on the lithium metal surface at low temperature to avoid the contamination of Mg and Ti targets under high temperature. The purity of this so formed LiF artificial layer surpasses 99% and the symmetric cell enables a stable CE of 99.5% for over 170 cycles at 0.4 mA cm^{-2}, much higher than that of bare lithium anode. Afterward, the abundant LiF interface substance could be formed in situ by the lithiation of the fluorinate-doped mesocarbon microbeads (MCMB-F) to improve the lithiophilicity and conductivity for the homogeneous lateral Li plating, preventing the vertical dendrite growth.[112] In comparison with the dendrite formation on the pristine copper foils, the negligible volume changes of MCMB-F and the high interfacial energy simultaneously guarantee the close contact (Figure 2G). Consequently, the MCMB-F decorated electrodes show an initial overpotential of 79 mV and are capable of stable cycling for 200 cycles without any CE decay in the following cycles, demonstrating excellent reversibility during the lithium plating/stripping.

Lithium phospho-oxynitride (LiPON) is also viable for the high mechanical and electrochemical stability. Wang et al. established a dense, but homogeneous LiPON coating layer on the lithium metal via nitrogen plasma-assisted deposition via electron beam reactive evaporation, which effectively inhibited the corrosion reaction with organic electrolytes and promoted uniform Li plating/stripping,[60] extending dendrite-free cycling performance to over 900 cycles. As such, the high-mass-loading lithium sulfur (Li-S) pouch cell based on LiPON-coated Li (sulfur loading: 7 mg cm^{-2}) achieved the energy density of ~300 Wh kg^{-1} and maintained an extended lifespan of over 120 cycles with stable CE ~ 91%.

Apart from metal nitrides and fluorides, the sulfides and selenides are also attractive candidates.[113,114] Yu and coworkers designed a hybridized lithium-ion conductive Li_2S/Li_2Se (LSSe) protection layer through a facile gas/solid (SeS_2/Li) chemical reaction at 150 °C, below metallic lithium's low melting point at 180 °C (Figure 2H).[115] Within this as-prepared hybrid film, the Li_2Se interphase could offer high mechanical resistance and enable rapid, but homogeneous Li-ion transfer to the entire electrode surface, strengthening the ion conductivity and robustness of the Li_2S for preventing the Li dendrite growth. The lifespan of the symmetric cell was extended from <50 h to ~300 h, realizing a stable lithium deposition without dendrite growth at the current density of 3 mA cm^{-2} under a stripping/plating capacity of 3 mA h cm^{-2}. Even paired with $LiFePO_4$ cathode, the full cell was able to maintain a high CE and high capacity stability over 450 cycles at 1 C. The density functional theory (DFT) calculation results further verified that the lithium-ion migration barrier energies of Li_2Se (0.89, 1.43, and 1.53 eV) were lower than those of Li_2S (0.94, 1.65, and 1.77 eV) across various crystal planes, demonstrating that the introduction of Li_2Se was beneficial to the Li-ion migration of the artificial SEI in spite of the similar antifluorite crystal structures of Li_2Se and Li_2S (Figure 2I). Above all, the adopted inorganic SEI layers should maintain relatively high lithium-ion conductivity to ensure satisfactory lithium transporting kinetics and to regulate the smooth electrodeposition with sufficient hardness and rigidity to resist the formation and growth of dendrite (Table 1).

2.2. Flexible Organic SEI Layer. Although inorganic materials endowed with high Li^+ conductivity regulate the electrodeposition to resist dendrite formation, most of the inorganic SEI layers, despite their hardness and electrochemical stability, are brittle with the propensity to crack under accumulated strain and so require complex structural designs to compensate these shortcomings (Table 1). Generally, organic layers at the anodes are electrochemically derived from organic liquid electrolyte solvents, exhibiting relatively high elasticity. Common strategies for fabricating organic

Table 1. Advantages and Disadvantages among the Constructed SEI Layers

SEI construction	Advantages	Disadvantages
Inorganic layer	➢ High lithium ion conductivity ➢ High stiffness ➢ High electrochemical stability	• Depressive flexibility • Fragile
Organic layer	❖ Excellent elastic strength ❖ High flexibility ❖ Good contact compatibility	• Low ion conductivity • Low stiffness
Organic/inorganic hybrid layer	➢ Robust "soft-rigid" mechanical property ➢ Good electrolyte compatibility ➢ High corrosion resistance ➢ Excellent lithium ion transport	• Weak interfacial contact

protective layers include the addition of electrolyte additives, such as FEC, VC, and ethylene sulfite (ES), to modify surface morphology and physicochemical properties of the formed SEI layer.[70] However, the electrochemically formed SEI layers are discontinuous and not uniform enough for complete dendrite inhibition. Methods for artificially constructing robust ion-conductive organic layer on metallic lithium surface are developed to help extend the lifespan of metallic Li electrode. Thanks to the rheological properties of organic or polymer layers, the organic/polymer layers are usually artificially coated on the metallic Li directly via dipping/spinning coating or other methods, acting as flexible SEI layers. The organic SEI layers can possess the high flexibility and elastic strength to accommodate the volumetric change during lithium stripping/plating (Table 1). Also, it maintains mechanical flexibility to withstand and suppress the concentrated stress exerted by dendrite growth.

Initially, in organic SEI layers, poly(ethylene oxide) (PEO), polyvinylidene fluoride (PVDF) or other polymers with ionic conductive structures were adopted due to their advantages for lithium ion transfer.[35,80] Cui's group simply coated a thin layer of Silly Putty (SP) as a smart dynamic protection layer for bearing the locally concentrated stress exerted by dendrite formation (Figure 3A).[116] The advanced volumetric adaptive polymer of SP was primarily formed based on polydimethylsiloxane (PDMS) with cross-linked transient boron-mediated networks. It uniformly covered the electrode through constantly changing its shape to adapt the morphological and volumetric evolutions of the Li electrode during the continuous plating and stripping process. Owing to the

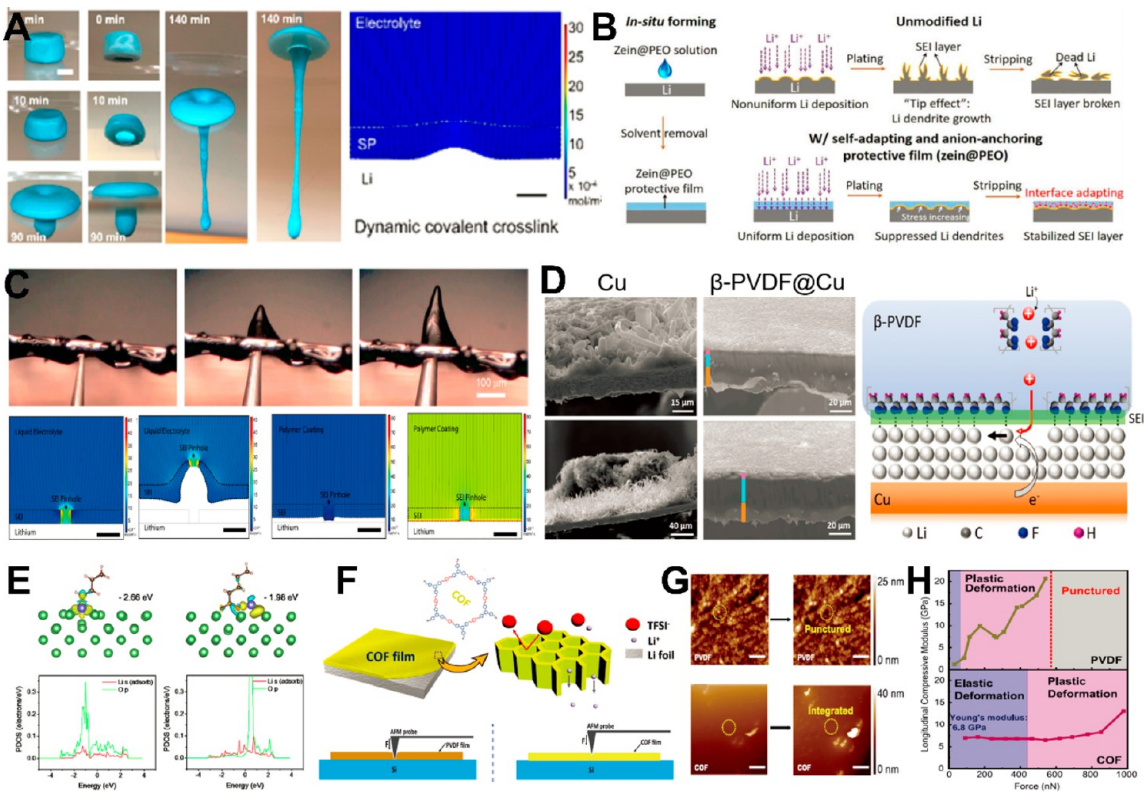

Figure 3. (A) Optical images of SP mounted over a hole punched on a Petri dish and simulation of lithium ion diffusion affected by polymer coatings. Reproduced with permission from ref 116. Copyright 2017, American Chemical Society. (B) In situ fabrication of forming zein@PEO protective film and functions in Li plating/stripping behaviors. Reproduced with permission from ref 117. Copyright 2021, Elsevier. (C) Mechanical piercing tests of the polymer with the needle and simulations of the lithium ion flux distribution with a pore in the SEI on metallic Li surface without/with polymer coating. Reproduced with permission from ref 118. Copyright 2016, American Chemical Society. (D) Morphologies of Li-deposited Cu (left column) and β-PVDF@Cu (right) anodes and mechanism of β-PVDF in achieving layer-by-layer deposition with preferential Li-ion diffusion pathways. Reproduced with permission from ref 119. Copyright 2017, Wiley-VCH. (E) The charge density difference and corresponding PDOS of the adsorbed Li atom with its nearest neighboring O atom. Reproduced with permission from ref 57. Copyright 2020, Elsevier. (F) Illustration of COF on lithium metal surface. (G) Mechanical measurements of PVDF and COF layers through AFM. (H) Longitudinal compressive modulus of PVDF and COF film under different force region. Reproduced with permission from ref 124. Copyright 2020, Wiley-VCH.

intrinsic thermal mobility of the polymer chains, the dynamic connections in SP are able to break and reform at a different location. Such a "break-reconnection" nature of the dynamic cross-links endows SP with a gradual spread and liquid like flow over time (Figure 3A), generating a rather flexible and self-healing SEI layer. More interestingly, the SP coating on the protruding Li can immediately increase stiffness to clamp the trend of fast local overgrowth or expansion when "hot-spots" are formed. However, once the aberrant dendrite growth rate is suppressed by SP, the coating layer recovers its fluid-like property and conformally adapts its shape according to the structure of the lithium metal electrode. Such flowability to stiffness transformation indicates the reversible switch of SP between its "liquid" and "solid" properties in response to the rate of lithium dendrite growth to provide uniform surface coverage and dendrite suppression, respectively, enabling the stable operation of lithium metal electrodes. As simulated in COMSOL, the defect-induced dendrite was immediately remediated by the polymer and the entire surface became uniform (Figure 3A). Thanks to this smart switching property, the SP-coated Li metal electrode showed superior cycling performance with an average CE ~ 97.6% for over 120 cycles at a current density of 1 mA cm^{-2}.

In addition, to directly use pristine organic polymers as artificial films, the modifications of the traditional polymers are further proposed to improve their mechanical and other unexpected properties. For example, a conformable zein-reinforced PEO protective film on the metallic Li surface facilitated diverse enhancements in flexibility, modulus, and adhesion strength, offering self-adapting and Li-ion anchoring abilities (Figure 3B).[117] Specifically, the zein@PEO on Li surface showed a significantly higher peeling force (2.3 N) than that of the PEO on Li film (0.75 N), implying a stronger adhesion improved by the rich functional groups of zein sustained with H-bonding, van der Waals force, and electrostatic forces. On the other hand, the Young's modulus of elasticity of the as-prepared film increased from 0.39 to 0.63 GPa and the ultimate tensile strength increased to 1.45 GPa. Because of the excellent mechanical properties of the zein@PEO SEI layer, the capacity, cycling stability and performance of the cells are greatly improved and the Li/Cu cell delivers prolonged cycle life for over 500 h with stable overpotentials.

For practical applications, high stripping/plating current densities above 3 mA cm^{-2} are usually desired for the potential high-energy-density EVs. According to the classical model of Sand's time, increasing current density means that the dendrite forms at an accelerated rate.[80] Such fast deposition usually exerts more aggregation and strain on the interface. Thanks to the presence of the cross-linked hydrogen bonds, a polymer layer with highly viscoelastic and flow properties is able to exhibit flexibility to withstand the focused strain and produce a homogenizing effect on Li^+ ion flux at hotspots.[118] The stretchability of this soft polymer was further verified by the mechanical piercing test (Figure 3C) where the polymer was so stretchable that it could bear the large local strains, indicating the robustness to endure the dendrite growth. Therefore, the pinhole-resistant polymer coating is expected to ensure uniform lithium ion flux during deposition and protect the Li surface from emerging hotspots and SEI breakage. Meanwhile, the COMSOL simulation depicted the ion changes in lithium deposition morphology with/without the soft polymer coating where a pinhole was placed in the SEI: The lithium metal grew quickly due to the reduction in resistance and subsequently amplified local ionic flux during Li electrodeposition. Even though the SEI was discontinuous with a defect in the native SEI layer, the lithium plating behaviors were normal and smooth at a high current density of 5 mA cm^{-2} (Figure 3C).

Apart from making use of robust flow flexibility, the improvement of Li-ion mobility through interface engineering can facilitate easy access to modulate ion flux distribution. The Li-ion diffusion can be accelerated by intrinsic phase transformation or synergetic corporation with other organic materials.[35] In some F-containing polymers, the active functional F-containing groups in the polymer layer will react with metallic Li to form LiF, further enhancing the lithium ion transport. For example, in terms of a more intact and robust PVDF layer, the transformation from α-phase to β-phase may trigger the superior ionic conductivity. The high-polarity β-phase PVDF also promotes the formation of LiF since F-rich interface favors layer-by-layer Li deposition.[119] Inspired by the nature of β-phase polyvinylidene fluoride (β-PVDF), Huang's group prepared a Li-ion pump based on its ferroelectric specialty for forming a piezoelectric field in an assembled coin cell.[120] The ionic conductivity of β-PVDF@separator is about 2.65 mS cm^{-1}, higher than the pristine separator (2.17 mS cm^{-1}). At the same time, the Li^+ transference number also increased from 0.19 to 0.53, suggesting fast ion transport propelled by β-PVDF. Consequently, in the asymmetric cell, the CE of Cu@β-PVDF reached ~99% even after 200 cycles. Needle-like protrusions and grass-like dendrites were observed on the copper with increased plating capacity (Figure 3D). In contrast, the β-PVDF-coated Cu electrodes exhibited smooth surface with hierarchical structure, which may be attributed to the PVDF layer's ability to withstand the large volume changes to form dense Li deposition with significantly decreased plating thickness. The aligned F atoms may have also facilitated a shorter lithium diffusion pathway across the interface. On the other hand, introducing other materials into the polymer systems can synergistically enhance the transfer rate of Li-ions. For example, when an ionic conductive 18-crown-6 was mixed into PVDF gel solution and then spin-coated on Li metal surface, it induced robust flexibility and high conductivity for uniform Li deposition.[121] The hybrid, high ionically conductive polymer film prevented the direct contact between metallic Li and the electrolyte, reducing the side reactions. Even after resting for 50 days, the 18-crown-6 and PVDF co-coated metallic Li remained on the fresh surface, showing high stability.

Regardless of the uniformity requisite of a coating layer, several tedious preparation processes are still necessary. In situ synthesis of organic SEI layer through direct reaction with Li metal is a promising alternative with good compatibility and tight junction stemming from chemical interactions. A carboxylic acid solution has been designed to spontaneously react with Li to form a dense organic layer with controllable thickness via spin coating.[57] The presence of the oxygen atoms in the lithium carboxylate layer significantly enhanced the adsorption energy to 2.66 eV, which can be ascribed to the high interaction between Li atom and carboxylic acid/Li via the hybridization between Li atom and O sites in the carboxylic acid revealed by the projected density of state (PDOS). This in situ grown organic layer could effectively protect the inner Li from corrosion by solvents in the electrolyte and suppress the dendrite growth, contributing to the increased lithiophilicity and decreased depositing over-

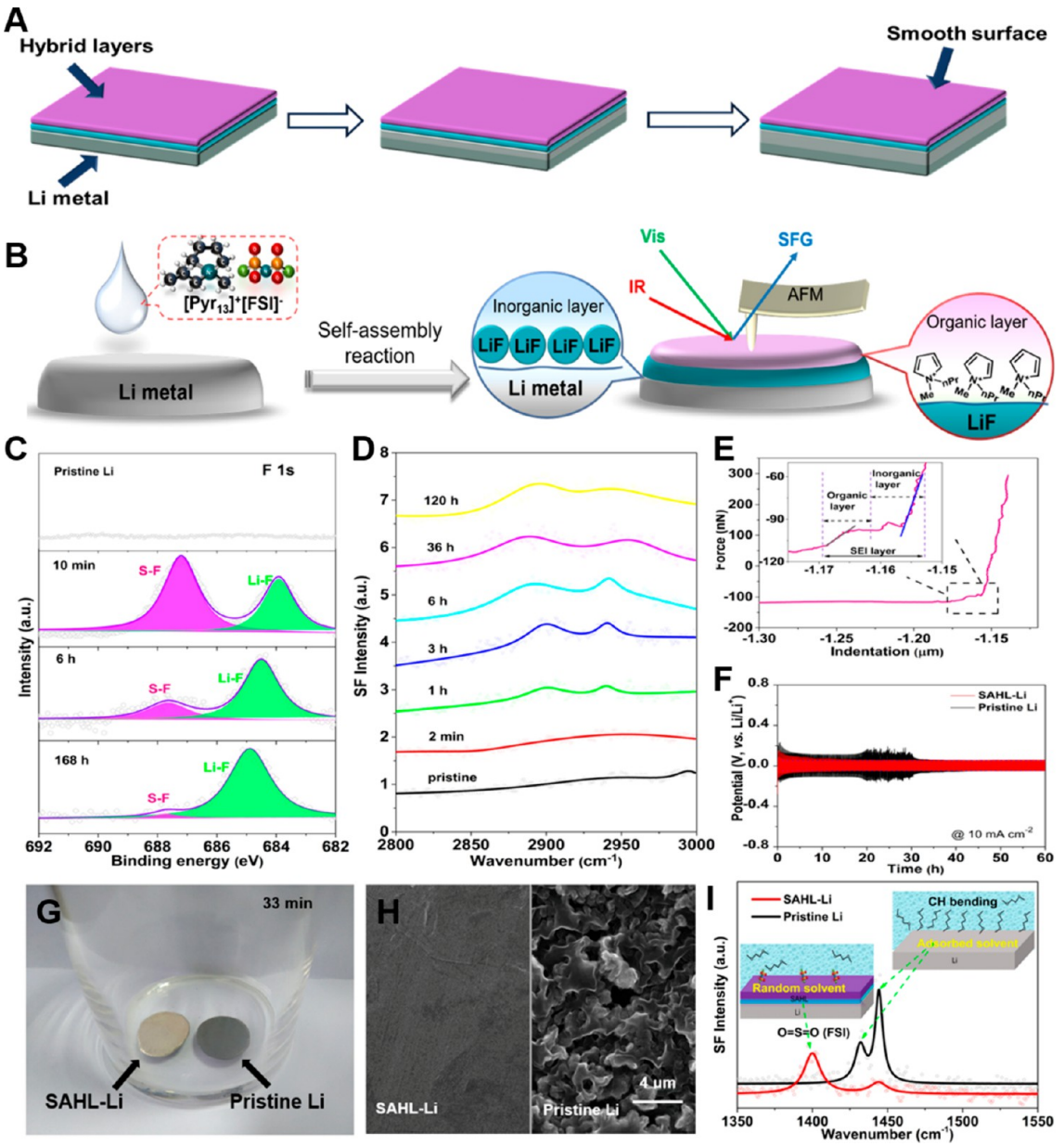

Figure 4. (A) Hybrid organic/inorganic SEI layers on lithium surface for smooth plating. (B) Schematic illustration of SAHL SEI formation on Li metal and corresponding evolution process probed by (C) XPS and (D) SFG. (E) Typical force curve of pretreated SAHL-Li via AFM. (F) Voltage curves of symmetric cells with/without SAHL layer at 10 mA cm^{-2}. (G) Optical photograph of the two Li foils exposed to dry air; corrosion investigation by (H) SEM and corresponding (I) SFG spectra probed in electrolyte/electrode interface. Reproduced with permission from ref 48. Copyright 2021, Wiley-VCH.

potential (Figure 3E). Lu et al. employed the $-CF_3$ functional group in the organic molecular structure to create the highly stable organic interphase (HSOI) through the chemical reactions between hexafluoroisopropanol (HFIP) and ethylene carbonate (EC), tuning the lowest unoccupied molecular orbital (LUMO) energy and achieving a relatively smooth surface with dendrite-free Li plating at as high as 5 mA cm^{-2}.[122] With the protection of HSOI, the treated Li electrode exhibited a lifespan of more than 1300 h, almost 5 times longer than that of the pristine Li electrode.

In virtue of organic polymers, recent covalent organic frameworks (COFs) have attracted growing attention owing to fast ion transfer through the porous structure, good mechanical strength and feasible modifiability of organic ligands.[18,106,123] Satisfactory lithiophilicity and lithium ion mobility can be achieved through adjusting the arrangements of functional groups in the COFs. A 10 nm-thick COF layer fabricated via in situ Schiff-base reaction between 1,3,5-tris(4-aminophenyl)-benzene and terephthaldehyde at room temperature (Figure 3F) can act as a SEI layer to modulate Li plating/stripping toward Li dendrite inhibition.[124] The micropores in the COF film permit the electrolyte penetration to facilitate ion conductivity and selectively block the bigger solvated anions from reaching the deposition sites, which is helpful for Li^+ desolvation toward homogeneous Li deposition and Li-electrolyte side reaction reduction. On the other hand, the thin COF film also ensures battery safety because with a high compressive modulus of 6.8 GPa, which is strong enough to suppress the dendrite formation (Figure 3G). Besides, COF film is also flexible, as evidenced in the stress−strain curves

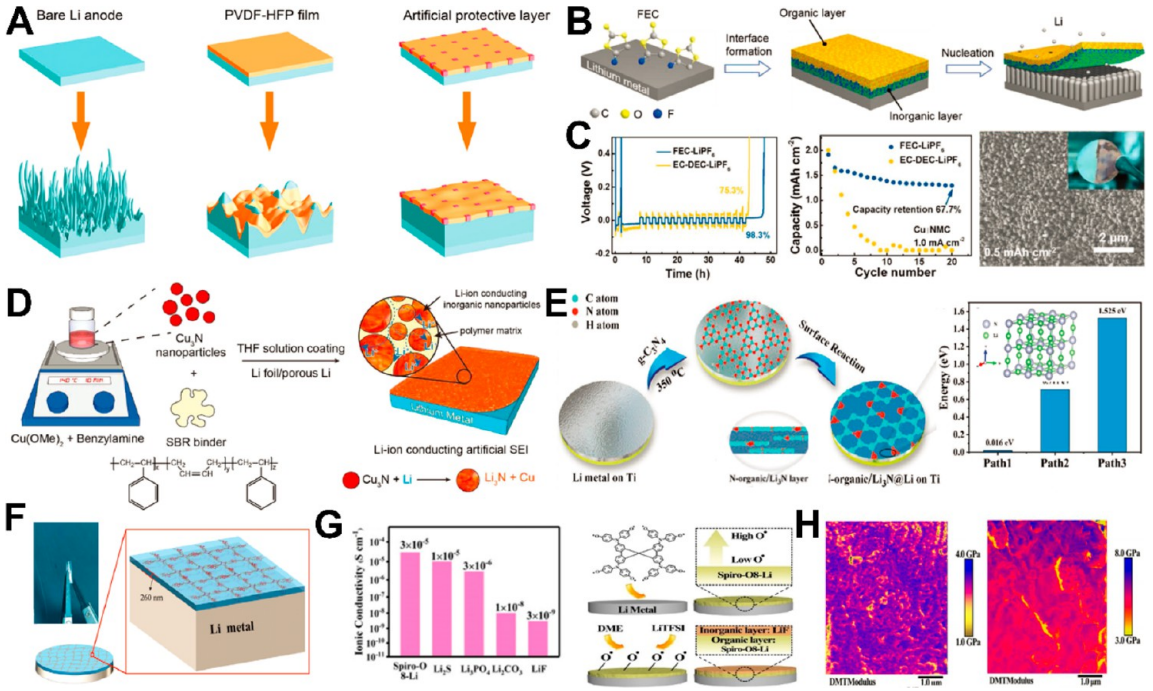

Figure 5. (A) Dynamic processes of metallic Li with different SEI when cycling. Reproduced with permission from ref 125. Copyright 2018, Wiley-VCH. (B) Dual-layered interphase formation derived from decomposing FEC solvent in the electrolyte. (C) The comparisons of CE, capacity retention, and surface SEM image of Li electrode with/without dual-layered SEI. Reproduced with permission from ref 70. Copyright 2018, Wiley-VCH. (D) Schematic illustration of coating artificial SEI on Li metal surface derived from "Cu_3N + SBR" hybrid composites. Reproduced with permission from ref 72. Copyright 2017, Wiley-VCH. (E) Schematic fabrication of N-organic/Li_3N@Li and Li atom migration barrier energy in Li_3N crystal. Reproduced with permission from ref 126. Copyright 2020, Wiley-VCH. (F) The structure and digital photograph of POSS-LiBMAB film. Reproduced with permission from ref 127. Copyright 2021, Wiley-VCH. (G) Comparison of ionic conductivity between common SEI films and Spiro-O8-Li@Li anode. (H) Young's modulus mapping of Spiro-O8-Li@Li anode before and after standing in the electrolyte for 12 h. Reproduced with permission from ref 128. Copyright 2021, Wiley-VCH.

where the COF film exhibits both elastic and plastic deformation rather than only plastic deformation exhibited by PVDF (Figure 3H). Beneficially, the internal short circuit is effectively blocked by COF-Li in Li-S batteries. At 1 mA cm^{-2}, a lifespan of 400 h was realized in the symmetric cells based on COF-decorated Li electrode.

2.3. Robust Hybrid Organic/Inorganic SEI Layer. Inheriting the flexibility and mechanical strength of organic compounds and rapid Li-ion conductivity of inorganic compounds, occurring, e.g., in the SEI on commercial graphite and lithium anodes,[116,117] organic/inorganic hybrid protective layers may not only effectively alleviate the volume expansion via the organic layer but also improve the uniform lithium ion diffusion through the inorganic layer (Figure 4A).[48] These synergistic effects are expected to suppress the Li dendrite growth and significantly improve the cycling stability and lifetime of LMBs without sacrificing the lithium ion/atom diffusion ability. Therefore, the organic/inorganic composite protective layers are ideal artificial coatings for regulating the deposition behaviors of lithium, which remains a hot topic in the field of functional SEI fabrication. The fabrications of organic/inorganic hybrid protective layers are usually comprised of electrolyte additives or artificial designs. The formation mechanism typically contains two steps: (1) the adsorption competition between electrolyte additives and ingredients in the normal electrolyte and (2) the decomposition of the more active adsorbed species by reacting with the metallic Li, forming the bottom inorganic layer and leaving the organic moieties to assemble into the upper layer.

Distinct from the conventional native mosaic structure (Figure 4B), the facile fabrication of organic/inorganic SEI with ordered dual-layer structure on the lithium surface via in situ self-assembly method (SAHL-Li) has been proposed.[48] Specifically, the ordered organic/inorganic hybrid layers were grown in situ by soaking the lithium metal anode in the highly reactive ionic liquid of *N*-methyl-*N*-propylpyrrolidinium bis-(fluorosulfonyl)imide ($Pyr_{13}FSI$) (Figure 4B), during which the active bis(fluorosulfonyl)imide anion (FSI^-) reacted with metallic Li to form LiF. The dynamic evolution of the inorganic layer was recorded with the high-resolution F 1s X-ray photoelectron spectroscopy (XPS) (Figure 4C), where the main peak centered at 684.8 eV was assigned to LiF phase. Over time, the relative peak intensity assigned to LiF increased gradually, while the peak attributed to the S−F bond in FSI^- anion decreased, strongly suggesting the gradual conversion from FSI^- to LiF. Meanwhile, the $S_{Li\text{-}F}/S_{S\text{-}F}$ ratio, with a value of 0 at the beginning with no spontaneous reaction, increased from 0.63 to 24.78 with sufficient formation of the self-assembled hybrid layer (SAHL). To accurately verify the dynamic evolution of the organic layer, the interface-sensitive sum frequency generation (SFG) spectroscopy was applied to probe the adsorption orientation states at the molecular level. Two peaks at 2940 and 2904 cm^{-1} assigned to $-CH_2$ and $-CH_3$ Fermi resonance signals, respectively, increased gradually until saturation (Figure 4D). After 5 days of extended reaction time, the coverage of organic monolayer with subnano thickness remained unchanged and stable. On the atomic force microscope (AFM) output curve, the slope

exhibited a two-stage change, namely an initial slow increase followed by a plateau, and a sharp increase (Figure 4E), suggesting mechanical differences among the substances in the SEI layer. In the symmetric cell, the pretreated Li electrode maintained stability at 10 mA cm^{-2} for 300 cycles without dendrite growth. It is well-known that the metallic lithium is sensitive to moist air which deteriorates the performance. Thanks to the uniformly formed dense and robust self-assembled organic/inorganic hybrid layer, the pretreated SAHL-Li could resist the moist air corrosion for more than 30 min (Figure 4G). In the battery, the carbonate solvents are also corrosive to the metallic Li surface and will make the surface more porous aiding dendrite formation (Figure 4H). As detected by the interface sensitive SFG, the electrolyte solvents displayed weak affinity with the hybrid dual layers (Figure 4I), which explains why the pretreated Li can survive for a long time without any cracks in the coating.

Due to the excellent film-forming properties of polymers, more efficient protective layers are expected to be obtained by rational hybridization of polymer components with ideal ion-conductive inorganic components for improving the performance of lithium metal anodes. Poly(vinylidene-*co*-hexafluoropropylene) (PVDF-HFP) is known to have a higher dielectric constant than other polymers.[35] LiF, with good compatibility with Li metal anode, is widely regarded as one of the most important components in managing Li deposition. It is thus rational to hybridize PVDF-HFP with LiF to serve as an artificial protective layer (APL) on Li metal anode (Figure 5A).[125] In reference to the typical diffraction peaks of LiF and PVDF-HFP, all the same peaks appear in the APL spectrum, suggesting the presence of the organic polymer and inorganic LiF. With rigid LiF incorporation, the Young's modulus of elasticity of the APL is enhanced to 6.72 GPa, far exceeding those of pristine SEI (150 MPa) and pristine PVDF-HFP film (0.8 GPa), improving the robustness of the formed SEI to tolerate focused stress of dendrite. As a result, a significantly longer cycle life was achieved. The hysteresis gap of symmetric cells without APL finally reached 1300 mV after cycling for 200 h at 2.0 mA cm^{-2}. The cell with APL-modified Li electrodes displayed highly stable voltage profiles, declaring a more stable deposition. The $LiFePO_4$ cathode paired full cell also exhibited high CE (>99.2%), indicating a high utilization of lithium atoms and no dendrite formation.

Although the hybrid artificial organic/inorganic SEI layers are feasible in solving the fragility, their weak interfacial contact remains an ineluctable issue. Thus, it is of great importance to build effective well-designed integral structures. In comparison to the mixed SEI structure, the ordered dual-layered SEI is more efficient to realize good uniformity, mechanical properties and flexibility as well as stability. Upon directly immersing Li metal into polyphosphoric ester (PPE) solvent, a dual-layered structure with dense organic layer ($-COPO_3-$, $-(CO)_2PO_2-$, and $-(CO)_3PO$) on the top and rigid inorganics (mainly Li_3PO_4) at the bottom were formed on the metallic Li surface.[49] Subsequently, the protected Li was stable to maintain successive electrodeposition over 800 cycles of plating/stripping at 2 mA cm^{-2}. Furthermore, beyond the formation of organic/inorganic components, elucidating the detailed formation mechanism is also crucial for establishing the guidelines for the future design of film structures to suppress Li dendrite growth. Zhang's group elaborated on the self-generated mechanism of a dual-layered SEI film constructed on Li metal anode by the spontaneous reaction between Li metal and FEC solvent (Figure 5B).[70] Ab initio molecular dynamics analysis depicted that pure FEC solvent would initially undergo decomposition reactions: The C−F bond in FEC became weakened and eventually broken due to the electrostatic attraction between the positively charged Li atom and negatively charged F atom, resulting in the formation of LiF, and then, the bond length of Li-F in FEC extended from 1.54 to 2.09 Å upon adsorption of a lithium atom into the FEC molecule. Along with these interactions, the organic compositions, such as CH_2CHOCO_2Li and CH_2CHOLi, were also formed to afford a typical dual-layered structure with compact organic components ($ROCO_2Li$ and ROLi) atop the rigid inorganic components (Li_2CO_3 and LiF). The average CE of the Li-Cu cell was as high as 98.3% with the FEC modification and the capacity retention improved to 67.7% after 20 cycles (Figure 5C). Benefiting from this evolved film, more dense and uniform columnar Li crystals with nearly the same height were generated to resist dendrite formation. The controllable uniformity of SEI coating and improved lithium ion conductivity further assisted the uniform deposition of lithium atoms. The styrene butadiene rubber and Cu_3N mixed solution has been fabricated to improve the mechanical strength and lithium ion transport (Figure 5D). As designed, the Cu_3N will spontaneously be reduced to Li_3N and Cu nanoparticle upon contact with metallic Li, decreasing the barrier of lithium ion across the surface.[72]

In contrast to the inorganic precursor of metal nitride, connecting nitrogen-containing organic groups possessing strong interaction with Li to generate lithium-ion conductive Li_3N could simultaneously produce a dense, but flexible N-rich layer, which combines the merits of organic/inorganic layers. Through chemical linking the nitrogen-containing organic Li_2CN_2 phase with high ionic conductive Li_3N phase (denoted as N-organic/Li_3N), Yu's group fabricated a conformal and compact artificial SEI layer rich in C−N═C, $N-(C)_3$ and Li_3N through the surface reactions (Figure 5E).[126] As demonstrated by DFT simulation, Li ions are able to diffuse within the Li−N plane (migration barrier energy of 0.016 eV, Path 1) as well as passing smoothly through the Li−N planes (0.711 and 1.525 eV), confirming the excellent Li-ion conductivity of bottom Li_3N crystal in the layer. In addition, the strong interplay between Li-ion and C−N═C and $N-(C)_3$ groups effectively confirms the organic group's functionality in regulating homogeneous distribution of Li ionic flux and providing abundant Li-ion nucleation sites simultaneously. With such beneficial structure reinforcement, the exchange density derived from the Tafel curve with the N-organic/Li_3N layer (≈0.0432 mA cm^{-2}) is higher than that of the native SEI (≈0.0011 mA cm^{-2}), suggesting faster Li-ion transport kinetics. Upon varying the testing temperatures within 30−60 °C, the fitted activation energy of the N-organic/Li_3N layer (19.03 kJ mol^{-1}) became lower than that of the native SEI (23.13 kJ mol^{-1}) due to the rapid Li-ion pathways supplied by Li_3N. Consequently, N-organic/Li_3N@Li composite electrodes can realize uniform lithium ion deposition and long lifespan over 1100 h at the current density of 1 mA cm^{-2}.

Another strategy for achieving a strong connection between inorganic and organic components to facilitate rapid lithium ion transport is by manipulating the chemical activity of organic molecules to generate more cross-linked frameworks. Liu and his co-workers designed a SEI layer with inorganic polyhedral oligomeric silsesquioxane containing eight-mercaptopropyl (POSS-SH) and lithium bis (allylmalonato) borate

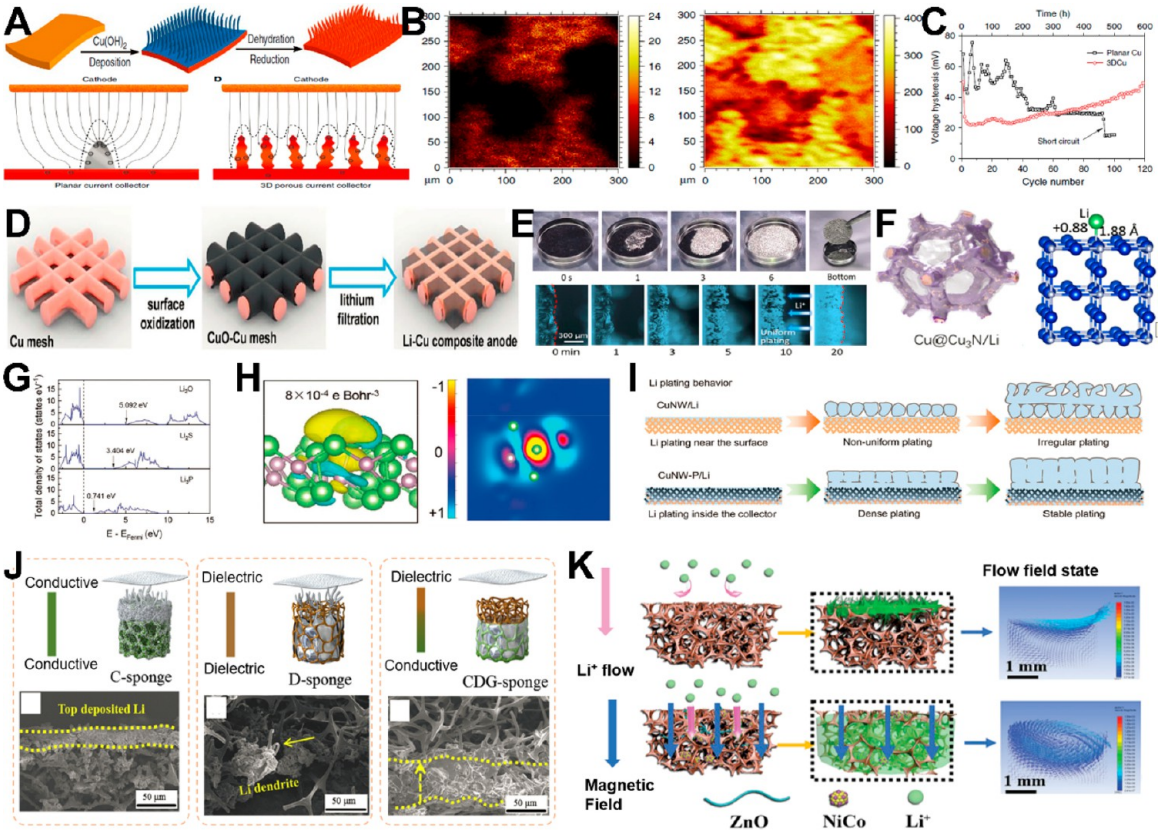

Figure 6. (A) Fabrication of 3D Cu foil and the proposed deposition processes on 3D Cu foil. (B) Cu^+ and Li^+ distributions in the Li@3D-Cu anode. (C) Summary of average voltage hysteresis in symmetric cells with different current collectors. Reprinted with permission under a Creative Commons Attribution 4.0 International License, ref 130. Copyright 2015, The Authors. (D) Fabrication illustration of the CuO−Cu mesh with melted Li. Reproduced with permission from ref 134. Copyright 2019, The Royal Society of Chemistry. (E) Optical images and in situ microscopy images of Li deposition in Cu@Cu_3N. (F) Calculations of structure optimization of Li in Cu_3N. Reproduced with permission from ref 65. Copyright 2021, Elsevier. (G) The corresponding density of states of various composites. (H) Surface charge transfer and distribution near Li* on Li_3P. (I) Schematic comparisons of Li plating behaviors on CuNW and CuNW-P current collectors. Reproduced with permission from ref 74. Copyright 2019, Wiley-VCH. (J) Illustration and SEM images of Li deposition in C-sponge, D-sponge, and CDG-sponge. Reproduced with permission from ref 136. Copyright 2020, Elsevier. (K) Schematic comparison of Li deposition and flow field state influenced by the magnetic field. Reproduced with permission from ref 63. Copyright 2022, Wiley-VCH.

(LiBMAB) on Li foil via the thiolene "click chemistry" reactions.[127] In this design, the organic and inorganic materials are closely cross-linked and self-reinforced through the S−C chemical bond formation. Benefiting from the porous polymeric covalent structure and noble inorganic Si_8O_{16}-type cubes, the organic/inorganic hybrid film appears to be self-standing and flexible enough to accommodate large volume changes after several cycles (Figure 5F). This synthesized film on the metallic Li significantly widened the working window from 2.5−4 V to 0.5−5 V, contributed to a high ionic conductivity (5.04×10^{-5} S cm^{-1}) with a Li-ion transference number of 0.9. With the protection of the POSS-LiBMAB layer, the Li metal anode exhibited stable performance for more than 1000 h with a voltage hysteresis (~40 mV) at a high current density of 5 mA cm^{-2}.

As stated above, the artificial bilayer usually contains the bottom inorganic layer and upper organic layer; alternatively, the bottom layer can also be organic. In virtue of the rapid hole transport in 2,2′,7,7′-tetrakis(*N*,*N*-di-*p*-methoxy-phenyl-amine)-9,9-spirobifluorene, the derivative of Spiro-O8 is known as the reactive phenoxy radicals and could be used to fabricate the double layer on the metallic surface.[128] A dual-layer artificial protective film with inorganic LiF on the top and Spiro-O8-Li at the bottom was achieved by a spontaneous assembly via redox reaction between the Spiro-O8 and Li metal and electrolyte (Figure 5G). This spontaneous reaction can be divided into two steps: first, the highly active phenoxy radical in Spiro-O8 reacts with metallic Li to form Spiro−O8-Li; second, the remaining radical acquires the hydrogen atoms from the solvents to form hydroxyl groups that facilitate the decomposition of lithium bis(trifluoromethanesulfonyl)imide into LiF. Different from the widely adopted dual-layer SEI structure, the upper LiF film in this formed dual-layer structure design can prevent the direct contact between the Li metal and the electrolyte. Meanwhile, the high ionic conductivity of the bottom Sprio-O8-Li layer is able to accelerate the uniform diffusion of Li ions across the SEI film to Li metal surface. In the AFM test, the single Spiro-O8-Li film showed a high initial Young's modulus of elasticity of 3.1 GPa, which was increased by 2-fold after immersing in the electrolyte (Figure 5H). As a result, Spiro-O8-Li@Li anode demonstrated long-term stability for 700 h at an ultrahigh current density of 10 mA cm^{-2} under high capacity of 10 mA h cm^{-2}. The 50 μm thick Spiro-O8-Li@Li electrode in full cells coupled with sulfur cathodes exhibited a greatly improved capacity of 635.6 mA h g^{-1} after 200 cycles.

In summary, the interface engineering by electrolyte additives or artificial designs can extend the life of metallic

lithium anodes as well as inhibiting dendrite growth. Understanding the original SEI model and constituents provides the option of the homogeneous organic, inorganic, or both hybrid layer to offer enhanced dendrite resistance and interfacial stability. Therefore, the ideal inorganic and organic materials in SEI interface should have the following features: (1) high lithium ion conductivity, (2) robust mechanical properties, (3) ample lithiophilic sites, and (4) feasible scalable fabrication. Given the future requirement in large industrial production of lithium metal batteries, it is urgent to explore more facile and effective approaches for preventing solvents and air corrosion on Li metal surface.

3. STRUCTURE DESIGNS OF 3D CURRENT COLLECTORS FOR LITHIUM HOSTS

Besides the SEI, the physicochemical properties of conductive plating hosts also influence the initial lithium nucleation and plating behavior. Currently, advanced porous Li hosts have been designed to investigate the coupling process between Li ion and electron and the plating morphologies during the plating/stripping process. With the cross-linked structure, hosts with high surface area can reduce the localized current density of lithium deposition and can supply enough void for tolerating the volume changes. In this section, the 3D metal networks and lightweight carbon as well as their derivatives are briefly summarized.

3.1. 3D Porous Cross-Linked Metal Current Collectors. Relatively smooth conductive surfaces are beneficial for the uniform electric field and the even distribution of electrons and Li ions toward preventing lithium dendrite formation in the initial plating.[129] However, the localized lithium dendrite still forms due to the difference in activity in the planar sites, such as the aggregations at the boundaries and the disturbed concentration distribution of the lithium ion flux, eventually forming the phenomenon of isolated "dead-Li". An effective strategy toward resolving these problems is to deposit lithium onto 3D rather than planar current collectors, changing the local scope of the electronic field.[130] Such conductive, porous and stable hosts with large surface areas not only buffer the volume change of the plating Li, but also provide large effective areas to adsorb more lithium ion in the interface so as to couple with electrons rapidly, reducing the deposition current density and thus inhibiting dendrite growth.

In the design of current collectors, two main factors must be considered: the high electrochemical stability during the plating/stripping process and the high electronic conductivity to transfer electrons.[42,66,68,131] Porous metal-based current collectors are suitable for effectively averaging the electric field distribution inside the electrode and at the electrolyte/Li interface to avoid large ion aggregation.[132] For working under the low stripping/plating potentials of lithium metal, inert copper (Cu), nickel (Ni), and titanium (Ti) are the most used metals. Combined with the advantages of 2D planar conductivity, a 3D Cu current collector with microscale conductive skeleton was proposed and synthesized on the metallic Cu surface.[130] As shown in Figure 6A, an in situ self-assembly method was adopted through etching planar Cu foil by immersion in ammonia solution to form porous $Cu(OH)_2$, which was then converted into 3D copper (fiber diameter of 2.1 μm) following dehydration and thermal reductions. In the surface morphology revealed by time-of-flight second-ion mass spectrometry measurement, the pores appear as dark circles on the Cu substrate while the Li atoms are mostly deposited on the 3D Cu fibers that fill in the pores (Figure 6B). AFM results show that the nucleation of Li on the planar Cu foil is accelerated by a sharp charge accumulation in several cycles. In contrast, the numerous fiber tips serve as the charge centers and nucleation sites, averaging the top localized electric fields (Figure 6A). With the efficient capability toward hosting Li, the optimized Li electrode was able to last for 600 h without any short circuits and exhibited very low voltage hysteresis and charge transfer resistance at 0.2 mA cm^{-2}. Also, it maintained a good CE of 98.5% at 0.5 mA cm^{-2}. The comparison of short-circuit times in Figure 6C proves that dendritic Li growth on 3D Cu foil is considerably slower than on the planar foils, and the cycle life is significantly improved by the multidimensional architectures. Following this, porous substrates with varying morphology and fabrication methods have been proposed. For example, the 3D hierarchical porous copper mesh coupled with commercial lithium foil is proposed by Lu et al.,[75] which provides more uniform reaction sites and "cages" for lithium redeposition, reducing the lithium dendrite formation. Its larger exchange area favors the electronic exchange and decreases the local deposition current density. Thus, the composite anode exhibits reduced interfacial impedance and better plating stability in comparison to the planar collector electrode. Other than Cu mesh, copper nanowires have also been used as 3D cross-linked conductive network to accommodate lithium within the confined nanostructures. A high capacity of metallic Li up to 7.5 mA h cm^{-2} was loaded and plated onto the nanowire-based current collector, and the 3D lithium electrode exhibited a high CE of 99% without dendrite generation during 200 cycles.[132] Besides Cu, other metals, such as Ni, have been developed and adopted due to their high stability and abundance in some cases.[133] The thermal infusion method within a specific temperature range was selected to explore the functions of Ni foam with preloaded Li. The hybrid lithium electrode exhibited uniform deposition/dissolution phenomenon during cycling without significant dendrite generation, and the assembled LMBs also have enhanced performance.[133]

Although relatively long lifespan and reduced overpotentials were achieved with the above 3D hosts, the long-term plating/stripping behaviors of the metallic Li anodes are dissatisfactory due to the large Li nucleation barriers caused by the weak lithiophilicity between the 3D metallic current collectors and lithium atoms.[63,134] To overcome these challenges, a large number of lithiophilic sites have been introduced into the hosts by surface coating and crystallization. Also, different scaffolds, such as 3D Cu foam derived from porous hydrogen compounds or other templates, have been explored to improve the lithiophilicity. The oxidation approach is widely employed to uniformly decorate the Cu mesh with a thin CuO layer to transform the lithiophobic nature to lithiophilic due to the strong chemical interaction between CuO and Li (Figure 6D).[134] Thermally filtrated Li was homogeneously preinfused into the lithiophilic CuO-decorated Cu mesh to obtain an ultrathin 3D Li-Cu hybrid metallic anode, simultaneously achieving a homogeneous distribution under the localized electric field and accommodating the volume fluctuations of Li plating during cycling. Consequently, the symmetric cell with 3D Li-Cu hybrid electrodes exhibited a stable cycling performance of 1000 cycles at 5 mA cm^{-2}, and the fabricated $LiFePO_4$||Li-Cu full cell maintained the capacity retention of 77.6% at 5 C after 1000 cycles, whereas the control only exhibited a capacity retention of 58.4%. Even though the

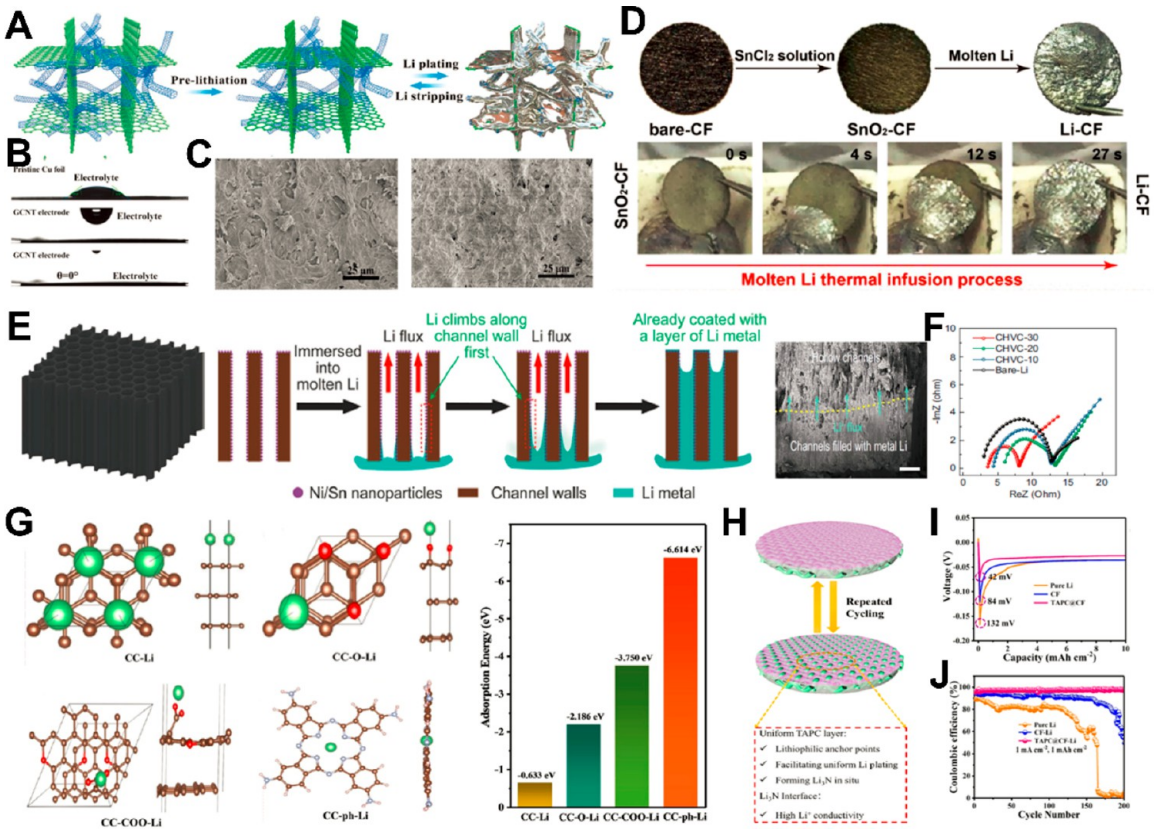

Figure 7. (A) Schematic diagrams of the deposition behaviors of lithium metal in GCNT. (B) Contact angle analysis on the current collectors. (C) SEM images of lithium deposition morphologies on the GCNT. Reproduced with permission from ref 64. Copyright 2021, Wiley-VCH. (D) Illustration of SnO_2-CF matrix with molten Li and the corresponding molten lithium infusion images in short time. Reproduced with permission from ref 66. Copyright 2018, Wiley-VCH. (E) Schematic evolution of lithium implantation into Sn/Ni-coated CHVC substrates. (F) Comparison of the impedance spectra of symmetric cells with different temperatures CHVC samples after 100 cycles. Reprinted with permission under a Creative Commons Attribution License 4.0, ref 153. Copyright 2019, The Authors. (G) Simulation models of Li atom on various substrates and the corresponding adsorption energy summary between Li and atoms of different functional groups. (H) The advantages of TAPC layer in modulating Li plating. The comparisons of (I) nucleation barriers and (J) CE with various Li anodes. Reproduced with permission from ref 154. Copyright 2022, Elsevier.

lithiophilicity of various hosts is significantly enhanced by the introduction of metal oxide (such as CuO and ZnO) on the 3D metal frameworks, the lithium ion diffusion is too sluggish to penetrate the as-formed insulating Li_2O layer. Alternatively, a universal strategy of combining lithiophilic surface with conductive cores could be realized through NH_3 atmosphere treatment, forming metal-nitrogen bond on the scaffolds, further increasing the lithiophilicity. For example, a strategy of decorating ultra-lithiophilic Cu_3N nanoparticles on 3D metal skeletons, such as Cu, Co, Ni, and Zn, for Li integration was proposed (Figure 6E).[65] It was discovered that the melted Li occupied the host matrix within several seconds and the lithium ion flux was uniformly plated on the Cu@Cu_3N matrix in the plating process. Further, the lithiophilic nature between lithium atoms and substrates was verified through first-principles theoretical calculations: The lower binding energy between Li atoms and Cu_3N(111) as well as the shorter bond length both indicated a stronger affinity through the formation of a stronger ionic bond (Li-N). With a lower migration energy barrier in Cu_3N, the Li ions could diffuse and redistribute on the Cu_3N surface with more ease than on Cu(111). Thanks to these advantages, the higher stripping/plating capacities of 3–5 mA h cm^{-2} were generated in the Cu@Cu_3N matrix and the asymmetric cells showed the overpotential gaps of 42–46 mV (Figure 6F).

Other substrate geometries have been further developed and the influence of porous nano/micro-structure have been studied.[74,132,135] Generally, through optimizing the nanostructure designs of current collectors, the lithium diffusion and deposition behaviors are accordingly regulated from the perspective of diffusion kinetics.[134] For instance, simulations and electrochemical experiment results confirmed the plating/stripping behaviors of lithium on a Cu current collector decorated with vertically aligned microchannels as such that lithium atoms preferentially deposited on the vertical channel walls rather than on the top surface.[129] Facilitated by the path channels, the modified Cu matrix exhibited lower overpotentials and higher CE of 98.5% during 200 cycles. Further, a lightweight Cu nanowire framework host with cross-sectional Cu_3P gradient was also trialed (Figure 6G).[74] Initially, the lithiophilic capability of the Cu-based compounds including CuO, Cu_3P and Cu_2S were compared through DFT calculations. Cu_3P and CuO are more suitable for serving as lithiophilic sites with relatively high adsorption energies by forming the byproducts of Li_3P and Li_2O after plating. The density of state results indicated the LUMO energy in Li_3P (0.741 eV) is much lower than that of Li_2S (3.404 eV) and Li_2O (5.092 eV). The surface charge transfer calculation further demonstrated fast kinetics in the surface charge transfer for Li deposition from Li_3P (Figure 6H). Therefore, the ionic

conductive Li_3P surface derived from the Cu_3P-decorated Cu nanowire (CuNW-P) is capable of averaging lithium ion flux. The low nucleation barrier and oriented morphology with dense and stable plating are formed owing to the uniform spatial electron distribution (Figure 6I).

Dielectric materials are electrical insulators that can be polarized by an applied electric field and their intrinsic voids are beneficial to accommodate lithium deposition. A hierarchical 3D conductive dielectric gradient (CDG) framework, formed by introducing conductive Ni nanolayer on the bottom of a dielectric melamine sponge, promoted preferential Li nucleation at the conductive bottom first, enhancing the plating capacity to >8 mA h cm^{-2} (Figure 6J).[136] While, the upper dielectric melamine sponge helps to stabilize the Li^+ flux distribution, inducing a "bottom-up" electrodeposition of Li^+ and "top-down" dissolution of Li metals during the stripping/plating process. Overall, the 3D conductive dielectric gradient framework guides uniform and near dendrite-free Li regulation and enhances the reversibility of the Li migration. As such, the fabricated Li-Cu cell exhibited a stable CE of 98.4% after 500 cycles and a long lifespan of 780 h at 1 mA cm^{-2}.

Besides various optimizations of the 3D host from structure design to coating layer, introducing an "external force" such as an additional magnetic field can be regarded as a pump to regulate Li deposition behavior in a 3D current collector. A magnetic current collector formed by loading ferromagnetic Ni-Co alloy together with lithiophilic ZnO onto a 3D Cu foam demonstrated an even Li-ion flux rate during cycling at 1 mA cm^{-2}.[63] This may be attributed to the micromagnetic field generated by Ni-Co alloy, whereby the pathway of Li^+ is deflected and redistributed due to the presence of Lorenz force (Figure 6K), and the enhanced movement of electrons and ions facilitated a dendrite-free anode with dense and deep lithium deposition.

3.2. Light-Weight 3D Nanocarbon Hybrid Current Collectors. Although the porous morphologies afford abundant lithiophilic sites in the 3D current collectors, capable of decreasing the localized current density with uniform plating, this is compromised by the weight of metal-based current collectors. In contrast, the carbon-based current collectors have many advantages: lightweight, abundance, tunable lithiophilicity toward enhancing the energy density of the entire Li anode.[137−139] The carbon-based materials, such as carbon nanotubes (CNTs), carbon fibers (CFs), graphene (G), carbon cloth (CC) and their derivatives, are commonly used to cross-link each other to form a conductive 3D network structure, where the voids have good spatial effects and the hierarchical pore channels can also reserve space for lithium deposition, effectively buffering its volume change.[66,135,140−145]

It has been discovered that both 3D graphitic carbon foam with rich nitrogen-containing functional groups and 3D porous structures formed by intertwining hierarchical dimensional scalable carbon materials have superior functions in reducing deposition current density and withstanding volume expansion. A 3D graphene/carbon nanotube composite (GCNT) aerogel formed by interweaving 2D graphene layers with 1D CNTs (Figure 7A) displayed a large specific surface area and high network electrical conductivity and affinity to electrolyte (Figure 7B).[64] This exhibited excellent reversibility. With the increase of plating time and capacity, the GNCT aerogel framework was gradually filled with metallic lithium and exhibited a morphology from nucleation to a smooth plane and upon stripping, and it recovered the original structure (Figure 7C).

Even though porous carbon materials have the advantages of structural diversity and tunable pore sizes, the number of lithiophilic sites in current collectors made from pure carbon materials are unsatisfactory since the lithium dendrite usually forms at the edges after several stripping/plating cycles. The surface chemical properties are important factors that affects the surface wettability.[6,15,146,147] Thus, recent studies have focused on the introduction of more lithiophilic sites on the carbon matrix, including the addition of metal oxide, metal particles and polymers. According to the Wenzel model, reasonable materials (Al, Cu, CNT, and NiO) with strong binding energy between molten Li and matrix materials may improve wettability.[148] Interweaving lithiophilic NiO nanospheres on highly conductive carbon nanotubes to construct lotus-leaf-like 3D porous structure was synthesized, improving its lithiophilicity along with accelerating lithium ion transport simultaneously. As observed, the CNT/NiO@Li electrode exhibited strong ability against the dendrite formation at the cross-section. However, the pristine lithium electrode surface had many protuberances and gradually evolved into an up-and-down interface within 60 min. The larger height of lithium plating in pristine Li evidenced the strong lithiophilic difference, strongly demonstrating the superiority of lithiophilic NiO in preventing dendrite formation. Besides metal oxides, the introduction of Ag nanoparticles,[149] Ni nanoparticles,[150] and ZnO nanoparticles,[151] etc., are also helpful in improving the wettability of the hybrid carbon matrix. To further modulate the lithium ion kinetics and increase the lithiophilicity and wettability of the carbon framework, the lithiated/delithiated metal oxide are proposed. For example, a SnO_2 layer is modified on cross-linked carbon fibers (CFs) via the solution reaction, and then molten lithium is injected into SnO_2−CF within half a minute (30 s) through a facile solution-based synthesis (Figure 7D), exhibiting higher affinity to the molten Li in a shorter time with the Li_2O formation.[66] The symmetric cell based on Li-CF electrodes displayed a smooth lithium deposition voltage profile over 120 h (180 cycles) at a current density of 3 mA cm^{-2} under a deposition capacity of 1 mA h cm^{-2}. These results demonstrate that the improved wettability and the 3D lithiated-type hybrid host can decrease the nucleation barrier and the local deposition current density.

Without changing the host material chemistry, shortening the ion pathway and averaging ion flux are also feasible to regulate the lithium behavior.[152] Inspired by natural wood, a carbonized resin-based artificial wood with tunable vertical microchannels (CHVC) was fabricated as a host that can incorporate nanosized Sn/Ni alloy nucleation sites (Figure 7E), facilitating the lithiophobic to lithiophilic transformation and reducing the local current density.[153] The charge transfer resistance (R_{ct}) value of the CHVC-30/Li composite electrode after cycling, as measured with electrochemical impedance spectroscopy (EIS), was lower than before (Figure 7F), implying the acceleration of the reaction kinetics and the fast plating/stripping behavior of Li atom.

In pursuit of higher energy density, changing the lithiophilic pristine metal-based materials with a lightweight layer or high-concentration heteroatom doping carbon matrix is a viable approach.[90,139,142] The incorporation of trace organic substances with special functional groups into the 3D carbon framework can enhance the robustness of the interface and

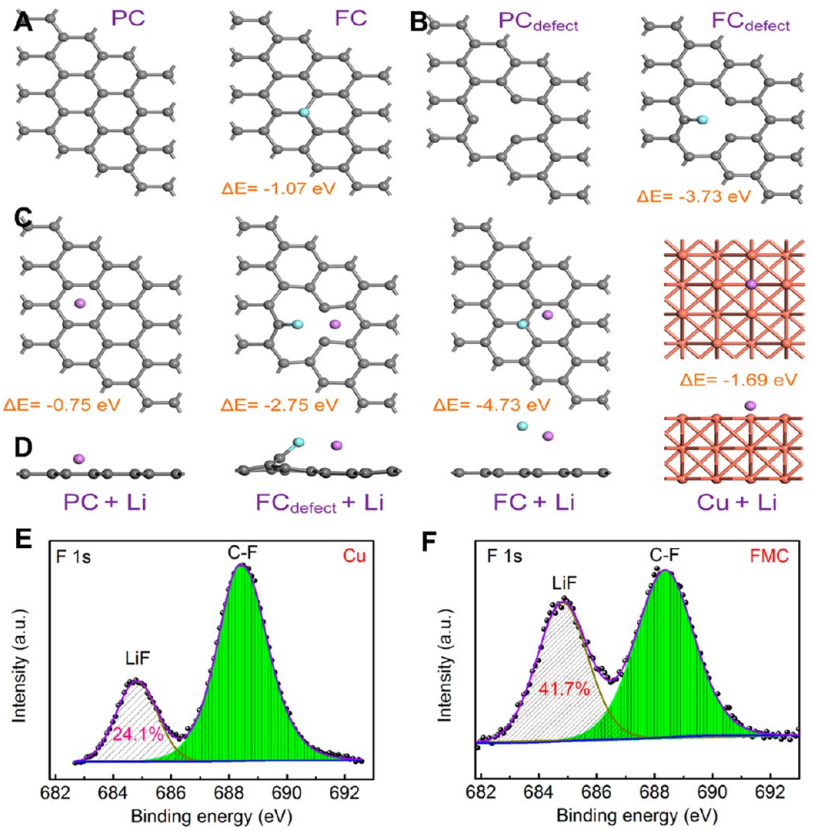

Figure 8. Bond formation energy of (A) C(sp^3)-F on pristine carbon and (B) C(sp^2)-F on defected carbon. The (C) top view and (D) corresponding side view of binding energies of a Li atom on various substrates. The high-resolution F 1s spectra after Li deposition on (E) Cu and (F) FMC@Cu current collector, respectively. Reproduced with permission from ref 90. Copyright 2020, Elsevier.

reduce the overall interfacial barrier, guiding the nonaggregated lithium deposition. Tetraaminophthalocyanine (TAPC) with abundant N-rich functional groups was loaded on the 3D CF cloth via a catalytic amidation reaction.[154] The ion-conductive, but electron-insulative Li_3N was formed in situ from the reaction between molten Li and the uniformly distributed TAPC nanoparticles, and this may act as lithiophilic sites on the skeleton. DFT calculations and experimental results helped elucidate the effects of TAPC on lithium metal deposition (Figure 7G): The adsorption energy between Li atom and M-N_4 structure in TAPC was estimated to be 6.614 eV, much higher than those between Li and several other materials, indicating the stronger interfacial interaction between Li and TAPC. Figure 7H demonstrates the plating/stripping behaviors of Li on TAPC-modified Li electrodes where alleviated volumetric expansion change with smooth plating layer was achieved. Among the three investigated electrodes, the TAPC-modified Li electrode exhibited the lowest nucleation voltage of 42 mV and highest CE during 200 cycles (Figure 7I,J). In addition, even at a high current density of 10 mA cm^{-2}, the symmetric cell based on TAPC-modified CF Li electrode was able to stabilize for 3500 h with average overpotential ~92.1 mV. Furthermore, the interactions between lithium and conductive lithiophilic heteroatom-doped carbon frameworks were systematically investigated through first-principles calculations identifying that the binding energies between lithium atoms and the fluoride-doped mesoporous carbon (FMC) have a significant effect on heterogeneous nucleation and the formation of stable SEI layer film.[90] Specifically, two characteristic bonds of C(sp^2)-F and C(sp^3)-F are found in the FMC matrix. In comparison with the pristine carbon, the formation energy of C(sp^3)-F in the matrix is about −1.07 eV, while introducing defects into the skeleton to form C(sp^2)-F could lower the binding energy down to −3.73 eV, indicating the stability of C(sp^2)-F bond (Figure 8). In general, the adsorption energy of Li atom on the matrix also reflects the lithiophilic capability and chemical stability. The simulation results and nucleation barriers reveal that the C(sp^2)-F is prone to supply lithiophilic site for nucleation, while the C(sp^3)-F bond is easy to break to generate LiF during Li plating. The charge transfers were further investigated with Bader charge and charge density difference analysis, which confirmed that the charge transfer between Li and C(sp^3)-F atoms increased significantly, implying the formation of Li-F bond. In contrast to the pristine Cu current collector, more LiF ratio in the XPS measurement was achieved when employed with FMC@Cu current collector (41.7% vs 24.1%), indicating the formation of LiF in enhancing lithium ion transport and averaging lithium ion flux for smooth plating.

Above all, for clear understanding of the protective effects, the electrochemical performances via interphase engineering and current collectors are summarized and compared from the aspects of the electrode material, overpotential, plating/stripping capacity, current density to cycling lifespan (Table 2).

4. ELECTROCHEMICAL REGULATIONS OF LITHIUM DIFFUSION

During the multi-processes of lithium plating (Figure 1B), the Li ion/atom undergoes desolvation, nucleation, and diffusion energy barriers owing to the depressed electrochemical

Table 2. Comparisons of the Overpotentials of the Reported Pretreated Electrodes

Electrodes	Overpotential (mV)	Plating/stripping capacity (mAh cm^{-2})	Current density (mA cm^{-2})	Cycling lifespan (h)	Ref
Aligned MgO-Li metal	140	5	10	2500	101
Li_3N-modified Li	200	1	0.5	500	109
Li_2S/Li_2Se-protected Li	80	1	2	400	115
Carboxylate-protected Li	50	2	0.5	1000	64
COF-modified Li	50	1	0.5	1000	124
SAHL-modified Li	35	1	0.5	1200	55
PVDF-HFP-protective Li	312	1	2	200	125
Organic Li salts decorated Li	350	0.5	2.5	90	77
N-organic/Li_3N-modified Li	72	1	2	1250	126
3D POSS-SH-protected Li	80	1	1	1000	127
Spiro-O_8-Li	80	1	1	2000	128
3D Cu-hosted Li	40	2	0.2	600	130
CuO-Cu mesh loaded Li	200	1	5	1000	134
3D Cu_3N decorated skeleton-Li	12	1	1	3000	72
CuNW-P loaded Li	100	1	2	300	81
CDG-sponge deposited Li	40	1	1	780	136
3D magnetic host loaded Li	50	1	2	550	70
GCNT-Li	68	2	2	200	71
3D CFs prestored Li	90	1	1	750	73
Carbon hosts with vertical channels molten Li	36	1	1	500	153
TAPC@CF infiltrated Li	41	0.5	1	5000	154

behaviors.[77,79,155] According to the diffusion model and spatial distribution theory, the generation and growth of lithium dendrite are mainly attributed to the random lithium ion behaviors and the sluggish surface atom diffusion.[77] Therefore, to electrochemically regulate the lithium ion/atom plating behaviors during these processes appears as a simpler and more straightforward approach (Figure 1C), sacrificing little negligible energy density of the entire lithium anode in comparison to heavy weight current collector hosts. In this section, the alloy materials are initially introduced to regulate the lithium ion/atom kinetics across the interface. More importantly, decreasing the alloy or metal down to atomic level, the capability of activity is the highest and reaches the maximum of 100%. The SACs applied in lithium anodes are highlighted to decrease the barriers from atom nucleation to atom diffusion.

4.1. Rapid Ion Diffusion across the SEI Layer Modulated by Lithiated Alloy Layer. The lithium ion plating and deposition between the SEI and metallic lithium must occur at a high current density in a short time for good high-rate performance. The uneven interface morphology and electrical field distribution easily lead to the inhomogeneous lithium deposition. In order to solve these problems, it is urgent to introduce a modulation layer that can average and homogenize lithium ion transport flux during the deposition process. Alloys, with the intrinsic ability to accelerate lithium ion/atom transport and reserve ion storage, can be applied as modulation coating layer on the metallic Li surface for preventing lithium dendrite growth.[156−158]

As typical anode materials, lithium alloy, with naturally higher Li^+ diffusion coefficients can also serve as modulators to accelerate the interfacial diffusion kinetics of lithium ions/atoms and to inhibit dendrite growth.[9,147,159,160] However, the addition of a large content of alloys as anodes into the lithium system inevitably burdens the entire battery with increased weight, sharply reducing the energy density and resulting in large volume change. Alternatively, a thin artificial alloy-based SEI only slightly increases the anode weight while maintaining its active role of regulating the Li deposition behaviors, retaining its integrity upon extended cycling. To avoid the phase aggregation upon simple mixing of two metal solids, a solution-based reaction method shows fabrication feasibility. In 2017, Nazar and Archer proposed to adopt the alloy coating layers to stabilize the surface of metallic lithium, applying an effective strategy of in situ formation of various kinds of lithium alloy compounds through the solution-based reactions.[82,161] After the fast reactions between the pristine Li and electrolyte additives of alloy precursors, the shiny pristine surface turned dark with the formation of metals (As, In, Bi) and alloys (Li_xAs, Li_xIn, Li_xBi) (Figure 9A).[161] A trilayer nanostructure composing of upper frozen electrolyte, a tin-rich middle layer with a particle size of 200 nm and bottom Li metal (Figure 9B) was observed in operation. Contrary to the pristine Li, the protected Li electrode had a smooth surface without any dendrites under the high plating capacity up to 4 mA h cm^{-2} (Figure 9C).[82] Besides the solution-based reaction, the direct use of the liquid metal may be an alternative method to coat the metallic Li surface since the metal in the liquid state possesses higher fluidity and surface affinity than chemically reduced solid particles. For instance, the spontaneous alloying process of spreading mercury droplets on the Li metal surface was completed within only a few minutes. As depicted in Figure 9D, the generated Hg-rich alloy (Li_3Hg), located on the outer side on the top surface, exhibited excellent flexibility and robustness, readily transferable onto other substrate surfaces without obvious mechanical rupture, indicating the potential in alleviating the focused stress of volume changes in flexible devices.[157] DFT simulations assist the explanation of the different behaviors of Li atoms on Li_3Hg and pristine Li: A higher electron density interaction was calculated between Li ions and Hg atoms at the anode surface and it increased significantly when Li atoms were adsorbed on the Hg sites of Li_3Hg on the (220) surface (Figure 9E). Meanwhile, for the crystal facet in Li_3Hg, molecular dynamics simulations also found that the surface diffusions along (110) and (100) direction show different energy barriers (0.09 eV for path I and 0.9 eV for path II), suggesting the possible "hopping" diffusion pathway of Li atom along the (110) direction (Figure 9F). In the symmetric cells, the protected Li electrodes exhibited fast ion transport under the high current density of 12 mA cm^{-2} and displayed stable cycling lifespan over 200 h at a high plating capacity of 12 mA h cm^{-2} (Figure 9G). Coupled with high-loading $LiFePO_4$ cathodes (12 mg cm^{-2}), the protected

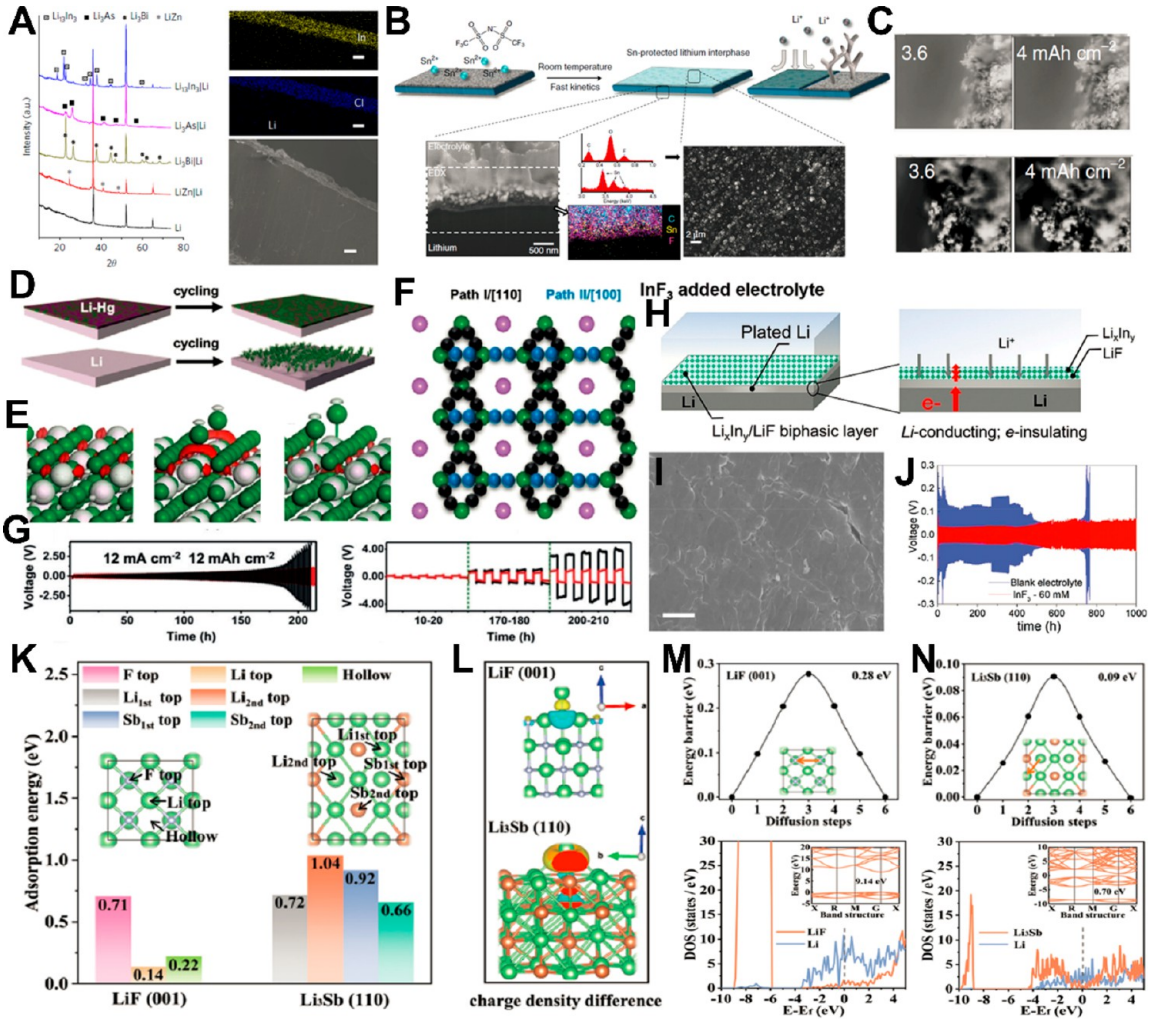

Figure 9. (A) XRD patterns of various alloy-protected Li metal and the corresponding cross-section EDS mapping images of $Li_{13}In_3$−Li. Reproduced with permission from ref 161. Copyright 2017, Nature Publishing Group. (B) Schematic illustration and SEM images of tin-protected lithium electrode through introducing $Sn(TFSI)_2$ additive. (C) Optical microscopy images of the electrolyte-electrode interface during electrodeposition on Sn−Li electrode (upper) and pristine Li (bottom). Reproduced with permission from ref 82. Copyright 2018, Nature Publishing Group. (D) Schematic illustrations of different Li deposition behaviors on pristine Li and Li-Hg anodes. (E) The deformation electron density of Li_3Hg and the interaction between Li atoms with Hg at the (220) surface of metallic Li. (F) Two possible Li migration path directions in Li_3Hg. (G) Stability test of symmetric cell. Reproduced with permission from ref 157. Copyright 2019, Wiley-VCH. (H) Schematic illustration of InF_3-added electrolyte additive before and after cycling on Li electrode. (I) The surface SEM image and (J) cycling performance of symmetric cells based on optimized electrolyte additive. Reproduced with permission from ref 162. Copyright 2018, Wiley-VCH. (K) Adsorption sites and corresponding adsorption energy of Li ion on the LiF (001) and Li_3Sb (110) surfaces. (L) Charge density differences of Li ion on the surfaces of LiF (001) and Li_3Sb (110). Kinetic energy barriers of Li-ion diffusion and DOS on the (M) LiF (001) and (N) Li_3Sb (110) surfaces, respectively. Reproduced with permission from ref 41. Copyright 2021, The Royal Society of Chemistry.

cells demonstrated improved capacity retention and over-potentials for over 100 cycles.

Although progress was achieved by applying liquid-state Hg, the environmental impact such as toxicity should also be taken into consideration. Therefore, it is more convenient and "green" to build thin lithiophilic alloy layers on the surface through the reaction between metal salts and lithium metal. In the successive research, Nazar's group further demonstrated a simple approach to achieve the biphase layer comprised of both $Li_{13}In_3$ alloy and Li-X halide phases by using indium halide additives (InX_3, X = F, Cl, Br, I) (Figure 9H).[162] The liquid-based electrolyte additives assist in the contact with metallic Li, exhibiting the uniform surface. The formed Li-In alloy provides efficient lithium-migration channels with the bulk diffusion coefficient as high as 10^{-8} to 10^{-6} cm^2 s^{-1}, allowing Li plating under the protecting layer. Meanwhile, the insulating Li-X such as LiF phase prevents electron transfer across the SEI layer and establishes an electric field to propel lithium ions. The deposited Li in the modified electrolyte displays a compact but smooth surface without any cracks (Figure 9I). Due to these advantages, a long-term stable plating/stripping behavior of symmetric cell over 1000 h in ether-based electrolyte was achieved (Figure 9J). Similar strategies utilized other additives such as magnesium bis-(trifluoromethanesulfonyl)imide ($Mg(TFSI)_2$) and indium bis(trifluoromethanesulfonyl)imide ($In(TFSI)_3$) on the lithium anode surface.[82,163,164]

Considerable efforts have been made to tune Li-ion/atom diffusion kinetics by engineering compositional and structural homogeneity of alloy layers on the surface. Although some

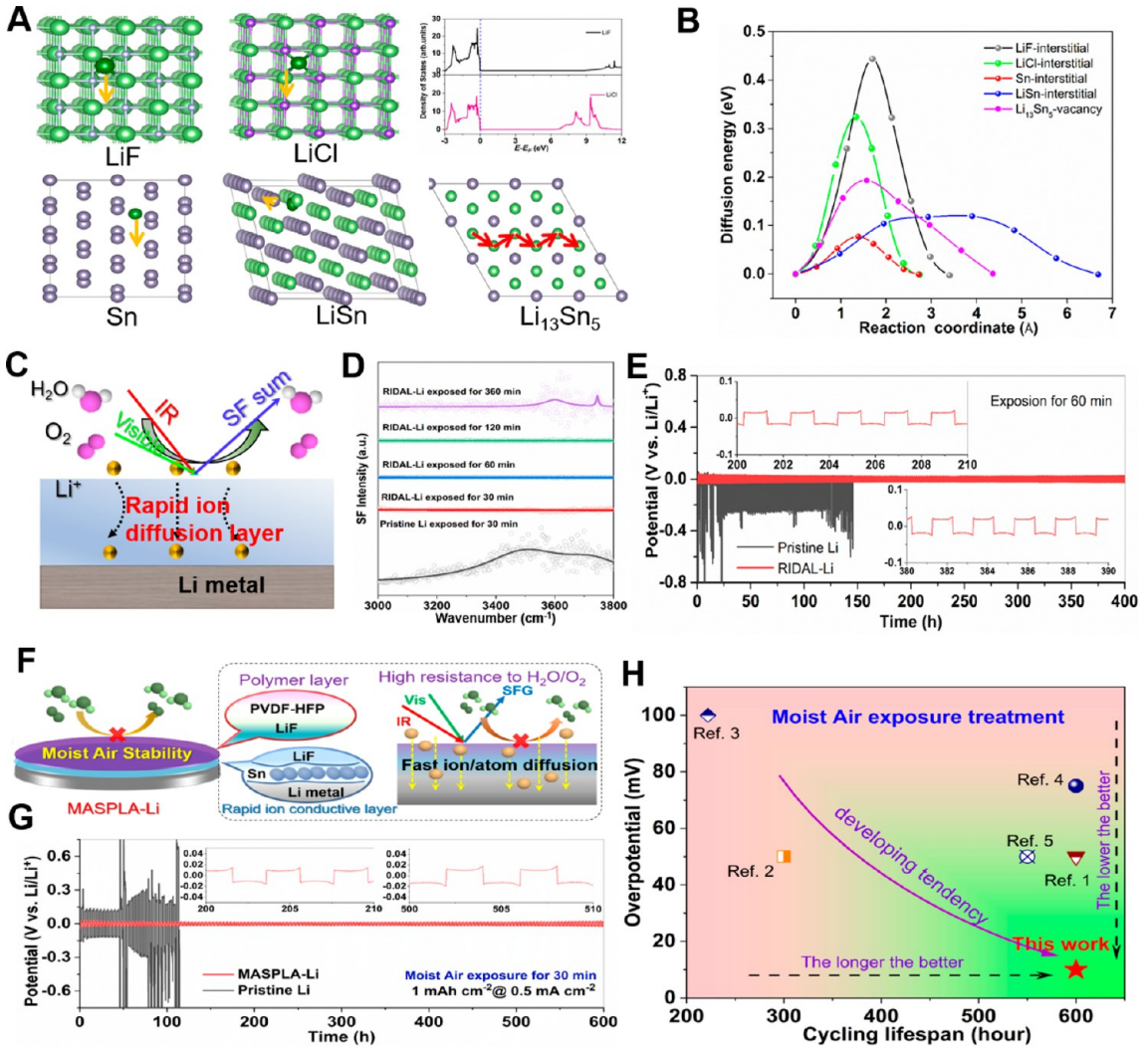

Figure 10. (A) Simulated structures of Li atom diffusion in LiF, LiCl, Sn, and LiSn and $Li_{13}Sn_5$ and the comparison of electronic density of states between LiF and LiCl; note: the yellow and red arrows indicate the diffusion. (B) The summary of the Li diffusion barriers in various materials with optimized diffusion path. (C) Schematic illustration of moisture on RIDAL layer modified Li and (D) the corresponding SFG spectra evolution of two lithium foils when exposed to moist air. (E) Cycling performance of symmetric cells based on moist air-treated anodes. Reproduced with permission from ref 77. Copyright 2022, Wiley-VCH. (F) Schematic illustration of MASPLA-Li structure and functions in accelerating ion diffusion and prohibiting moist corrosion. (G) Comparison of galvanostatic plating/stripping stability of the symmetric cells. (H) Comparison of cycling lifespan and overpotential in the reported literatures. Reproduced with permission from ref 15. Copyright 2022, Elsevier.

works have partially revealed the diffusion mechanism of the lithium atom/ion on the internal and outer surfaces, the specific behaviors of lithium ion/atom through the alloy SEI layer remains elusive. Therefore, theoretical and experimental understanding of the internal mechanism of Li^+ transport within the alloy SEI layer is crucial for the realization of stable Li metal anodes at practically high rates. Thus, an artificial hybrid SEI layer consisting of lithium-antimony (Li_3Sb) and LiF were constructed by immersing Li metal into antimony trifluoride (SbF_3) solution.[32] DFT simulations (Figure 9K) confirmed that among the four discovered potential Li-ion adsorption sites on the Li_3Sb (110) surface, the "Li second-top site" was the most stable position with a high adsorption energy of 1.04 eV, and the F-top site on the LiF (001) surface was the stable site for Li-ion adsorption with the energy of 0.71 eV, while the Li ion on metallic Li (001) surface is ~0.39 eV. The higher adsorption energy means that the Li_3Sb alloy has the highest affinity toward Li ions/atoms. Based on the charge density differences (Figure 9L), the Li_3Sb (110) alloy shows a stronger interaction with Li atom than LiF (001). However, with the introduction of Li_3Sb (110) and LiF (001) surfaces, the diffusion energy barriers of Li ion are decreased to 0.09 and 0.28 eV, respectively (Figure 9M,N), which may indicate that the Li_3Sb (110) surface can strongly adsorb Li ions/atoms and then drive the rapid transport of Li through the SEI layer. The higher work of adhesion (1.513 J m^{-2}) and lower interfacial energy (0.159 J m^{-2}) than those of LiF/Li interface evidence the excellent stability of the Li_3Sb/Li interface. In the density of state, the LiF shows a high band gap, preventing electron tunneling across the LiF layer (Figure 9M), while the Li_3Sb is comparable to the Fermi level of interfacial metallic Li surface, indicating the electrons could migrate from the Li side to the Li_3Sb side and then couple with Li^+ to generate the nucleation sites (Figure 9N). Overall, the symmetric cells based on SbF_3-modified Li anodes offer excellent Li plating/stripping stability over 1360 cycles with a very low polarization of 100 mV at an

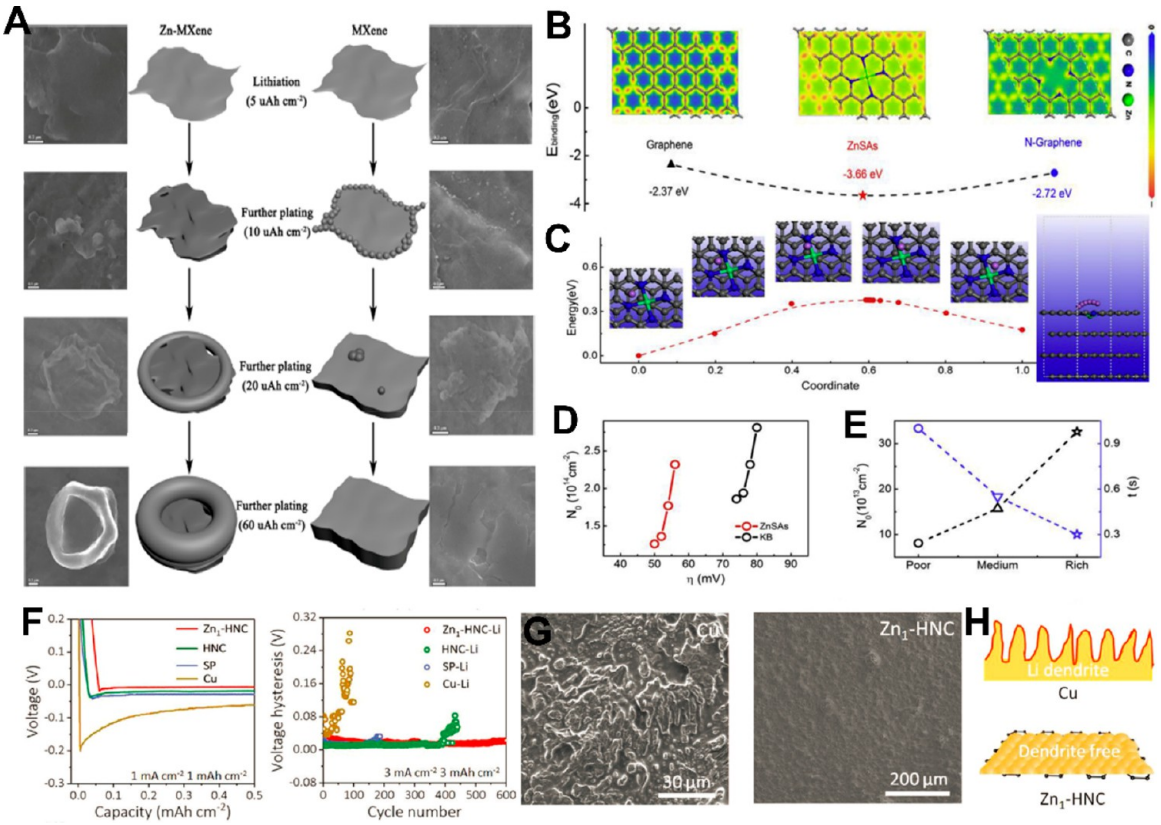

Figure 11. (A) The gradual nucleation and growth process of Li atoms on Zn-MXene and MXene nanosheets observed by SEM. Reproduced with permission from ref 175. Copyright 2020, American Chemical Society. (B) Comparisons of electron density difference and surface binding energy of graphene, ZnSAs, and N-graphene. (C) Li migration pathways and barriers on ZnSAs. (D) Nucleus formation number under different polarized deposition potential. (E) Nucleus number and nucleation relaxation time induced by ZnSAs with different density of single-atom Zn sites. Reproduced with permission from ref 173. Copyright 2019, Elsevier. (F) Comparisons of Li nucleation Li and voltage hysteresis variation on different substrates. (G) The surface SEM images of Li plating on Cu or Zn_1-HNC. (H) The corresponding schematic illustration of electrochemical deposition of Cu and Zn_1-HNC electrode. Reproduced with permission from ref 176. Copyright 2020, Wiley-VCH.

ultrahigh current density of up to 20 mA cm^{-2}. The prepared pouch cell exhibited a practical energy density of 325.28 Wh kg^{-1} under a high sulfur loading of 6 mg cm^{-2} with lean electrolyte of 3 μL mg^{-1}.[32]

Alloy layers generally exhibit excellent Li wettability, which can induce uniform Li-ion/atom flux and lower the Li nucleation barrier during electroplating. Although all the aforementioned alloy layers are efficacious to a certain extent for improving Li diffusion and suppressing dendritic Li growth, the practical assembly and application of the metallic Li anode is limited by the surrounding environment, such as moisture and oxygen content. This is due to the high activity of Li, the surface color of Li metal turns from shiny to dark rapidly upon exposure to moist air, which leads to a rough surface that deteriorates the performance of the lithium electrode. Some of us have reported a "rapid ion diffusion bilayer" on metallic Li (RIDAL-Li) via a solution-based chemical reaction between Li and liquid $SnCl_4$, generating the Sn/Li_xSn alloy layer with a trace amount of insoluble LiCl on the Li foil surface (Figure 10).[77] To reveal the mechanism of rapid ion diffusion across the SEI layer, simulations and electrochemical measurements have been performed. Also, the behaviors of ion/atom diffusion across the alloy layer have been comprehensively calculated. Two kinds of diffusion models, i.e., interstitial diffusion and vacancy diffusion are compared and optimized in all possible systems of Li-X and Li-alloy (Figure 10A). Within various structure optimizations, the lithium ion/atom tends to exhibit an interstitial diffusion behavior in Sn with extremely low diffusion energy barrier (0.08 eV). In the various Li-Sn alloys, the transport behaviors are changed gradually from interstitial diffusion to vacancy diffusion model along with the gradual lithiation in the alloy (Figure 10B). Also, the generated LiCl exhibited lower diffusion barriers than the commonly used LiF. As a result, the pretreated RIDAL-Li exhibited an improved CE of 99% lasting up to 350 cycles without dendrite formation at 1 mA cm^{-2}. At the same time, the binding/adsorption energy between moisture and pristine Li is ~0.79 eV, since the spontaneous reaction will happen, and was significantly decreased to 0.45 eV on the Sn/Li_xSn alloy surface, demonstrating the chemical stability. As revealed by sum-frequency generation spectroscopy (SFG), no H_2O peaks appeared on the RIDAL-Li even after exposure to moist air for 120 min (Figure 10C,D), suggesting the exclusion of moisture on the surface. Similarly, by separating the inner Li from the electrolyte, the RIDAL functional layer can resist corrosion by electrolyte solvents. Even after exposure to the ambient environment with relative humidity of 51% for 60 min, the RIDAL-Li can maintain stripping/plating for 400 h and exhibit a low overpotential of 18 mV (Figure 10E). These electrochemical results show the rapid ion diffusion is also reflected in the increased lithium ion transfer number. Besides $SnCl_4$, other metal fluoride composites including AlF_3 and CuF_2 are used on

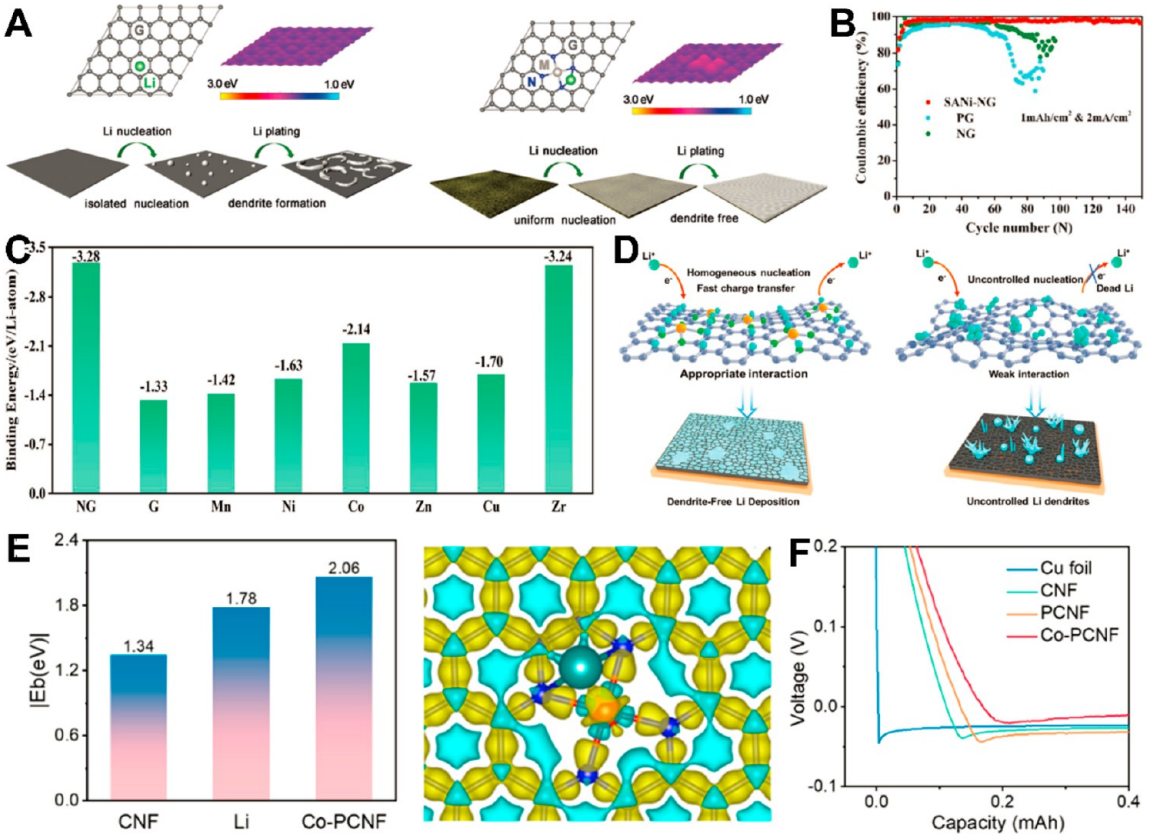

Figure 12. (A) Li adsorption energy and distribution mappings on PG electrode and SAM-NG (M = Ni, Pt, Cu) and corresponding schematic illustration of modulating Li behaviors. (B) The CE measurement of corresponding samples in Li-Cu asymmetric cells. Reproduced with permission from ref 172. Copyright 2019, Wiley-VCH. (C) Binding energy summary between Li atoms and a series of metal atom decorated graphene. (D) Proposed mechanism of Li deposition on the carbon electrode with/without single metal atom. Reproduced with permission from ref 92. Copyright 2022, Wiley-VCH. (E) Binding energy summary of Li atom on CNF, Li, and Co-PCNF and the corresponding charge density distribution of Li atom on Co-PCNF. (F) Li nucleation barriers on different substrates in the enlarged voltage plating profiles. Reproduced with permission from ref 177. Copyright 2021, American Chemical Society.

the metallic Li surface to modulate the lithium ion kinetics for smooth plating. For example, the assembled cells with the interphases of LiF and Li-Al alloy, produced via direct reduction of aluminum fluoride on Li foil as the protected anode and a $LiFePO_4$ cathode, exhibited a long cycle life of 300 cycles with an extraordinary capacity retention of over 95%.[165] Further, even with the surrounding humid air (25% relative humidity, RH), the protected Li was capable of surviving for over 24 h. To enhance the resistance to moist air corrosion, a hydrophobic ion-conductive organic layer was introduced into the system. Figure 10F displays the dense moist-air-stable polymer-LiF-alloy hybrid layer on the metallic Li (MASPLA-Li) through optimizing the upper thickness of PVDF-HFP layer.[15] As revealed by SFG, the hybrid MASPLA layer stabilized for more than 4 h under the humidity of ~50 RH. Even after exposure for various times, the MASPLA-Li showed extended lifespan and lower overpotentials. For example, being treated for 30 min, in comparison with pristine Li electrode with dendrite formation within 50 h, the exposed MASPLA-Li electrode was capable of surviving for ~600 h with the overpotential of 20 mV (Figure 10G). These results are among the best in the reported literature on moist stability (Figure 10H), indicating the designed hydrophobic ion-accelerated polymer-LiF-alloy diffusion layer could strongly resist the corrosion and uniformize lithium ion flux for smooth deposition.

4.2. Li Nucleation and Diffusion Catalyzed by Single Atomic Catalysts. Although alloy layers can modulate the lithium ion/atom behaviors and average the lithium flux across the interface, the insufficient lithiophilic sites and the relatively high weight may compromise some energy density. When the size of the alloy is reduced to monodispersed metal atoms, the specific surface area and atomic utilization reach the maximum to gain the highest reactivity, forming SACs.[76,85−87,166−172] By bringing the metal-based modulator down to atomic level, the active sites are fully exposed, approaching the atomic efficiency of 100%.[6,76,86,87,173] To this end, a single atomic iron catalyst was transplanted into the nitrogen-doped carbon (Fe_{SA}-N-C) matrix as lithophilic sites to decrease Li nucleation potential.[174] Molecular dynamics simulations verified that the lithium ions spatially spread around the SAC-decorated nanocarbon rather than the random distribution on the pristine carbon matrix. The high peak at 0.2 nm instead of ~0.7 nm was achieved in the radial distribution function, indicating the possibility of close interaction between Li and Fe_{SA}-N-C. Thereafter, single Zn atom immobilized on MXene layers (denoted as Zn-MXene) as SAC host was developed.[175] With a plating areal capacity of 10 μAh cm^{-2}, the lithium atoms are deposited in planes on the Zn-MXene electrode (Figure 11A), in contrast to the lithium spheres growth from the outer edge to the inner center on the pristine MXene layer. Upon further increasing the lithium plating, aggregations are formed at the edge side

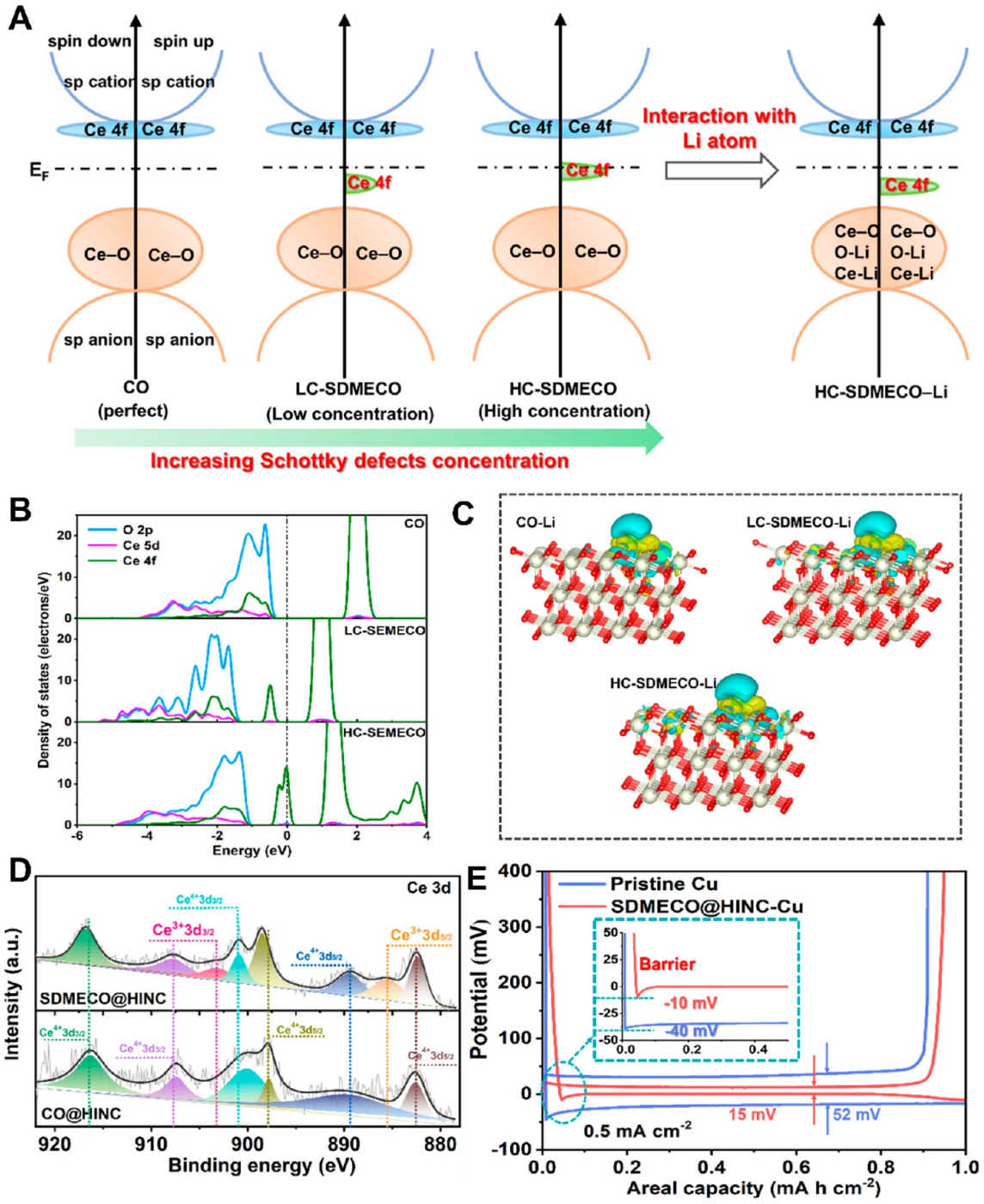

Figure 13. (A) Schematic explanation of the 4f electron modulation strategy by increasing the Schottky defects concentration, and the subsequent electron transfer interaction of the modulated structure with Li atom. (B) The projected density of states (PDOS) simulated from the surface atoms in the unabsorbed configurations of CO, LC-SDMECO, and HC-SDMECO. (C) The corresponding charge density difference of the three models. (D) Ce 3d between the SDMECO@HINC and CO@HINC. (E) The comparison curve of the Li nucleation barriers on different electrodes in asymmetric cell. Reprinted with permission under a Creative Commons Attribution License 4.0, ref 16. Copyright 2022, The Authors.

with a bowl-like morphology, indicating the strong "lightning tip effect" of the edge to promote rapid lithium plating. To understand the specific roles of single atomic Zn (ZnSAs), DFT calculations and chronoamperometry methods were carried out.[173] In comparison to the converged electron density of graphene among chemical bonds, the introduction of ZnSAs helps to delocalize the electronic density on the entire plane, indicating the improved electronic conductivity. Also, the plating behaviors have a close relation with the surface binding energy and lithium ion migration energy (Figure 11B). The calculated surface energy to bind lithium atom shifted from −2.37 eV for the pristine graphene to −3.66 eV for the ZnSAs, indicating the higher plating capability of ZnSAs, which is beneficial for the release of surface tension. The lithium atom can easily migrate to the nearest neighbor with the lowest barrier energy (Figure 11C). In the

chronoamperometry measurement, the ZnSAs only took the extra potential of 50 mV to overcome the nucleation barrier, while the Ketjen black exerts the nucleation potential of 74 mV (Figure 11D). The abundant active sites can achieve uniform nucleation in a shorter time (Figure 11E). As a result, the ZnSAs-decorated Li electrode exhibited the lower overpotential of 12 mV and high CE above 98%. Accordingly, the symmetric cell based on ZnSAs-decorated Li electrode could operate for 800 h without dendrite growth. For the Li-S full battery, a "nanoreactor" anode composed of well-dispersed Zn atom-decorated hollow carbon spheres (Zn_1-HNC) was also constructed to regulate the lithium plating behaviors.[176] Charge density difference analysis demonstrated that the plated lithium atom tends to nucleate around Zn_1 sites with higher affinity to the Li atom than bare carbon sites (−2.04 *vs* −0.48 eV). CE measurements revealed that the single atomic Zn in HNC increased lithium atom utilization to 99.9% with much lower voltage dip and stabilized the overpotential to within 15 mV, suggesting high ion conductivity in the Zn_1-HNC-modified electrode (Figure 11F). Moreover, this electrode also stabilized the lower voltage hysteresis for 600 cycles at 3 mA cm^{-2} (Figure 11F). SEM results in Figure 11G verified that, contrary to the random deposition and dendrite growth on bare Cu, uniform Li nucleation and uniform smooth surface (Figure 11H) were both achieved in the Zn_1-HNC electrode.

To date, the application of SACs on the metallic lithium anodes is still in its infancy, and further effort is required to screen more SACs to sculpt the lithium system. To discern the catalytic essence from the interfacial functional bonds, various metal atoms supported by the nitrogen-doped graphene to generate metal-nitrogen-carbon (M-N_x-C) nanostructure to regulate lithium nucleation and deposit behaviors have been investigated (Figure 12A).[172] The high concentration of single metal atoms anchored by nitrogen sites increased the local adsorption energy to Li atom by increasing the localized area. In addition, this M-N_x-C nanostructure can direct the Li atom deposition and recast the nanostructure during long life cycles. DFT simulations revealed that the single-atom nickel supported on nitrogen-doped graphene matrix (SANi-NG) showed the highest feasibility for experiments due to its low Fermi energy of 0.8 eV, and the SANi-NG decorated electrode displayed the highest CE and stability for 150 cycles (Figure 12B). To further probe the lithiophilicity in SACs, six types of single metal atom-doped graphene materials (SAM@NG, M = Mn, Ni, Co, Zn, Cu, Zr) were synthesized via the NaCl-templating method and investigated.[92] Although single-atom zirconium supported on nitrogen-doped graphene matrix (SAZr@NG) has a larger calculated binding energy than the other systems, which is similar to that of NG (Figure 12C), it does not perform better experimentally. This implies that the host needs a moderate lithiophilicity to the lithium atom, so that the atoms can diffuse freely. Different from the weak adsorption with dendrite formation, the case in moderate binding energy between single-atom (SA) metals supported on nitrogen-doped graphene matrix (SAM@NG) and Li will achieve a uniform nucleation and smooth lithium plating. Stable M-N_x-C structures and abundant lithiophilic sites can be realized by introducing single atoms, which appropriately tunes the local chemistry around metal atoms, thereby changing the binding capability of lithiophilic sites. Meanwhile, the 3D nitrogen-doped anchor architecture provides SAM@NG with a large surface area, which not only provides sufficient space for Li deposition but also efficiently reduces the local current density to realize uniform charge distribution (Figure 12D). Besides serving as host materials for metallic lithium, SACs can also be used as artificial protective interlayers so that the flexible carbon substrate can adapt to volume changes, thereby providing a stable interface that facilitates the uniform lithium deposition. Most importantly, SACs interlayer with abundant isolated lithiophilic sites can guide lithium deposition and suppress the formation of Li dendrites during electroplating. A fibrous carbon skeleton implanted with single atom dispersed Co-N_x (Co-PCNF) was used as an advanced regulator for Li electrodes (Figure 12E).[177] The interconnected porous framework endows the whole structure with good mechanical strength and fast electron/ion transport. Implanting atomic Co-N_x dispersions could effectively alter the fibrous carbon skeleton from lithiophobic to lithiophilic, as evidenced by the Co-PCNF's high adsorption energy toward Li atom (2.06 eV), exhibiting enhanced charge transfer between Li and the atomic Co-N_x sites. In particular, the nucleation overpotential for the Co-PCNF was as low as 10 mV (Figure 12F), suggesting a favorable lithiophilic property. The Co-PCNF-modified cell exhibited superior stability with an excellent cycle life over 1500 h without any observable increase of polarization.[177]

Currently, the heteroatom-doped nanocarbon matrix, such as nitrogen-doped, is still a popular method to hold the single metal atoms via the chemical formation of metal-N bond. To the best of our knowledge, the lithium nucleation and plating behaviors have a close connection with the active site number in the artificial layer. However, the anchoring sites of M-N_x-C are limited by the number of heteroatom doping. The presence of defects enables the electronic density of the metal center to be tuned to provide more active polar sites than the perfect (defect-free) counterpart.[36,178,173] Defect engineering is a feasible approach to redistribute the internal electrons and generate intrinsic active sites or synergistic sites.[179−181] Different from popular architecture designs, our group initially proposed a 4f-center electron reconstruction strategy by introducing Schottky defects (SDMECO) to modulate lithium diffusion behaviors to suppress dendrites, taking advantage of CeO_2 (CO)'s easily adjustable intrinsic electronic structure.[16] As initially simulated (Figure 13A), the introduction of defects in the system induced a shift in the 4f-band electronic state, which was recovered upon interaction (charge transfer) with Li atoms, indicating the capture of Li atom to decrease the initial nucleation barrier. As disclosed, the Fermi level state in Figure 13B is strengthened in high concentration of Schottky defects (HC-SDMECO) and the corresponding spin polarity originating from Ce-4f electrons is significantly enhanced. Furthermore, the formation of Ce-Li bond was weakened due to the reduction of Ce-4f electrons that participate in bonding, indicating the essential role of Ce-4f electrons in modulating Li atoms. At the same time, the oxygen defects are able to enhance the adsorption ability toward Li through interfering with the charge balance of perfect CeO_2 (111) surface to form an internal electric field. Such electronic transfer between the SDMECO and Li atom can also be reflected by the charge density difference (Figure 13C). As further verified by the XPS experimental results, the coexisting Ce^{3+} $3d_{3/2}$ and Ce^{3+} $3d_{5/2}$ peak changes in the high-resolution Ce 3d spectrum are evidence of the 4f-center electron density transfer inducing valence band restructuring upon the inception of the Schottky defects (Figure 13D). Consequently, the Schottky defects-modulated CeO_2 within highly conductive and interconnected

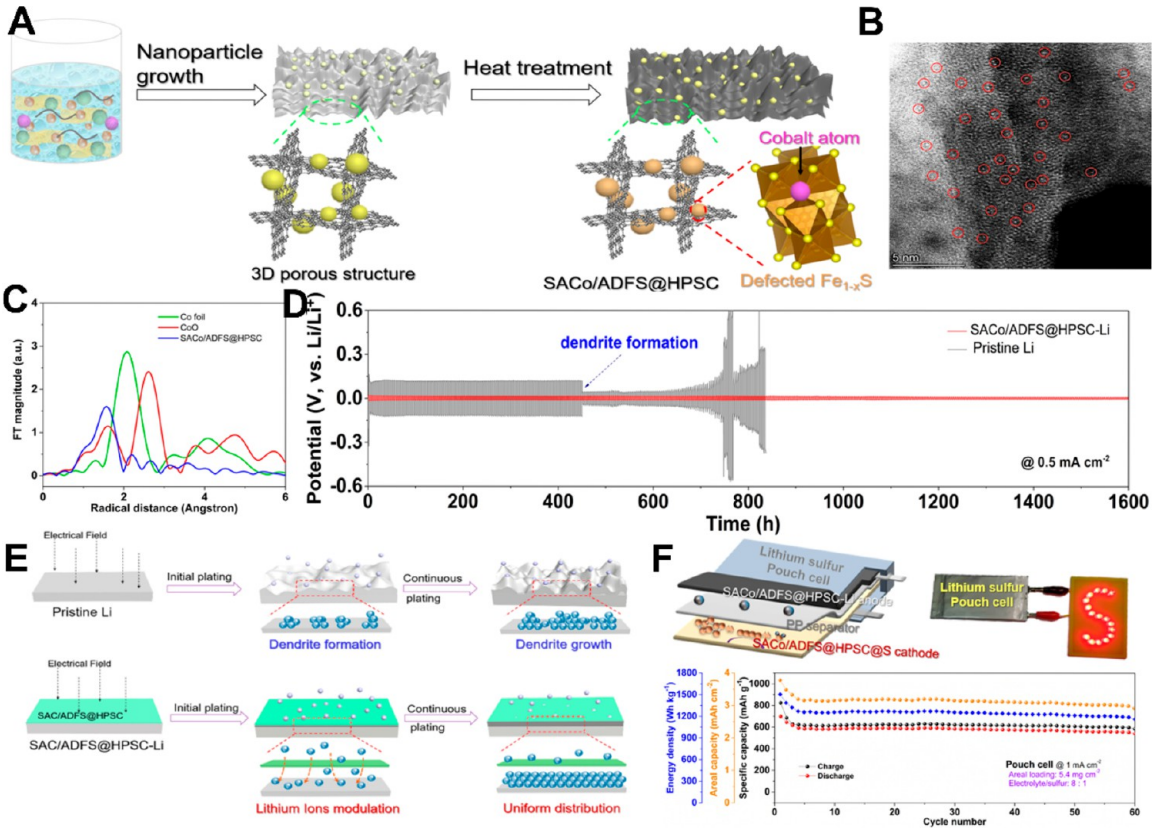

Figure 14. (A) Schematic synthesis of the SACo/ADFS@HPSC modulator via the strategy of "SAC-in-Defects". The characterizations of SAC by (B) HAADF-STEM and (C) XAS. (D) Plating/stripping stability of the symmetric cells at 0.5 mA cm^{-2}. (E) Schematic illustration of plated lithium behaviors on SACo/ADFS@HPSC modified Li surface. (F) Configuration of large areal pouch cell and the lightened series of LED lights and the cycling performance of so-fabricated large areal pouch cell. Reproduced with permission from ref 76. Copyright 2021, American Chemical Society.

N-doped carbon nanotubes networks (SDMECO@HINC) exhibited superior electrocatalytic activity in propelling the desolvation and Li diffusion kinetics, achieving smooth dendrite-free lithium plating. Serving as modulators for lithium electrode, the initial nucleation energy barrier decreased to nearly four times lower than that of the bare Cu substrate (Figure 13E). What's more, a long lifespan (1200 h at 0.5 mA cm^{-2}) and high CE (98% after 100 cycles) were achieved without dendrite formation.

The defects may also preferentially act as the host sites for other metal heteroatoms. Recently, the methodology of "SAC-in-Defects", utilizing abundant defective sites to trap single metal atomic catalyst, was proposed and successfully realized.[76] Briefly, highly active atomic Co was anchored in defective iron sulfide embedded on the hierarchical porous sulfur-doped nanocarbon through the hydrothermal reactions (denoted as SACo/ADFS@HPSC), as displayed in Figure 14. Aberration corrected scanning transmission electron microscopy, electronic energy loss spectroscopy, and XAS were applied to identify the atomic Co anchored at the defected $Fe_{1-x}S$ (Figure 14B,C). For example, the bright dots in the high-resolution TEM indicated the well-distributed Co atoms, forming the Co−S bond in the ADFS (Figure 14C). The Li electrode decorated by SACo/ADFS@HPSC (SACo/ADFS@HPSC-Li) showed a much lower charge transfer resistance (23 Ω) than the pristine Li. In the nucleation process, the highly active atomic Co closely interacted with the plated lithium atoms to decrease the initial nucleation barrier. At 0.5 mA cm^{-2}, the SACo/ADFS@HPSC-Li electrode extended the lifespan from 500 h for pristine Li to 1600 h with a stable and lower overpotential of about 13 mV (Figure 14D). During the entire stripping/plating process, no short-circuit phenomena was observed. Overall, the electrode exhibited superior capacity in modulating lithium nucleation and plating behaviors along the horizontal deposition, smoothing the lithium surface without dendrite growth (Figure 14E). The so-fabricated high-loading Li-S pouch cell (5.4 mg cm^{-2}) based on SACo/ADFS@HPSC-Li (Figure 14F) was able to deliver an outstanding areal capacity up to 3.78 mA h cm^{-2} corresponding to the energy density of 1505 W h kg^{-1}.

The rapid vertical deposition of Li atom will result in dendrite formation. Regulating the surface activation helps to increase diffusion kinetics to realize homogeneous deposition (Figure 15A).[83] As reported in our previous finding, the SAC is available to modulate the Li nucleation by decreasing the barrier. Furthermore, in comparison with the pristine Li metal with high diffusion barriers (Figure 15B,C), a significant decrease of lithium atom diffusion barrier was realized down to 0.09 eV by introducing SAC activators into the system, suggesting the enhanced lateral diffusion for evenly distributed Li plating. Under the practical stripping/plating capacity of 3.0 mA h cm^{-2}, the single iron/nickel atom catalyst on light nitrogen-doped carbon layer modified metallic Li (SAFeNi@LNCP-Li) showed a reversible lifespan of 450 cycles with the overpotential of 50 mV at 3.0 mA cm^{-2}. After cycling and peeling off the upper SAC modulated layer, the ex situ low-

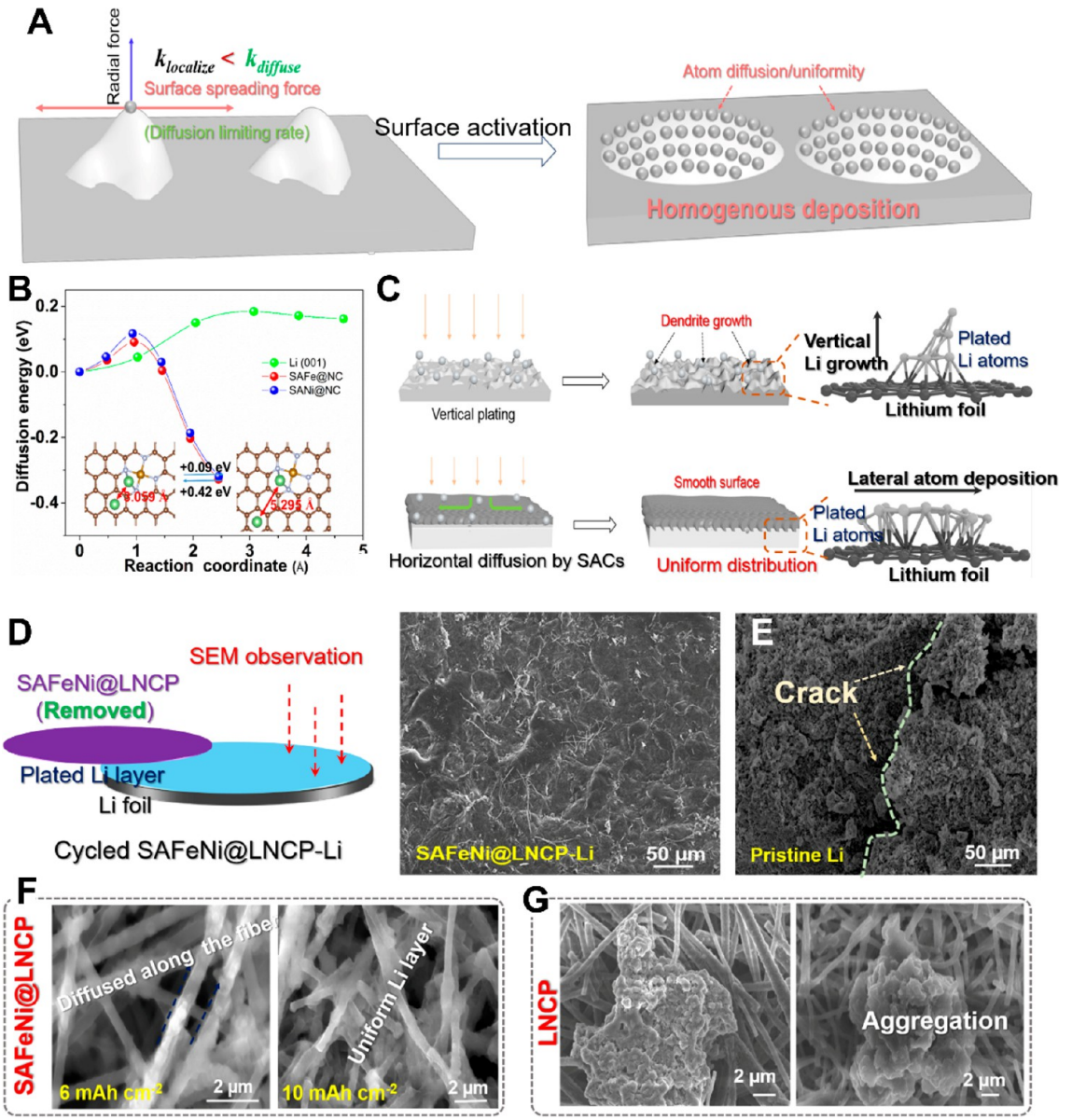

Figure 15. (A) Schematic illustration of Li atom diffusion kinetics by surface activation. (B) Comparison of diffusion barriers on metallic Li and SAC-modulated carbon. (C) Lateral diffusion for smooth plating surface on metallic Li with SAC activation. Surface morphologies of the (D) cycled SAFeNi@LNCP-Li after peeling off SAC-modulator layer and (E) cycled pristine Li. Morphology of Li atom plating on (F) bare SAFeNi@LNCP and (G) LNCP to verify lateral deposition modulated by SACs. Reproduced with permission from ref 83. Copyright 2022, American Chemical Society.

resolution SEM image of pretreated Li exhibited the smoother plating morphology instead of cracks and large volumetric changes on pristine Li (Figure 15D,E). To visualize the lateral atom diffusion modulated by SACs, the plating morphologies on bare SAFeNi@LNCP or LNCP without bottom Li were further observed under different plating capacities. In comparison with the aggregation of lithium on the LNCP (Figure 15G), smooth thin plating layers were obtained along the fiber, suggesting the catalytic modulation ability of SACs in propelling lateral atom diffusion (Figure 15F). These results explain the crucial role of the SACs in promoting the lateral diffusion of lithium atoms instead of decreasing current density of deposition with large surface area.

5. SUMMARY AND FUTURE PERSPECTIVES

LMBs have attracted significant research interest in the pursuit of high-energy-density batteries in recent years. Unfortunately, the large-scale utilization of LMBs has encountered hindrances such as uncontrolled dendrite formation, large volumetric changes, SEI deformation or even breakdown and electrolyte exhaustion. In this review, we have systematically summarized and discussed the latest strategies on modulating Li electrodeposition behavior for stable Li anodes and optimization of the SEI layer structure designs toward robust layer formations for stabilizing Li metal electrode performances. In addition, we have explored the design of lithiophilic current collectors for hosting metallic lithium to decrease local deposition current density. Finally, modulating the kinetics of Li-ion/atom diffusion by applying alloy layer or highly active SACs was

explored. However, the diffusion strategies of using alloys or SACs are still in their infancy with further studies requisite to develop LMBs for practical high energy storage systems. Future research should focus on the four areas outlined in Sections 5.1−5.4 and Figure 16.

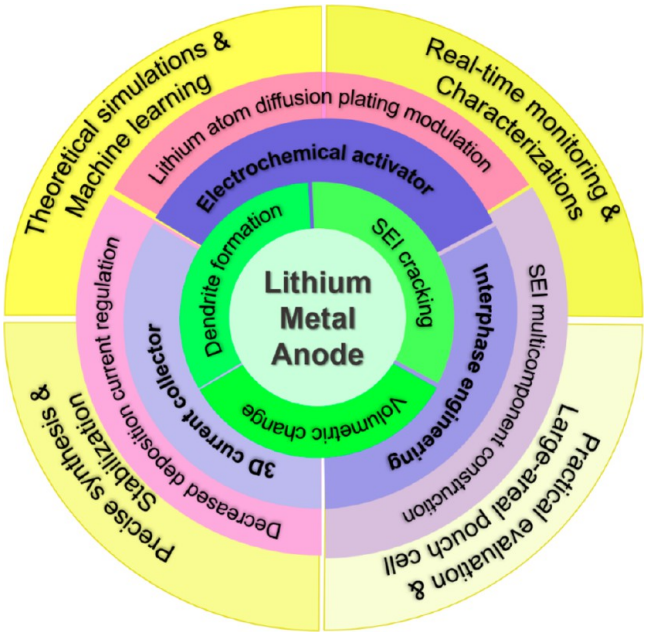

Figure 16. Summary and prospects of Li metal batteries for future development.

5.1. Precise Fabrication and Stabilization: High-Concentration SAC Modulation Layer. It has been established that the lithium diffusion capability in interphase engineering or current collector is difficult to enhance since it is the intrinsic property of the perfect inorganic/organic materials. Introducing heteroatoms or defects in the inorganic species is a potential approach for modulating the electronic density distribution to decrease the atom diffusion barriers and improve the kinetic behaviors. By virtue of the proper hosts, SACs appear to be the most efficient for modulating the Li-ions/atoms diffusion. However, the reliance on the heteroatom numbers in the nanocarbon matrix via forming M-N_x-C structure restricts the high-concentration loading of SACs. The metal−support interaction mechanism should be investigated to support high metal concentrations and provide more active sites for smooth morphology, i.e., promoting the lateral Li-ion/atom diffusion. Besides, the various optimizations of atomic metal species in terms of modulation capability for practical utilization should be evaluated.

5.2. Real-Time Monitoring and Characterizations: In Situ Visualizations to Trace Lithium Atom Plating/Stripping Evolution within Deep Electrodeposition Behavior. Unfortunately, the lack of effective methods to visualize diffusion and uniform Li deposition means that the exact mechanism guiding Li atoms deposition is still not fully understood. A transition to employ in situ techniques to observe the dynamic plating/stripping process is advantageous in exploring the plating evolution and dendrite formation mechanisms. In situ/operando visualization tools such as operando AFM, TEM, and SEM provide information on SEI formation, the interface evolution at the molecular/atomic level, and the atom diffusion in an operating battery.[96−98,182]

5.3. Theoretical Simulations and Machine Learning: Understandings of Li Electrodeposition at Electrified Interfaces. With the development of artificial intelligence, machine learning offers an approach to screen more suitable catalysts or structure designs without the need of tedious experiments.[16,90,172,180] For instance, besides the binding adsorption energy between lithium ion/atom and interface/host, machine learning can offer more distinction criteria for the suitability of the materials for application in Li anodes. Also, the use of machine learning is expected to accurately guide material synthesis and significantly simplify the experimental steps. In terms of electrochemical kinetics, the finite element method and molecular dynamics simulations can describe the atom diffusion influence on dendrite formation. Therefore, it is imperative to simulate the lithiophilicity and diffusion behavior between the substrate or interface layer and lithium flux to elucidate the mechanism. To understand the ion/atom transformation mechanism and electrochemical kinetics of Li electrodeposition, combining the in situ/operando visualization tools with the theoretical calculations or simulations may clarify the extent of Li electrodeposition.

5.4. Practical Evaluation and Large-Areal Pouch Cells: Demonstration of Fabricated Li Metal Anodes in Large Pouch Cells. For the wide application of Li metal anode in high-energy-density batteries, the anode must be evaluated in large-areal pouch cells or high current stripping/plating for potential application of fast charging. For example, in the pursuit of energy density of 500 Wh kg^{-1}, the areal stripping/plating capacity should be improved to above 3 mA h cm^{-2} and the charging current density should be enhanced to 3.0 mA cm^{-2}, meaning the high-energy-density batteries are requested to be fully charged within 1 h. Most of the reported strategies must be reassessed to determine if they can achieve these thresholds. In such instances, the higher barriers of desolvation, nucleation and diffusion should be significantly reduced to realize the capability of fast lithium plating/stripping. Meanwhile, the evaluation of the pretreated cell is performed by assembling coin cells with excessive lithium, in contrast to the limited Li inventory in practical battery cells. Pouch cells have long been considered as the pilot attempt for the implementation of batteries on a large scale, while the success of interfacial engineering (or matrix) from coin cell to practical battery without sacrificing energy density remains a challenge. Incorporating machine learning can aid the designs of constructing rapid ion diffusion tunnel or modulating the lithium behaviors for the practical Li metal anode as well as its assessment under high capacity in pouch cells; this represents a viable method for realizing high-power-density lithium batteries.

AUTHOR INFORMATION

Corresponding Authors

Jian Wang − *i-Lab and CAS Key Laboratory of Nanophotonic Materials and Devices, Suzhou Institute of Nano-tech and Nano-bionics, Chinese Academy of Sciences, Suzhou 215123, China; Helmholtz Institute Ulm (HIU), Ulm D89081, Germany; Karlsruhe Institute of Technology (KIT), Karlsruhe D-76021, Germany;* orcid.org/0000-0002-7945-0826; Email: jian.wang@kit.edu, wangjian2014@sinano.ac.cn

Jing Zhang − *School of Materials Science and Engineering, Xi'an University of Technology, Xi'an 710048, China*; Email: zhangjing2020@xaut.edu.cn

Stefano Passerini − *Helmholtz Institute Ulm (HIU), Ulm D89081, Germany; Karlsruhe Institute of Technology (KIT), Karlsruhe D-76021, Germany;* orcid.org/0000-0002-6606-5304; Email: stefano.passerini@kit.edu

Hongzhen Lin − *i-Lab and CAS Key Laboratory of Nanophotonic Materials and Devices, Suzhou Institute of Nano-tech and Nano-bionics, Chinese Academy of Sciences, Suzhou 215123, China*; Email: hzlin2010@sinano.ac.cn

Authors

Linge Li − *i-Lab and CAS Key Laboratory of Nanophotonic Materials and Devices, Suzhou Institute of Nano-tech and Nano-bionics, Chinese Academy of Sciences, Suzhou 215123, China*

Huimin Hu − *i-Lab and CAS Key Laboratory of Nanophotonic Materials and Devices, Suzhou Institute of Nano-tech and Nano-bionics, Chinese Academy of Sciences, Suzhou 215123, China*

Hongfei Hu − *i-Lab and CAS Key Laboratory of Nanophotonic Materials and Devices, Suzhou Institute of Nano-tech and Nano-bionics, Chinese Academy of Sciences, Suzhou 215123, China*

Qinghua Guan − *i-Lab and CAS Key Laboratory of Nanophotonic Materials and Devices, Suzhou Institute of Nano-tech and Nano-bionics, Chinese Academy of Sciences, Suzhou 215123, China*

Min Huang − *i-Lab and CAS Key Laboratory of Nanophotonic Materials and Devices, Suzhou Institute of Nano-tech and Nano-bionics, Chinese Academy of Sciences, Suzhou 215123, China*

Lujie Jia − *i-Lab and CAS Key Laboratory of Nanophotonic Materials and Devices, Suzhou Institute of Nano-tech and Nano-bionics, Chinese Academy of Sciences, Suzhou 215123, China*

Henry Adenusi − *Hong Kong Quantum AI Lab (HKQAI), Hong Kong 999077, China*

Kun V. Tian − *Department of Chemistry and Chemical Sciences of Pharmacy, Sapienza University of Rome, Rome 00186, Italy; Department of Chemistry and Biological Chemistry, McMaster University, Hamilton L8S 4L8, Canada; Faculty of Land and Food Systems, The University of British Columbia, Vancouver V6T 1Z4, Canada;* orcid.org/0000-0003-0102-0620

Complete contact information is available at: https://pubs.acs.org/10.1021/acsnano.2c08480

Notes

The authors declare no competing financial interest.

ACKNOWLEDGMENTS

The authors acknowledge the funding from National Key R&D Program (2021YFA1201503), Natural Science Foundation of Jiangsu Province (BK 20210130), the Innovative and Entrepreneurial Doctor in Jiangsu Province (JSSCBS20211428), Natural Science Foundation of China (21972164; 22279161), and Shanxi Natural Science Basic Research Plan (no. 2022JQ-137). J.W. and S.P. acknowledge the financial support by the Alexander von Humboldt Foundation and the basic funding of the Helmholtz Association. H.A. acknowledges the Hong Kong Quantum AI Lab (HKQAI) for supporting his fellowship. K.V.T. thanks EU-Horizon 2020 and BEIS, UK for supporting the FUNMIN project (ACT, no. 299668), the Natural Sciences and Engineering Research Council, Canada (RGPIN 04598, RYY), the Department of Chemistry and Chemical sciences of Pharmacy (Sapienza University of Rome), the Department of Chemistry and Chemical Biology (McMaster University), and the Faculty of Land and Food Systems (University of British Columbia) for support.

VOCABULARY

Lithium dendrite, an accumulation of plated Li atom in one site with metallic microstructure morphology; it will penetrate through the separator, affected by the current density, electrolyte ingredients, and temperature; **dead lithium**, the main composition of inactive lithium detached or escaped from the conductive Li or matrix surface without any electron exchange; **solid electrolyte interphase**, a byproduct generated from the side reaction between metallic Li and electrolyte/solvents, which is electronically insulative but ionically conductive; **single atomic catalyst**, the ultimate size state of metal particles with 100% atomic exposure, which is usually dispersed or located on functional supports; **diffusion kinetics**, the evaluation of the migration rate of the carriers to the electrode/electrolyte surface or in the electrode interior

REFERENCES

(1) He, X.; Bresser, D.; Passerini, S.; Baakes, F.; Krewer, U.; Lopez, J.; Mallia, C. T.; Shao-Horn, Y.; Cekic-Laskovic, I.; Wiemers-Meyer, S.; Soto, F. A.; Ponce, V.; Seminario, J. M.; Balbuena, P. B.; Jia, H.; Xu, W.; Xu, Y.; Wang, C.; Horstmann, B.; Amine, R.; Su, C.-C.; Shi, J.; Amine, K.; Winter, M.; Latz, A.; Kostecki, R. The Passivity of Lithium Electrodes in Liquid Electrolytes for Secondary Batteries. *Nat. Rev. Mater.* **2021**, *6* (11), 1036−1052.

(2) Liu, B.; Zhang, J.-G.; Xu, W. Advancing Lithium Metal Batteries. *Joule* **2018**, *2* (5), 833−845.

(3) Larcher, D.; Tarascon, J. M. Towards Greener and More Sustainable Batteries for Electrical Energy Storage. *Nat. Chem.* **2015**, *7* (1), 19−29.

(4) Elia, G. A.; Marquardt, K.; Hoeppner, K.; Fantini, S.; Lin, R.; Knipping, E.; Peters, W.; Drillet, J. F.; Passerini, S.; Hahn, R. An Overview and Future Perspectives of Aluminum Batteries. *Adv. Mater.* **2016**, *28* (35), 7564−79.

(5) Assat, G.; Tarascon, J.-M. Fundamental Understanding and Practical Challenges of Anionic Redox Activity in Li-Ion Batteries. *Nat. Energy* **2018**, *3* (5), 373−386.

(6) Zhang, J.; You, C.; Lin, H.; Wang, J. Electrochemical Kinetic Modulators in Lithium−Sulfur Batteries: From Defect-Rich Catalysts to Single Atomic Catalysts. *Energy Environ. Mater.* **2022**, *5* (3), 731−750.

(7) Braga, M. H.; Grundish, N. S.; Murchison, A. J.; Goodenough, J. B. Alternative Strategy for a Safe Rechargeable Battery. *Energy Environ. Sci.* **2017**, *10* (1), 331−336.

(8) Huang, X.; Yang, J.; Mao, S.; Chang, J.; Hallac, P. B.; Fell, C. R.; Metz, B.; Jiang, J.; Hurley, P. T.; Chen, J. Controllable Synthesis of Hollow Si Anode for Long-Cycle-Life Lithium-Ion Batteries. *Adv. Mater.* **2014**, *26* (25), 4326−32.

(9) Li, X.; Su, H.; Ma, C.; Hou, K.; Wang, J.; Lin, H.; Shang, Y.; Liu, H. Optimizations of Graphitic Carbon/Silicon Hybrids for Scalable Preparation with High-Performance Lithium-Ion Storage. *ACS Sustain. Chem. Engi.* **2022**, *10* (17), 5590−5598.

(10) Elia, G. A.; Ulissi, U.; Jeong, S.; Passerini, S.; Hassoun, J. Exceptional Long-Life Performance of Lithium-Ion Batteries using Ionic Liquid-Based Electrolytes. *Energy Environ. Sci.* **2016**, *9* (10), 3210−3220.

(11) Wang, Q.; Jia, Z.; Li, L.; Wang, J.; Xu, G.; Ding, X.; Liu, N.; Liu, M.; Zhang, Y. Coupling Niobia Nanorods with a Multicomponent Carbon Network for High Power Lithium-Ion Batteries. *ACS Appl. Mater. Interfaces* **2019**, *11* (47), 44196−44203.
(12) Kang, Q.; Zhao, J.; Li, X.; Zhu, G.; Feng, X.; Ma, Y.; Huang, W.; Liu, J. A Single Wire as All-Inclusive fully Functional Supercapacitor. *Nano Energy* **2017**, *32*, 201−208.
(13) Fang, K.; Liu, D.; Xiang, X.; Zhu, X.; Tang, H.; Qu, D.; Xie, Z.; Li, J.; Qu, D. Air-Stable Red Phosphorus Anode for Potassium/Sodium-Ion Batteries Enabled through Dual-Protection Design. *Nano Energy* **2020**, *69*, 104451.
(14) Asadi, M.; Sayahpour, B.; Abbasi, P.; Ngo, A. T.; Karis, K.; Jokisaari, J. R.; Liu, C.; Narayanan, B.; Gerard, M.; Yasaei, P.; Hu, X.; Mukherjee, A.; Lau, K. C.; Assary, R. S.; Khalili-Araghi, F.; Klie, R. F.; Curtiss, L. A.; Salehi-Khojin, A. A Lithium-Oxygen Battery with a Long Cycle Life in an Air-Like Atmosphere. *Nature* **2018**, *555* (7697), 502−506.
(15) Wang, J.; Hu, H.; Zhang, J.; Li, L.; Jia, L.; Guan, Q.; Hu, H.; Liu, H.; Jia, Y.; Zhuang, Q.; Cheng, S.; Huang, M.; Lin, H. Hydrophobic Lithium Diffusion-Accelerating Layers Enables Long-Life Moisture-Resistant Metallic Lithium Anodes in Practical Harsh Environments. *Energy Storage Mater.* **2022**, *52*, 210−219.
(16) Zhang, J.; He, R.; Zhuang, Q.; Ma, X.; You, C.; Hao, Q.; Li, L.; Cheng, S.; Lei, L.; Deng, B.; Li, X.; Lin, H.; Wang, J. Tuning 4f-Center Electron Structure by Schottky Defects for Catalyzing Li Diffusion to Achieve Long-Term Dendrite-Free Lithium Metal Battery. *Adv. Sci. (Weinh)* **2022**, *9* (23), 2202244.
(17) Zhang, J.; Jia, L.; Lin, H.; Wang, J. Advances and Prospects of 2D Graphene-Based Materials/Hybrids for Lithium Metal−Sulfur Full Battery: From Intrinsic Property to Catalysis Modification. *Adv. Energy Sustain. Res.* **2022**, *3* (4), 2100187.
(18) Xu, J.; Tang, W.; Yang, C.; Manke, I.; Chen, N.; Lai, F.; Xu, T.; An, S.; Liu, H.; Zhang, Z.; Cao, Y.; Wang, N.; Zhao, S.; Niu, D.; Chen, R. A Highly Conductive COF@CNT Electrocatalyst Boosting Polysulfide Conversion for Li-S Chemistry. *ACS Energy Lett.* **2021**, *6* (9), 3053−3062.
(19) Cheng, X. B.; Zhang, R.; Zhao, C. Z.; Wei, F.; Zhang, J. G.; Zhang, Q. A Review of Solid Electrolyte Interphases on Lithium Metal Anode. *Adv. Sci. (Weinh)* **2016**, *3* (3), 1500213.
(20) Agostini, M.; Scrosati, B.; Hassoun, J. An Advanced Lithium-Ion Sulfur Battery for High Energy Storage. *Adv. Energy Mater.* **2015**, *5* (16), 1500481.
(21) Wang, J.; Zhang, J.; Duan, S.; Li, T.; Jia, L.; Liu, H.; Li, L.; Cheng, S.; Hu, H.; Huang, M.; Hu, H.; Zhang, S.; Xiao, Q.; Lin, H. Interfacial Lithium-Nitrogen Bond Catalyzes Sulfide Oxidation Reactions in High-Loading Li_2S Cathode. *Chem. Eng. J.* **2022**, *429*, 132352.
(22) Zhang, J.; You, C.; Zhang, W.; Wang, J.; Guo, S.; Yang, R.; Xu, Y. Conductive Bridging Effect of TiN Nanoparticles on the Electrochemical Performance of TiN@CNT-S Composite Cathode. *Electrochim. Acta* **2017**, *250*, 159−166.
(23) Dubal, D. P.; Ayyad, O.; Ruiz, V.; Gomez-Romero, P. Hybrid Energy Storage: the Merging of Battery and Supercapacitor Chemistries. *Chem. Soc. Rev.* **2015**, *44* (7), 1777−90.
(24) Zhang, J.; Su, Y.; Zhang, Y. Recent Advances in Research on Anodes for Safe and Efficient Lithium-Metal Batteries. *Nanoscale* **2020**, *12* (29), 15528−15559.
(25) Zhang, J.; Duan, S.; You, C.; Wang, J.; Liu, H.; Guo, S.; Zhang, W.; Yang, R. In situ-Grown Tungsten Carbide Nanoparticles on Nanocarbon as an Electrocatalyst to Promote the Redox Reaction Kinetics of High-Mass Loading Sulfur Cathode for High Volumetric Performance. *J. Mater. Chem. A* **2020**, *8* (42), 22240−22250.
(26) Zhou, G.; Chen, H.; Cui, Y. Formulating Energy Density for Designing Practical Lithium−Sulfur Batteries. *Nat. Energy* **2022**, *7* (4), 312−319.
(27) Zhao, C.; Xu, G. L.; Yu, Z.; Zhang, L.; Hwang, I.; Mo, Y. X.; Ren, Y.; Cheng, L.; Sun, C. J.; Ren, Y.; Zuo, X.; Li, J. T.; Sun, S. G.; Amine, K.; Zhao, T. A High-Energy and Long-Cycling Lithium-Sulfur Pouch Cell via a Macroporous Catalytic Cathode with Double-End Binding Sites. *Nat. Nanotechnol.* **2021**, *16* (2), 166−173.
(28) Li, H.; Liu, D.; Zhu, X.; Qu, D.; Xie, Z.; Li, J.; Tang, H.; Zheng, D.; Qu, D. Integrated 3D Electrodes Based on Metal-Nitrogen-Doped Graphitic Ordered Mesoporous Carbon and Carbon Paper for High-Loading Lithium-Sulfur Batteries. *Nano Energy* **2020**, *73*, 104763.
(29) Wang, D.; Zhang, W.; Zheng, W.; Cui, X.; Rojo, T.; Zhang, Q. Towards High-Safe Lithium Metal Anodes: Suppressing Lithium Dendrites via Tuning Surface Energy. *Adv. Sci. (Weinh)* **2017**, *4* (1), 1600168.
(30) Zheng, Z. J.; Ye, H.; Guo, Z. P. Recent Progress in Designing Stable Composite Lithium Anodes with Improved Wettability. *Adv. Sci. (Weinh)* **2020**, *7* (22), 2002212.
(31) Peng, H. J.; Huang, J. Q.; Cheng, X. B.; Zhang, Q. Review on High-Loading and High-Energy Lithium-Sulfur Batteries. *Adv. Energy Mater.* **2017**, *7* (24), 1700260.
(32) Zhang, K.; Lee, G.-H.; Park, M.; Li, W.; Kang, Y.-M. Recent Developments of the Lithium Metal Anode for Rechargeable Non-Aqueous Batteries. *Adv. Energy Mater.* **2016**, *6* (20), 1600811.
(33) Qian, J.; Adams, B. D.; Zheng, J.; Xu, W.; Henderson, W. A.; Wang, J.; Bowden, M. E.; Xu, S.; Hu, J.; Zhang, J.-G. Anode-Free Rechargeable Lithium Metal Batteries. *Adv. Funct. Mater.* **2016**, *26* (39), 7094−7102.
(34) Chang, Z.; Qiao, Y.; Deng, H.; Yang, H.; He, P.; Zhou, H. A Liquid Electrolyte with De-Solvated Lithium Ions for Lithium-Metal Battery. *Joule* **2020**, *4* (8), 1776−1789.
(35) Kang, Q.; Li, Y.; Zhuang, Z.; Wang, D.; Zhi, C.; Jiang, P.; Huang, X. Dielectric Polymer Based Electrolytes for High-Performance All-Solid-State Lithium Metal Batteries. *J. Energy Chem.* **2022**, *69*, 194−204.
(36) Wang, D.; Liu, Y.; Li, G.; Qin, C.; Huang, L.; Wu, Y. Liquid Metal Welding to Suppress Li Dendrite by Equalized Heat Distribution. *Adv. Funct. Mater.* **2021**, *31* (47), 2106740.
(37) Wang, J.; Kang, Q.; Yuan, J.; Fu, Q.; Chen, C.; Zhai, Z.; Liu, Y.; Yan, W.; Li, A.; Zhang, J. Dendrite-Free Lithium and Sodium Metal Anodes with Deep Plating/Stripping Properties for Lithium and Sodium Batteries. *Carbon Energy* **2021**, *3* (1), 153−166.
(38) Wang, D.; Luan, C.; Zhang, W.; Liu, X. F.; Sun, L. S.; Liang, Q.; Qin, T. T.; Zhao, Z. Z.; Zhou, Y.; Wang, P.; Zheng, W. T. Zipper-Inspired SEI Film for Remarkably Enhancing the Stability of Li Metal Anode via Nucleation Barriers Controlled Weaving of Lithium Pits. *Adv. Energy Mater.* **2018**, *8* (21), 1800650.
(39) Chang, Z.; Qiao, Y.; Yang, H.; Deng, H.; Zhu, X.; He, P.; Zhou, H. Beyond the Concentrated Electrolyte: further Depleting Solvent Molecules within a Li^+ Solvation Sheath to Stabilize High-Energy-Density Lithium Metal Batteries. *Energy Environ. Sci.* **2020**, *13* (11), 4122−4131.
(40) Chu, C.; Li, R.; Cai, F.; Bai, Z.; Wang, Y.; Xu, X.; Wang, N.; Yang, J.; Dou, S. Recent Advanced Skeletons in Sodium Metal Anodes. *Energy Environ. Sci.* **2021**, *14* (8), 4318−4340.
(41) Hu, A.; Chen, W.; Du, X.; Hu, Y.; Lei, T.; Wang, H.; Xue, L.; Li, Y.; Sun, H.; Yan, Y.; Long, J.; Shu, C.; Zhu, J.; Li, B.; Wang, X.; Xiong, J. An Artificial Hybrid Interphase for an Ultrahigh-Rate and Practical Lithium Metal Anode. *Energy Environ. Sci.* **2021**, *14* (7), 4115−4124.
(42) Horstmann, B.; Shi, J.; Amine, R.; Werres, M.; He, X.; Jia, H.; Hausen, F.; Cekic-Laskovic, I.; Wiemers-Meyer, S.; Lopez, J.; Galvez-Aranda, D.; Baakes, F.; Bresser, D.; Su, C.-C.; Xu, Y.; Xu, W.; Jakes, P.; Eichel, R.-A.; Figgemeier, E.; Krewer, U.; Seminario, J. M.; Balbuena, P. B.; Wang, C.; Passerini, S.; Shao-Horn, Y.; Winter, M.; Amine, K.; Kostecki, R.; Latz, A. Strategies towards Enabling Lithium Metal in Batteries: Interphases and Electrodes. *Energy Environ. Sci.* **2021**, *14* (10), 5289−5314.
(43) Liu, Y.; Gao, D.; Xiang, H.; Feng, X.; Yu, Y. Research Progress on Copper-Based Current Collector for Lithium Metal Batteries. *Energy Fuels* **2021**, *35* (16), 12921−12937.
(44) Tao, X.; Wang, J.; Liu, C.; Wang, H.; Yao, H.; Zheng, G.; Seh, Z. W.; Cai, Q.; Li, W.; Zhou, G.; Zu, C.; Cui, Y. Balancing Surface Adsorption and Diffusion of Lithium-Polysulfides on Nonconductive

Oxides for Lithium−Sulfur Battery Design. *Nat. Commun.* **2016**, *7*, 11203.
(45) Holoubek, J.; Liu, H.; Wu, Z.; Yin, Y.; Xing, X.; Cai, G.; Yu, S.; Zhou, H.; Pascal, T. A.; Chen, Z.; Liu, P. Tailoring Electrolyte Solvation for Li Metal Batteries Cycled at Ultra-Low Temperature. *Nat. Energy* **2021**, *6*, 303.
(46) Chang, Z.; Yang, H.; Zhu, X.; He, P.; Zhou, H. A Stable Quasi-Solid Electrolyte Improves the Safe Operation of Highly Efficient Lithium-Metal Pouch Cells in Harsh Environments. *Nat. Commun.* **2022**, *13* (1), 1510.
(47) Yang, Y.; Yao, S.; Liang, Z.; Wen, Y.; Liu, Z.; Wu, Y.; Liu, J.; Zhu, M. A Self-Supporting Covalent Organic Framework Separator with Desolvation Effect for High Energy Density Lithium Metal Batteries. *ACS Energy Lett.* **2022**, *7* (2), 885−896.
(48) Wang, J.; Yang, J.; Xiao, Q.; Zhang, J.; Li, T.; Jia, L.; Wang, Z.; Cheng, S.; Li, L.; Liu, M.; Liu, H.; Lin, H.; Zhang, Y. In Situ Self-Assembly of Ordered Organic/Inorganic Dual-Layered Interphase for Achieving Long-Life Dendrite-Free Li Metal Anodes in LiFSI-Based Electrolyte. *Adv. Funct. Mater.* **2021**, *31* (7), 2007434.
(49) Liu, X.; Liu, J.; Qian, T.; Chen, H.; Yan, C. Novel Organophosphate-Derived Dual-Layered Interface Enabling Air-Stable and Dendrite-Free Lithium Metal Anode. *Adv. Mater.* **2020**, *32* (2), 1902724.
(50) Qin, B.; Cai, Y.; Si, X.; Li, C.; Cao, J.; Fei, W.; Qi, J. Ultra-Lightweight Ion-Sieving Membranes for High-Rate Lithium Sulfur Batteries. *Chem. Eng. J.* **2022**, *430*, 132698.
(51) Qian, S.; Xing, C.; Zheng, M.; Su, Z.; Chen, H.; Wu, Z.; Lai, C.; Zhang, S. $CuCl_2$-Modified Lithium Metal Anode via Dynamic Protection Mechanisms for Dendrite-Free Long-Life Charging/Discharge Processes. *Adv. Energy Mater.* **2022**, *12* (15), 2103480.
(52) Liu, X.; Mariani, A.; Zarrabeitia, M.; Di Pietro, M. E.; Dong, X.; Elia, G. A.; Mele, A.; Passerini, S. Effect of Organic Cations in Locally Concentrated Ionic Liquid Electrolytes on the Electrochemical Performance of Lithium Metal Batteries. *Energy Storage Mater.* **2022**, *44*, 370−378.
(53) Hou, L. P.; Yao, N.; Xie, J.; Shi, P.; Sun, S. Y.; Jin, C. B.; Chen, C. M.; Liu, Q. B.; Li, B. Q.; Zhang, X. Q.; Zhang, Q. Modification of Nitrate Ion Enables Stable Solid Electrolyte Interphase in Lithium Metal Batteries. *Angew. Chem., Int. Ed. Engl.* **2022**, *61* (20), 202201406.
(54) Zhang, Q.; Liu, S.; Lu, Y.; Xing, L.; Li, W. Artificial Interphases Enable Dendrite-Free Li-Metal Anodes. *J. Energy Chem.* **2021**, *58*, 198−206.
(55) Wu, J.; Rao, Z.; Liu, X.; Shen, Y.; Fang, C.; Yuan, L.; Li, Z.; Zhang, W.; Xie, X.; Huang, Y. Polycationic Polymer Layer for Air-Stable and Dendrite-Free Li Metal Anodes in Carbonate Electrolytes. *Adv. Mater.* **2021**, *33* (12), 2007428.
(56) Fu, L.; Wang, X.; Wang, L.; Wan, M.; Li, Y.; Cai, Z.; Tan, Y.; Li, G.; Zhan, R.; Seh, Z. W.; Sun, Y. A Salt-in-Metal Anode: Stabilizing the Solid Electrolyte Interphase to Enable Prolonged Battery Cycling. *Adv. Funct. Mater.* **2021**, *31* (19), 2010602.
(57) Kang, D.; Sardar, S.; Zhang, R.; Noam, H.; Chen, J.; Ma, L.; Liang, W.; Shi, C.; Lemmon, J. P. In-situ Organic SEI Layer for Dendrite-Free Lithium Metal Anode. *Energy Storage Mater.* **2020**, *27*, 69−77.
(58) Eshetu, G. G.; Elia, G. A.; Armand, M.; Forsyth, M.; Komaba, S.; Rojo, T.; Passerini, S. Electrolytes and Interphases in Sodium-Based Rechargeable Batteries: Recent Advances and Perspectives. *Adv. Energy Mater.* **2020**, *10* (20), 2000093.
(59) Xu, R.; Cheng, X.-B.; Yan, C.; Zhang, X.-Q.; Xiao, Y.; Zhao, C.-Z.; Huang, J.-Q.; Zhang, Q. Artificial Interphases for Highly Stable Lithium Metal Anode. *Matter* **2019**, *1* (2), 317−344.
(60) Wang, W.; Yue, X.; Meng, J.; Wang, J.; Wang, X.; Chen, H.; Shi, D.; Fu, J.; Zhou, Y.; Chen, J.; Fu, Z. Lithium Phosphorus Oxynitride as an Efficient Protective Layer on Lithium Metal Anodes for Advanced Lithium-Sulfur Batteries. *Energy Storage Mater.* **2019**, *18*, 414−422.
(61) Wang, J.; Yan, W.; Zhang, J. High Area Capacity and Dendrite-Free Anode Constructed by Highly Potassiophilic Pd/Cu Current Collector for Low-Temperature Potassium Metal Battery. *Nano Energy* **2022**, *96*, 107131.
(62) Wang, J.; Yuan, J.; Chen, C.; Wang, L.; Zhai, Z.; Fu, Q.; Liu, Y.; Dong, L.; Yan, W.; Li, A.; Zhang, J. Cu_3Pt Alloy-Functionalized Cu Mesh as Current Collector for Dendritic-Free Anodes of Potassium Metal Batteries. *Nano Energy* **2020**, *75*, 104914.
(63) Zhang, J.; Chen, H.; Wen, M.; Shen, K.; Chen, Q.; Hou, G.; Tang, Y. Lithiophilic 3D Copper-Based Magnetic Current Collector for Lithium-Free Anode to Realize Deep Lithium Deposition. *Adv. Funct. Mater.* **2022**, *32* (13), 2110110.
(64) Yang, T.; Li, L.; Zhao, T.; Ye, Y.; Ye, Z.; Xu, S.; Wu, F.; Chen, R. From Flower-Like to Spherical Deposition: A GCNT Aerogel Scaffold for Fast-Charging Lithium Metal Batteries. *Adv. Energy Mater.* **2021**, *11* (42), 2102454.
(65) Li, Z.; He, Q.; Zhou, C.; Li, Y.; Liu, Z.; Hong, X.; Xu, X.; Zhao, Y.; Mai, L. Rationally Design Lithiophilic Surfaces toward High−Energy Lithium Metal Battery. *Energy Storage Mater.* **2021**, *37*, 40−46.
(66) Zhang, Y.; Wang, C.; Pastel, G.; Kuang, Y.; Xie, H.; Li, Y.; Liu, B.; Luo, W.; Chen, C.; Hu, L. 3D Wettable Framework for Dendrite-Free Alkali Metal Anodes. *Adv. Energy Mater.* **2018**, *8* (18), 1800635.
(67) Xie, J.; Wang, J.; Lee, H. R.; Yan, K.; Li, Y.; Shi, F.; Huang, W.; Pei, A.; Chen, G.; Subbaraman, R.; Christensen, J.; Cui, Y. Engineering Stable Interfaces for Three-Dimensional Lithium Metal Anodes. *Sci. Adv.* **2018**, *4* (7), eaat5168.
(68) Wang, G.; Xiong, X.; Lin, Z.; Zheng, J.; Fenghua, Z.; Li, Y.; Liu, Y.; Yang, C.; Tang, Y.; Liu, M. Uniform Li Deposition Regulated via Three-Dimensional Polyvinyl Alcohol Nanofiber Networks for Effective Li Metal Anodes. *Nanoscale* **2018**, *10* (21), 10018−10024.
(69) Rong, G.; Zhang, X.; Zhao, W.; Qiu, Y.; Liu, M.; Ye, F.; Xu, Y.; Chen, J.; Hou, Y.; Li, W.; Duan, W.; Zhang, Y. Liquid-Phase Electrochemical Scanning Electron Microscopy for In Situ Investigation of Lithium Dendrite Growth and Dissolution. *Adv. Mater.* **2017**, *29* (13), 1606187.
(70) Yan, C.; Cheng, X. B.; Tian, Y.; Chen, X.; Zhang, X. Q.; Li, W. J.; Huang, J. Q.; Zhang, Q. Dual-Layered Film Protected Lithium Metal Anode to Enable Dendrite-Free Lithium Deposition. *Adv. Mater.* **2018**, *30* (25), 1707629.
(71) Choudhury, S.; Archer, L. A. Lithium Fluoride Additives for Stable Cycling of Lithium Batteries at High Current Densities. *Adv. Electron. Mater.* **2016**, *2* (2), 1500246.
(72) Liu, Y.; Lin, D.; Yuen, P. Y.; Liu, K.; Xie, J.; Dauskardt, R. H.; Cui, Y. An Artificial Solid Electrolyte Interphase with High Li-Ion Conductivity, Mechanical Strength, and Flexibility for Stable Lithium Metal Anodes. *Adv. Mater.* **2017**, *29* (10), 1605531.
(73) Bai, M.; Xie, K.; Yuan, K.; Zhang, K.; Li, N.; Shen, C.; Lai, Y.; Vajtai, R.; Ajayan, P.; Wei, B. A Scalable Approach to Dendrite-Free Lithium Anodes via Spontaneous Reduction of Spray-Coated Graphene Oxide Layers. *Adv. Mater.* **2018**, *30*, 1801213.
(74) Zhang, C.; Lyu, R.; Lv, W.; Li, H.; Jiang, W.; Li, J.; Gu, S.; Zhou, G.; Huang, Z.; Zhang, Y.; Wu, J.; Yang, Q. H.; Kang, F. A Lightweight 3D Cu Nanowire Network with Phosphidation Gradient as Current Collector for High-Density Nucleation and Stable Deposition of Lithium. *Adv. Mater.* **2019**, *31* (48), 1904991.
(75) Li, Q.; Zhu, S.; Lu, Y. 3D Porous Cu Current Collector/Li-Metal Composite Anode for Stable Lithium-Metal Batteries. *Adv. Funct. Mater.* **2017**, *27* (18), 1606422.
(76) Wang, J.; Zhang, J.; Cheng, S.; Yang, J.; Xi, Y.; Hou, X.; Xiao, Q.; Lin, H. Long-Life Dendrite-Free Lithium Metal Electrode Achieved by Constructing a Single Metal Atom Anchored in a Diffusion Modulator Layer. *Nano Lett.* **2021**, *21* (7), 3245−3253.
(77) Wang, J.; Hu, H.; Duan, S.; Xiao, Q.; Zhang, J.; Liu, H.; Kang, Q.; Jia, L.; Yang, J.; Xu, W.; Fei, H.; Cheng, S.; Li, L.; Liu, M.; Lin, H.; Zhang, Y. Construction of Moisture-Stable Lithium Diffusion-Controlling Layer toward High Performance Dendrite-Free Lithium Anode. *Adv. Funct. Mater.* **2022**, *32* (12), 2110468.
(78) Hu, Y. Z.; Li, L. G.; Tu, H. F.; Yi, X. H.; Wang, J.; Xu, J. J.; Gong, W. B.; Lin, H. Z.; Wu, X. D.; Liu, M. N. Janus Electrolyte with Modified Li^+ Solvation for High-Performance Solid-State Lithium Batteries. *Adv. Funct. Mater.* **2022**, *32*, 2203336.

(79) Chen, X. R.; Yao, Y. X.; Yan, C.; Zhang, R.; Cheng, X. B.; Zhang, Q. A Diffusion–Reaction Competition Mechanism to Tailor Lithium Deposition for Lithium-Metal Batteries. *Angew. Chem., Int. Ed. Engl.* **2020**, *59* (20), 7743−7747.
(80) Li, L.; Wang, M.; Wang, J.; Ye, F.; Wang, S.; Xu, Y.; Liu, J.; Xu, G.; Zhang, Y.; Zhang, Y.; Yan, C.; Medhekar, N. V.; Liu, M.; Zhang, Y. Asymmetric Gel Polymer Electrolyte with High Lithium Ion Conductivity for Dendrite-Free Lithium Metal Batteries. *J. Mater. Chem. A* **2020**, *8* (16), 8033−8040.
(81) Liu, Y.; Liu, Q.; Xin, L.; Liu, Y.; Yang, F.; Stach, E. A.; Xie, J. Making Li-Metal Electrodes Rechargeable by Controlling the Dendrite Growth Direction. *Nat. Energy* **2017**, *2*, 17083.
(82) Tu, Z.; Choudhury, S.; Zachman, M. J.; Wei, S.; Zhang, K.; Kourkoutis, L. F.; Archer, L. A. Fast Ion Transport at Solid−Solid Interfaces in Hybrid Battery Anodes. *Nat. Energy* **2018**, *3* (4), 310−316.
(83) Wang, J.; Zhang, J.; Duan, S.; Jia, L.; Xiao, Q.; Liu, H.; Hu, H.; Cheng, S.; Zhang, Z.; Li, L.; Duan, W.; Zhang, Y.; Lin, H. Lithium Atom Surface Diffusion and Delocalized Deposition Propelled by Atomic Metal Catalyst towards Ultrahigh-capacity Dendrite-free Lithium Anode. *Nano Lett.* **2022**, *22*, 8008−8017.
(84) Tu, Z.; Choudhury, S.; Zachman, M. J.; Wei, S.; Zhang, K.; Kourkoutis, L. F.; Archer, L. A. Designing Artificial Solid-Electrolyte Interphases for Single-Ion and High-Efficiency Transport in Batteries. *Joule* **2017**, *1* (2), 394−406.
(85) Wang, J.; Jia, L.; Lin, H.; Zhang, Y. Single-Atomic Catalysts Embedded on Nanocarbon Supports for High Energy Density Lithium-Sulfur Batteries. *ChemSusChem* **2020**, *13* (13), 3404−3411.
(86) Wang, J.; Jia, L.; Duan, S.; Liu, H.; Xiao, Q.; Li, T.; Fan, H.; Feng, K.; Yang, J.; Wang, Q.; Liu, M.; Zhong, J.; Duan, W.; Lin, H.; Zhang, Y. Single Atomic Cobalt Catalyst Significantly Accelerates Lithium Ion Diffusion in High Mass Loading Li_2S Cathode. *Energy Storage Mater.* **2020**, *28*, 375−382.
(87) Wang, J.; Jia, L.; Zhong, J.; Xiao, Q.; Wang, C.; Zang, K.; Liu, H.; Zheng, H.; Luo, J.; Yang, J.; Fan, H.; Duan, W.; Wu, Y.; Lin, H.; Zhang, Y. Single-Atom Catalyst Boosts Electrochemical Conversion Reactions in Batteries. *Energy Storage Mater.* **2019**, *18*, 246−252.
(88) Biswal, P.; Stalin, S.; Kludze, A.; Choudhury, S.; Archer, L. A. Nucleation and Early Stage Growth of Li Electrodeposits. *Nano Lett.* **2019**, *19* (11), 8191−8200.
(89) Hou, T. Z.; Xu, W. T.; Chen, X.; Peng, H. J.; Huang, J. Q.; Zhang, Q. Lithium Bond Chemistry in Lithium-Sulfur Batteries. *Angew. Chem., Int. Ed. Engl.* **2017**, *56* (28), 8178−8182.
(90) Liu, T.; Lin, Z.; Wang, D.; Zhang, M.; Hu, Q.; Tan, L.; Wu, Y.; Zhang, X.; Huang, H.; Wang, J. Aluminum Electrolysis Derivative Spent Cathodic Carbon for Dendrite-Free Li Metal Anode. *Mater. Today Energy* **2020**, *17*, 100465.
(91) Sheng, L.; Wang, Q.; Liu, X.; Cui, H.; Wang, X.; Xu, Y.; Li, Z.; Wang, L.; Chen, Z.; Xu, G. L.; Wang, J.; Tang, Y.; Amine, K.; Xu, H.; He, X. Suppressing Electrolyte-Lithium Metal Reactivity via Li(+)-Desolvation in Uniform Nano-porous Separator. *Nat. Commun.* **2022**, *13* (1), 172.
(92) Yang, Z.; Dang, Y.; Zhai, P.; Wei, Y.; Chen, Q.; Zuo, J.; Gu, X.; Yao, Y.; Wang, X.; Zhao, F.; Wang, J.; Yang, S.; Tang, P.; Gong, Y. Single-Atom Reversible Lithiophilic Sites toward Stable Lithium Anodes. *Adv. Energy Mater.* **2022**, *12* (8), 2103368.
(93) Dong, K.; Xu, Y.; Tan, J.; Osenberg, M.; Sun, F.; Kochovski, Z.; Pham, D. T.; Mei, S.; Hilger, A.; Ryan, E.; Lu, Y.; Banhart, J.; Manke, I. Unravelling the Mechanism of Lithium Nucleation and Growth and the Interaction with the Solid Electrolyte Interface. *ACS Energy Lett.* **2021**, *6* (5), 1719−1728.
(94) Wang, J.; Cheng, S.; Li, L.; Jia, L.; Wu, J.; Li, X.; Guan, Q.; Hu, H.; Zhang, J.; Lin, H. Robust Interfacial Engineering Construction to Alleviate Polysulfide Shuttling in Metal Sulfide Electrodes for Achieving Fast-Charge High-Capacity Lithium Storages. *Chem. Eng. J.* **2022**, *446*, 137291.
(95) Jiang, C.; Gu, Y.; Tang, M.; Chen, Y.; Wu, Y.; Ma, J.; Wang, C.; Hu, W. Toward Stable Lithium Plating/Stripping by Successive Desolvation and Exclusive Transport of Li Ions. *ACS Appl. Mater. Interfaces* **2020**, *12* (9), 10461−10470.
(96) Ye, Y.; Song, M.-K.; Xu, Y.; Nie, K.; Liu, Y.-s.; Feng, J.; Sun, X.; Cairns, E. J.; Zhang, Y.; Guo, J. Lithium Nitrate: A Double-Edged Sword in the Rechargeable Lithium-Sulfur Cell. *Energy Storage Mater.* **2019**, *16*, 498−504.
(97) Um, J. H.; Yu, S. H. Unraveling the Mechanisms of Lithium Metal Plating/Stripping via In Situ/Operando Analytical Techniques. *Adv. Energy Mater.* **2021**, *11* (27), 2003004.
(98) Sun, H.; Liu, Q.; Chen, J.; Li, Y.; Ye, H.; Zhao, J.; Geng, L.; Dai, Q.; Yang, T.; Li, H.; Wang, Z.; Zhang, L.; Tang, Y.; Huang, J. In Situ Visualization of Lithium Penetration through Solid Electrolyte and Dead Lithium Dynamics in Solid-State Lithium Metal Batteries. *ACS Nano* **2021**, *15* (12), 19070−19079.
(99) Cha, E.; Patel, M. D.; Park, J.; Hwang, J.; Prasad, V.; Cho, K.; Choi, W. 2D MoS_2 as an Efficient Protective Layer for Lithium Metal Anodes in High-Performance Li-S Batteries. *Nat. Nanotechnol.* **2018**, *13* (4), 337−344.
(100) Wang, L.; Zhang, L.; Wang, Q.; Li, W.; Wu, B.; Jia, W.; Wang, Y.; Li, J.; Li, H. Long Lifespan Lithium Metal Anodes Enabled by Al_2O_3 Sputter Coating. *Energy Storage Mater.* **2018**, *10*, 16−23.
(101) Zhou, Y.; Zhang, X.; Ding, Y.; Bae, J.; Guo, X.; Zhao, Y.; Yu, G. Redistributing Li-Ion Flux by Parallelly Aligned Holey Nanosheets for Dendrite-Free Li Metal Anodes. *Adv. Mater.* **2020**, *32* (38), 2003920.
(102) Chen, L.; Connell, J. G.; Nie, A.; Huang, Z.; Zavadil, K. R.; Klavetter, K. C.; Yuan, Y.; Sharifi-Asl, S.; Shahbazian-Yassar, R.; Libera, J. A.; Mane, A. U.; Elam, J. W. Lithium Metal Protected by Atomic Layer Deposition Metal Oxide for High Performance Anodes. *J. Mater. Chem. A* **2017**, *5* (24), 12297−12309.
(103) Guo, Y.; Li, H.; Zhai, T. Reviving Lithium-Metal Anodes for Next-Generation High-Energy Batteries. *Adv. Mater.* **2017**, *29* (29), 1700007.
(104) Tao, T.; Lu, S.; Fan, Y.; Lei, W.; Huang, S.; Chen, Y. Anode Improvement in Rechargeable Lithium-Sulfur Batteries. *Adv. Mater.* **2017**, *29* (48), 1700542.
(105) Wang, J.; Cheng, S.; Li, W.; Jia, L.; Xiao, Q.; Hou, Y.; Zheng, Z.; Li, H.; Zhang, S.; Zhou, L.; Liu, M.; Lin, H.; Zhang, Y. Robust Electrical "Highway" Network for High Mass Loading Sulfur Cathode. *Nano Energy* **2017**, *40*, 390−398.
(106) Xu, J.; An, S.; Song, X.; Cao, Y.; Wang, N.; Qiu, X.; Zhang, Y.; Chen, J.; Duan, X.; Huang, J.; Li, W.; Wang, Y. Towards High Performance Li-S Batteries via Sulfonate-Rich COF-Modified Separator. *Adv. Mater.* **2021**, *33*, 2105178.
(107) Li, S.; Lin, J.; Ding, Y.; Xu, P.; Guo, X.; Xiong, W.; Wu, D. Y.; Dong, Q.; Chen, J.; Zhang, L. Defects Engineering of Lightweight Metal-Organic Frameworks-Based Electrocatalytic Membrane for High-Loading Lithium-Sulfur Batteries. *ACS Nano* **2021**, *15*, 13803−13813.
(108) Qin, K.; Holguin, K.; Mohammadiroudbari, M.; Huang, J.; Kim, E. Y. S.; Hall, R.; Luo, C. Strategies in Structure and Electrolyte Design for High-Performance Lithium Metal Batteries. *Adv. Funct. Mater.* **2021**, *31* (15), 2009694.
(109) Chen, K.; Pathak, R.; Gurung, A.; Adhamash, E. A.; Bahrami, B.; He, Q.; Qiao, H.; Smirnova, A. L.; Wu, J. J.; Qiao, Q.; Zhou, Y. Flower-Shaped Lithium Nitride as a Protective Layer via Facile Plasma Activation for Stable Lithium Metal Anodes. *Energy Storage Mater.* **2019**, *18*, 389−396.
(110) Chen, C.; Liang, Q.; Wang, G.; Liu, D.; Xiong, X. Grain-Boundary-Rich Artificial SEI Layer for High-Rate Lithium Metal Anodes. *Adv. Funct. Mater.* **2022**, *32* (4), 2107249.
(111) Chen, L.; Chen, K. S.; Chen, X.; Ramirez, G.; Huang, Z.; Geise, N. R.; Steinruck, H. G.; Fisher, B. L.; Shahbazian-Yassar, R.; Toney, M. F.; Hersam, M. C.; Elam, J. W. Novel ALD Chemistry Enabled Low-Temperature Synthesis of Lithium Fluoride Coatings for Durable Lithium Anodes. *ACS Appl. Mater. Interfaces* **2018**, *10* (32), 26972−26981.
(112) Cui, C.; Yang, C.; Eidson, N.; Chen, J.; Han, F.; Chen, L.; Luo, C.; Wang, P. F.; Fan, X.; Wang, C. A Highly Reversible,

Dendrite-Free Lithium Metal Anode Enabled by a Lithium-Fluoride-Enriched Interphase. *Adv. Mater.* **2020**, *32* (12), 1906427.
(113) Li, W.; Yao, H.; Yan, K.; Zheng, G.; Liang, Z.; Chiang, Y. M.; Cui, Y. The Synergetic Effect of Lithium Polysulfide and Lithium Nitrate to Prevent Lithium Dendrite Growth. *Nat. Commun.* **2015**, *6*, 7436.
(114) Yao, Y.; Wang, H.; Yang, H.; Zeng, S.; Xu, R.; Liu, F.; Shi, P.; Feng, Y.; Wang, K.; Yang, W.; Wu, X.; Luo, W.; Yu, Y. A Dual-Functional Conductive Framework Embedded with TiN-VN Heterostructures for Highly Efficient Polysulfide and Lithium Regulation toward Stable Li-S Full Batteries. *Adv. Mater.* **2020**, *32* (6), 1905658.
(115) Liu, F.; Wang, L.; Zhang, Z.; Shi, P.; Feng, Y.; Yao, Y.; Ye, S.; Wang, H.; Wu, X.; Yu, Y. A Mixed Lithium-Ion Conductive Li_2S/Li_2Se Protection Layer for Stable Lithium Metal Anode. *Adv. Funct. Mater.* **2020**, *30* (23), 2001607.
(116) Liu, K.; Pei, A.; Lee, H. R.; Kong, B.; Liu, N.; Lin, D.; Liu, Y.; Liu, C.; Hsu, P. C.; Bao, Z.; Cui, Y. Lithium Metal Anodes with an Adaptive "Solid-Liquid" Interfacial Protective Layer. *J. Am. Chem. Soc.* **2017**, *139* (13), 4815−4820.
(117) Wang, C.; Fu, X.; Lin, S.; Liu, J.; Zhong, W.-H. A Protein-Enabled Protective Film with Functions of Self-Adapting and Anion-Anchoring for Stabilizing Lithium-Metal Batteries. *J. Energy Chem.* **2022**, *64*, 485−495.
(118) Zheng, G.; Wang, C.; Pei, A.; Lopez, J.; Shi, F.; Chen, Z.; Sendek, A. D.; Lee, H.-W.; Lu, Z.; Schneider, H.; Safont-Sempere, M. M.; Chu, S.; Bao, Z.; Cui, Y. High-Performance Lithium Metal Negative Electrode with a Soft and Flowable Polymer Coating. *ACS Energy Lett.* **2016**, *1* (6), 1247−1255.
(119) Luo, J.; Fang, C.-C.; Wu, N.-L. High Polarity Poly(vinylidene difluoride) Thin Coating for Dendrite-Free and High-Performance Lithium Metal Anodes. *Adv. Energy Mater.* **2018**, *8* (2), 1701482.
(120) Xiang, J.; Cheng, Z.; Zhao, Y.; Zhang, B.; Yuan, L.; Shen, Y.; Guo, Z.; Zhang, Y.; Jiang, J.; Huang, Y. A Lithium-Ion Pump Based on Piezoelectric Effect for Improved Rechargeability of Lithium Metal Anode. *Adv. Sci. (Weinh)* **2019**, *6* (22), 1901120.
(121) Dong, H.; Xiao, X.; Jin, C.; Wang, X.; Tang, P.; Wang, C.; Yin, Y.; Wang, D.; Yang, S.; Wu, C. High lithium-Ion Conductivity Polymer Film to Suppress Dendrites in Li Metal Batteries. *J. Power Sources* **2019**, *423*, 72−79.
(122) Zhang, W.; Zhang, S.; Fan, L.; Gao, L.; Kong, X.; Li, S.; Li, J.; Hong, X.; Lu, Y. Tuning the LUMO Energy of an Organic Interphase to Stabilize Lithium Metal Batteries. *ACS Energy Lett.* **2019**, *4* (3), 644−650.
(123) Wang, J.; Si, L.; Wei, Q.; Hong, X.; Cai, S.; Cai, Y. Covalent Organic Frameworks as the Coating Layer of Ceramic Separator for High-Efficiency Lithium−Sulfur Batteries. *ACS Appl. Nano Mater.* **2018**, *1* (1), 132−138.
(124) Chen, D.; Huang, S.; Zhong, L.; Wang, S.; Xiao, M.; Han, D.; Meng, Y. In Situ Preparation of Thin and Rigid COF Film on Li Anode as Artificial Solid Electrolyte Interphase Layer Resisting Li Dendrite Puncture. *Adv. Funct. Mater.* **2020**, *30* (7), 1907717.
(125) Xu, R.; Zhang, X.-Q.; Cheng, X.-B.; Peng, H.-J.; Zhao, C.-Z.; Yan, C.; Huang, J.-Q. Artificial Soft-Rigid Protective Layer for Dendrite-Free Lithium Metal Anode. *Adv. Funct. Mater.* **2018**, *28* (8), 1705838.
(126) Ye, S.; Wang, L.; Liu, F.; Shi, P.; Wang, H.; Wu, X.; Yu, Y. g-C3N4 Derivative Artificial Organic/Inorganic Composite Solid Electrolyte Interphase Layer for Stable Lithium Metal Anode. *Adv. Energy Mater.* **2020**, *10* (44), 2002647.
(127) Liu, P.; Zhang, J.; Zhong, L.; Huang, S.; Gong, L.; Han, D.; Wang, S.; Xiao, M.; Meng, Y. Interphase Building of Organic-Inorganic Hybrid Polymer Solid Electrolyte with Uniform Intermolecular Li(+) Path for Stable Lithium Metal Batteries. *Small* **2021**, *17* (41), 2102454.
(128) Chen, C.; Liang, Q.; Chen, Z.; Zhu, W.; Wang, Z.; Li, Y.; Wu, X.; Xiong, X. Phenoxy Radical-Induced Formation of Dual-Layered Protection Film for High-Rate and Dendrite-Free Lithium-Metal Anodes. *Angew. Chem., Int. Ed. Engl.* **2021**, *60* (51), 26718−26724.
(129) Niu, C.; Pan, H.; Xu, W.; Xiao, J.; Zhang, J. G.; Luo, L.; Wang, C.; Mei, D.; Meng, J.; Wang, X.; Liu, Z.; Mai, L.; Liu, J. Self-Smoothing Anode for Achieving High-Energy Lithium Metal Batteries under Realistic Conditions. *Nat. Nanotechnol.* **2019**, *14* (6), 594−601.
(130) Yang, C. P.; Yin, Y. X.; Zhang, S. F.; Li, N. W.; Guo, Y. G. Accommodating Lithium into 3D Current Collectors with a Submicron Skeleton towards Long-Life Lithium Metal Anodes. *Nat. Commun.* **2015**, *6*, 8058.
(131) Zhang, J.; You, C.; Wang, J.; Guo, S.; Zhang, W.; Yang, R.; Fu, P. Synergistic Catalytic Effect of Ion Tunnels with Polar Dopants to Boost the Electrochemical Kinetics for High-Performance Sulfur Cathodes. *ChemElectroChem.* **2019**, *6* (19), 5051−5059.
(132) Lu, L. L.; Ge, J.; Yang, J. N.; Chen, S. M.; Yao, H. B.; Zhou, F.; Yu, S. H. Free-Standing Copper Nanowire Network Current Collector for Improving Lithium Anode Performance. *Nano Lett.* **2016**, *16* (7), 4431−7.
(133) Chi, S.-S.; Liu, Y.; Song, W.-L.; Fan, L.-Z.; Zhang, Q. Prestoring Lithium into Stable 3D Nickel Foam Host as Dendrite-Free Lithium Metal Anode. *Adv. Funct. Mater.* **2017**, *27* (24), 1700348.
(134) Wu, S.; Jiao, T.; Yang, S.; Liu, B.; Zhang, W.; Zhang, K. Lithiophilicity Conversion of the Cu Surface through Facile Thermal Oxidation: Boosting a Stable Li−Cu Composite Anode through Melt Infusion. *J. Mater. Chem. A* **2019**, *7* (10), 5726−5732.
(135) Xue, P.; Liu, S.; Shi, X.; Sun, C.; Lai, C.; Zhou, Y.; Sui, D.; Chen, Y.; Liang, J. A Hierarchical Silver-Nanowire-Graphene Host Enabling Ultrahigh Rates and Superior Long-Term Cycling of Lithium-Metal Composite Anodes. *Adv. Mater.* **2018**, *30* (44), 1804165.
(136) Li, J.; Zou, P.; Chiang, S. W.; Yao, W.; Wang, Y.; Liu, P.; Liang, C.; Kang, F.; Yang, C. A Conductive-Dielectric Gradient Framework for Stable Lithium Metal Anode. *Energy Storage Mater.* **2020**, *24*, 700−706.
(137) Zhang, R.; Chen, X.; Shen, X.; Zhang, X.-Q.; Chen, X.-R.; Cheng, X.-B.; Yan, C.; Zhao, C.-Z.; Zhang, Q. Coralloid Carbon Fiber-Based Composite Lithium Anode for Robust Lithium Metal Batteries. *Joule* **2018**, *2* (4), 764−777.
(138) Kong, L.-L.; Zhang, Z.; Zhang, Y.-Z.; Liu, S.; Li, G.-R.; Gao, X.-P. Porous Carbon Paper as Interlayer to Stabilize the Lithium Anode for Lithium−Sulfur Battery. *ACS Appl. Mater. Interfaces* **2016**, *8* (46), 31684−31694.
(139) Liu, L.; Yin, Y. X.; Li, J. Y.; Wang, S. H.; Guo, Y. G.; Wan, L. J. Uniform Lithium Nucleation/Growth Induced by Lightweight Nitrogen-Doped Graphitic Carbon Foams for High-Performance Lithium Metal Anodes. *Adv. Mater.* **2018**, *30* (10), 1706216.
(140) Deng, W.; Zhou, X.; Fang, Q.; Liu, Z. Microscale Lithium Metal Stored inside Cellular Graphene Scaffold toward Advanced Metallic Lithium Anodes. *Adv. Energy Mater.* **2018**, *8* (12), 1703152.
(141) Yu, B.; Fan, Y.; Mateti, S.; Kim, D.; Zhao, C.; Lu, S.; Liu, X.; Rong, Q.; Tao, T.; Tanwar, K. K.; Tan, X.; Smith, S. C.; Chen, Y. I. An Ultra-Long-Life Flexible Lithium-Sulfur Battery with Lithium Cloth Anode and Polysulfone-Functionalized Separator. *ACS Nano* **2021**, *15* (1), 1358−1369.
(142) Zhang, F.; Liu, P.; Tian, Y.; Wu, J.; Wang, X.; Li, H.; Liu, X. Uniform Lithium Nucleation/Deposition Regulated by N/S co-doped Carbon Nanospheres towards Ultra-Stable Lithium Metal Anodes. *J. Mater. Chem. A* **2022**, *10* (3), 1463−1472.
(143) Wang, H.; Li, Y.; Li, Y.; Liu, Y.; Lin, D.; Zhu, C.; Chen, G.; Yang, A.; Yan, K.; Chen, H.; Zhu, Y.; Li, J.; Xie, J.; Xu, J.; Zhang, Z.; Vila, R.; Pei, A.; Wang, K.; Cui, Y. Wrinkled Graphene Cages as Hosts for High-Capacity Li Metal Anodes Shown by Cryogenic Electron Microscopy. *Nano Lett.* **2019**, *19* (2), 1326−1335.
(144) Liu, S.; Wang, A.; Li, Q.; Wu, J.; Chiou, K.; Huang, J.; Luo, J. Crumpled Graphene Balls Stabilized Dendrite-free Lithium Metal Anodes. *Joule* **2018**, *2* (1), 184−193.
(145) Yan, K.; Lu, Z.; Lee, H.-W.; Xiong, F.; Hsu, P.-C.; Li, Y.; Zhao, J.; Chu, S.; Cui, Y. Selective Deposition and Stable Encapsulation of Lithium through Heterogeneous Seeded Growth. *Nat. Energy* **2016**, *1* (3), 16010.

(146) Zhang, J.; You, C.; Wang, J.; Xu, H.; Zhu, C.; Guo, S.; Zhang, W.; Yang, R.; Xu, Y. Confinement of Sulfur Species into Heteroatom-Doped, Porous Carbon Container for High Areal Capacity Cathode. *Chem. Eng. J.* **2019**, *368*, 340−349.
(147) Wang, J.; Yang, J.; Xiao, Q.; Jia, L.; Lin, H.; Zhang, Y. Hierarchical Sulfur-Doped Graphene Foam Embedded with Sn Nanoparticles for Superior Lithium Storage in LiFSI-Based Electrolyte. *ACS Appl. Mater. Interfaces* **2019**, *11* (33), 30500−30507.
(148) Mei, Y.; Zhou, J.; Hao, Y.; Hu, X.; Lin, J.; Huang, Y.; Li, L.; Feng, C.; Wu, F.; Chen, R. High-Lithiophilicity Host with Micro/Nanostructured Active Sites based on Wenzel Wetting Model for Dendrite-Free Lithium Metal Anodes. *Adv. Funct. Mater.* **2021**, *31* (50), 2106676.
(149) Yang, C.; Yao, Y.; He, S.; Xie, H.; Hitz, E.; Hu, L. Ultrafine Silver Nanoparticles for Seeded Lithium Deposition toward Stable Lithium Metal Anode. *Adv. Mater.* **2017**, *29* (38), 1702714.
(150) Zeng, W.; Zhang, X.; Yang, C.; Zhang, C.; Shi, H.; Hu, J.; Zhao, Y.; Zhang, W.; Zhang, G.; Duan, H. Regulating Alkali Metal Deposition Behavior via Li/Na-philic Ni Nanoparticles Modified 3D Hierarchical Carbon Skeleton. *Chem. Eng. J.* **2021**, *412*, 128661.
(151) Tang, L.; Zhang, R.; Zhang, X.; Zhao, N.; Shi, C.; Liu, E.; Ma, L.; Luo, J.; He, C. ZnO Nanoconfined 3D Porous Carbon Composite Microspheres to Stabilize Lithium Nucleation/Growth for High-Performance Lithium Metal Anodes. *J. Materials Chem. A* **2019**, *7* (33), 19442−19452.
(152) Zhang, R.; Li, N. W.; Cheng, X. B.; Yin, Y. X.; Zhang, Q.; Guo, Y. G. Advanced Micro/Nanostructures for Lithium Metal Anodes. *Adv. Sci. (Weinh)* **2017**, *4* (3), 1600445.
(153) Yin, Y. C.; Yu, Z. L.; Ma, Z. Y.; Zhang, T. W.; Lu, Y. Y.; Ma, T.; Zhou, F.; Yao, H. B.; Yu, S. H. Bio-Inspired Low-Tortuosity Carbon Host for High-Performance Lithium-Metal Anode. *Natl. Sci. Rev.* **2019**, *6* (2), 247−256.
(154) Chen, Z.; Chen, W.; Wang, H.; Zhang, C.; Qi, X.; Qie, L.; Wu, F.; Wang, L.; Yu, F. Lithiophilic Anchor Points Enabling Endogenous Symbiotic Li_3N Interface for Homogeneous and Stable Lithium Electrodeposition. *Nano Energy* **2022**, *93*, 106836.
(155) Mukherjee, S.; Banwait, A.; Grixti, S.; Koratkar, N.; Singh, C. V. Adsorption and Diffusion of Lithium and Sodium on Defective Rhenium Disulfide: A First Principles Study. *ACS Appl. Mater. Interfaces* **2018**, *10* (6), 5373−5384.
(156) Choudhury, S.; Tu, Z.; Stalin, S.; Vu, D.; Fawole, K.; Gunceler, D.; Sundararaman, R.; Archer, L. A. Electroless Formation of Hybrid Lithium Anodes for Fast Interfacial Ion Transport. *Angew. Chem., Int. Ed. Engl.* **2017**, *56* (42), 13070−13077.
(157) He, G.; Li, Q.; Shen, Y.; Ding, Y. Flexible Amalgam Film Enables Stable Lithium Metal Anodes with High Capacities. *Angew. Chem., Int. Ed. Engl.* **2019**, *58* (51), 18466−18470.
(158) Ye, H.; Zheng, Z. J.; Yao, H. R.; Liu, S. C.; Zuo, T. T.; Wu, X. W.; Yin, Y. X.; Li, N. W.; Gu, J. J.; Cao, F. F.; Guo, Y. G. Guiding Uniform Li Plating/Stripping through Lithium-Aluminum Alloying Medium for Long-Life Li Metal Batteries. *Angew. Chem., Int. Ed. Engl.* **2019**, *58* (4), 1094−1099.
(159) Wang, G.; Wang, B.; Wang, X.; Park, J.; Dou, S.; Ahn, H.; Kim, K. Sn/Graphene Nanocomposite with 3D Architecture for Enhanced Reversible Lithium Storage in Lithium Ion Batteries. *J. Mater. Chem.* **2009**, *19* (44), 8378.
(160) Horowitz, Y.; Han, H. L.; Ross, P. N.; Somorjai, G. A. In Situ Potentiodynamic Analysis of the Electrolyte/Silicon Electrodes Interface Reactions–A Sum Frequency Generation Vibrational Spectroscopy Study. *J. Am. Chem. Soc.* **2016**, *138* (3), 726−729.
(161) Liang, X.; Pang, Q.; Kochetkov, I. R.; Sempere, M. S.; Huang, H.; Sun, X.; Nazar, L. F. A Facile Surface Chemistry Route to a Stabilized Lithium Metal Anode. *Nat. Energy* **2017**, *2* (9), 17119.
(162) Pang, Q.; Liang, X.; Kochetkov, I. R.; Hartmann, P.; Nazar, L. F. Stabilizing Lithium Plating by a Biphasic Surface Layer Formed In Situ. *Angew. Chem., Int. Ed. Engl.* **2018**, *57* (31), 9795−9798.
(163) Chu, F.; Hu, J.; Tian, J.; Zhou, X.; Li, Z.; Li, C. In Situ Plating of Porous Mg Network Layer to Reinforce Anode Dendrite Suppression in Li-Metal Batteries. *ACS Appl. Mater. Interfaces* **2018**, *10* (15), 12678−12689.
(164) Choudhury, S.; Tu, Z.; Stalin, S.; Vu, D.; Fawole, K.; Gunceler, D.; Sundararaman, R.; Archer, L. A. Electroless Formation of Hybrid Lithium Anodes for Fast Interfacial Ion Transport. *Angew. Chem.-Int. Ed.* **2017**, *56* (42), 13070−13077.
(165) Wang, Z.; Xu, Z.; Jin, X.; Li, J.; Xu, Q.; Chong, Y.; Ye, C.; Li, W.; Ye, D.; Lu, Y.; Qiu, Y. Dendrite-Free and Air-Stable Lithium Metal Batteries Enabled by Electroless Plating with Aluminum Fluoride. *J. Mater. Chem. A* **2020**, *8* (18), 9218−9227.
(166) Zhang, D.; Wang, S.; Hu, R.; Gu, J.; Cui, Y.; Li, B.; Chen, W.; Liu, C.; Shang, J.; Yang, S. Catalytic Conversion of Polysulfides on Single Atom Zinc Implanted MXene toward High-Rate Lithium−Sulfur Batteries. *Adv. Funct. Mater.* **2020**, *30* (30), 2002471.
(167) Du, Z.; Chen, X.; Hu, W.; Chuang, C.; Xie, S.; Hu, A.; Yan, W.; Kong, X.; Wu, X.; Ji, H.; Wan, L. J. Cobalt in Nitrogen-Doped Graphene as Single-Atom Catalyst for High-Sulfur Content Lithium-Sulfur Batteries. *J. Am. Chem. Soc.* **2019**, *141* (9), 3977−3985.
(168) Zhang, L.; Liu, D.; Muhammad, Z.; Wan, F.; Xie, W.; Wang, Y.; Song, L.; Niu, Z.; Chen, J. Single Nickel Atoms on Nitrogen-Doped Graphene Enabling Enhanced Kinetics of Lithium-Sulfur Batteries. *Adv. Mater.* **2019**, *31* (40), 1903955.
(169) Lu, C.; Chen, Y.; Yang, Y.; Chen, X. Single-atom Catalytic Materials for Lean-electrolyte Ultrastable Lithium-Sulfur Batteries. *Nano Lett.* **2020**, *20* (7), 5522−5530.
(170) Zhou, G.; Zhao, S.; Wang, T.; Yang, S. Z.; Johannessen, B.; Chen, H.; Liu, C.; Ye, Y.; Wu, Y.; Peng, Y.; Liu, C.; Jiang, S. P.; Zhang, Q.; Cui, Y. Theoretical Calculation Guided Design of Single-Atom Catalysts toward Fast Kinetic and Long-Life Li-S Batteries. *Nano Lett.* **2020**, *20* (2), 1252−1261.
(171) Yan, K.; Lee, H. W.; Gao, T.; Zheng, G.; Yao, H.; Wang, H.; Lu, Z.; Zhou, Y.; Liang, Z.; Liu, Z.; Chu, S.; Cui, Y. Ultrathin Two-Dimensional Atomic Crystals as Stable Interfacial Layer for Improvement of Lithium Metal Anode. *Nano Lett.* **2014**, *14* (10), 6016−22.
(172) Zhai, P.; Wang, T.; Yang, W.; Cui, S.; Zhang, P.; Nie, A.; Zhang, Q.; Gong, Y. Uniform Lithium Deposition Assisted by Single-Atom Doping toward High-Performance Lithium Metal Anodes. *Adv. Energy Mater.* **2019**, *9* (18), 1804019.
(173) Xu, K.; Zhu, M.; Wu, X.; Liang, J.; Liu, Y.; Zhang, T.; Zhu, Y.; Qian, Y. Dendrite-Tamed Deposition Kinetics using Single-Atom Zn Sites for Li Metal Anode. *Energy Storage Mater.* **2019**, *23*, 587−593.
(174) Sun, Y.; Zhou, J.; Ji, H.; Liu, J.; Qian, T.; Yan, C. Single-Atom Iron as Lithiophilic Site To Minimize Lithium Nucleation Overpotential for Stable Lithium Metal Full Battery. *ACS Appl. Mater. Interfaces* **2019**, *11* (35), 32008−32014.
(175) Gu, J.; Zhu, Q.; Shi, Y.; Chen, H.; Zhang, D.; Du, Z.; Yang, S. Single Zinc Atoms Immobilized on MXene ($Ti_3C_2Cl_x$) Layers toward Dendrite-Free Lithium Metal Anodes. *ACS Nano* **2020**, *14* (1), 891−898.
(176) Shi, H.; Ren, X.; Lu, J.; Dong, C.; Liu, J.; Yang, Q.; Chen, J.; Wu, Z. S. Dual-Functional Atomic Zinc Decorated Hollow Carbon Nanoreactors for Kinetically Accelerated Polysulfides Conversion and Dendrite Free Lithium Sulfur Batteries. *Adv. Energy Mater.* **2020**, *10* (39), 2002271.
(177) Huang, T.; Sun, Y.; Wu, J.; Jin, J.; Wei, C.; Shi, Z.; Wang, M.; Cai, J.; An, X. T.; Wang, P.; Su, C.; Li, Y. Y.; Sun, J. A Dual-Functional Fibrous Skeleton Implanted with Single-Atomic Co-Nx Dispersions for Longevous Li-S Full Batteries. *ACS Nano* **2021**, *15* (9), 14105−14115.
(178) Wang, J.; Jia, L.; Liu, H.; Wang, C.; Zhong, J.; Xiao, Q.; Yang, J.; Duan, S.; Feng, K.; Liu, N.; Duan, W.; Lin, H.; Zhang, Y. Multi-ion Modulated Single-Step Synthesis of a Nanocarbon Embedded with a Defect-Rich Nanoparticle Catalyst for a High Loading Sulfur Cathode. *ACS Appl. Mater. Interfaces* **2020**, *12* (11), 12727−12735.
(179) Li, X.; Su, H.; Ma, C.; Cong, Y.; Wang, J.; Lin, H.; Shang, Y.; Liu, H. In-situ Self-Assembly Robust Defected Graphene Wrapped Silicon/Nanorod Carbon for High-Performance Binder-Free Li Ion Battery. *Mater. Lett.* **2022**, *324*, 132636.

(180) Xi, Y.; Ye, X.; Duan, S.; Li, T.; Zhang, J.; Jia, L.; Yang, J.; Wang, J.; Liu, H.; Xiao, Q. Iron Vacancies and Surface Modulation of Iron Disulfide Nanoflowers as a High Power/Energy Density Cathode for Ultralong-Life Stable Li Storage. *J. Mater. Chem. A* **2020**, *8* (29), 14769−14777.
(181) Zhang, L.; Zhao, X.; Yuan, Z.; Wu, M.; Zhou, H. Oxygen Defect-Stabilized Heterogeneous Single Atom Catalysts: Preparation, Properties and Catalytic Application. *J. Mater. Chem. A* **2021**, *9* (7), 3855−3879.
(182) Jia, L.; Wang, J.; Ren, S.; Ren, G.; Jin, X.; Kao, L.; Feng, X.; Yang, F.; Wang, Q.; Pan, L.; Li, Q.; Liu, Y. s.; Wu, Y.; Liu, G.; Feng, J.; Fan, S.; Ye, Y.; Guo, J.; Zhang, Y. Unraveling Shuttle Effect and Suppression Strategy in Lithium/Sulfur Cells by In Situ/Operando X-ray Absorption Spectroscopic Characterization. *Energy Environ. Mater.* **2021**, *4* (2), 222−228.